NONLINEAR VIBRATION ANALYSIS OF L-SHAPED BEAMS AND THEIR USE IN VIBRATION REDUCTION

A THESIS SUBMITTED TO
THE GRADUATE SCHOOL OF NATURAL AND APPLIED SCIENCES
OF
MIDDLE EAST TECHNICAL UNIVERSITY

BY

YIGITCAN EKICI

IN PARTIAL FULFILLMENT OF THE REQUIREMENTS
FOR
THE DEGREE OF MASTER OF SCIENCE
IN
MECHANICAL ENGINEERING

SEPTEMBER 2022

Approval of the thesis:

NONLINEAR VIBRATION ANALYSIS OF L-SHAPED BEAMS AND THEIR USE IN VIBRATION REDUCTION

submitted by **YİĞİTCAN EKİCİ** in partial fulfillment of the requirements for the degree of **Master of Science** i**n Mechanical Engineering, Middle East Technical University** by,

Prof. Dr. Halil Kalıpçılar
Dean, Graduate School of **Natural and Applied Sciences** _____

Prof. Dr. Mehmet Ali Sahir Arıkan
Head of the Department, **Mechanical Eng.** _____

Prof. Dr. Ender Ciğeroğlu
Supervisor, **Mechanical Eng., METU** _____

Prof. Dr. Yiğit Yazıcıoğlu
Co-Supervisor, **Mechanical Eng., METU** _____

Examining Committee Members:

Prof. Dr. Fevzi Suat Kadıoğlu
Mechanical Eng., METU _____

Prof. Dr. Ender Ciğeroğlu
Mechanical Eng., METU _____

Prof. Dr. Yiğit Yazıcıoğlu
Mechanical Eng., METU _____

Asst. Prof. Dr. Gökhan Osman Özgen
Mechanical Eng., METU _____

Asst. Prof. Dr. Saeed Lotfan
Mechanical Eng., Gebze Technical Uni. _____

Date: 02.09.2022

I hereby declare that all information in this document has been obtained and presented in accordance with academic rules and ethical conduct. I also declare that, as required by these rules and conduct, I have fully cited and referenced all material and results that are not original to this work.

Name Last name : Yiğitcan Ekici

Signature :

ABSTRACT

NONLINEAR VIBRATION ANALYSIS OF L-SHAPED BEAMS AND THEIR USE IN VIBRATION REDUCTION

Ekici, Yiğitcan
Master of Science, Mechanical Engineering
Supervisor : Prof. Dr. Ender Ciğeroğlu
Co-Supervisor: Prof. Dr. Yiğit Yazıcıoğlu

September 2022, 106 pages

In this thesis, nonlinear vibration analysis of both fixed L-shaped beam and L-shaped beam attached to a single degree of freedom (SDOF) system is performed for several cases with different structural parameters to observe the effect of these parameters. Then these beams are proposed to reduce the vibration amplitudes of certain structures, and the nonlinear effects on the dynamic responses of these structures are investigated. The nonlinear dynamic model of the L-shaped beam is obtained by using Euler-Bernoulli Beam Theory and Hamilton's principle. The equations are simplified by disregarding the beams' axial motions; only the transverse motions are considered in calculations. Galerkin's method is utilized to discretize the obtained nonlinear partial differential equations into a set of nonlinear ordinary differential equations. These equations are converted into a set of nonlinear algebraic equations using Harmonic Balance Method, which are then solved numerically using Newton's method with arc length continuation.

Keywords: Nonlinear Beams, Nonlinear L-Shaped Beams, Structural Dynamics, Euler Bernoulli Beam Theory

ÖZ

L-ŞEKİLLİ KİRİŞLERİN DOĞRUSAL OLMAYAN TİTREŞİM ANALİZİ VE BUNLARIN TİTREŞİM AZALTIMI İÇİN KULLANIMI

Ekici, Yiğitcan
Yüksek Lisans, Makina Mühendisliği
Tez Yöneticisi: Prof. Dr. Ender Ciğeroğlu
Ortak Tez Yöneticisi: Prof. Dr. Yiğit Yazıcıoğlu

Eylül 2022, 106 sayfa

Bu tezde, hem sabit L-şekilli kirişin hem de tek serbestlik dereceli sisteme bağlanmış L-şekilli kirişin doğrusal olmayan titreşim analizi, yapısal parametrelerin etkisini gözlemlemek için farklı parametreli çeşitli vaka çalışmaları için yapılmıştır. Sonrasında bu kirişlerin belirli yapıların titreşim genliklerini azaltması önerilmiştir ve bu yapıların dinamik tepkileri üzerindeki doğrusal olmayan etkiler araştırılmıştır. L-şekilli kirişin doğrusal olmayan dinamik modeli, Euler-Bernoulli kiriş teorisi ve Hamilton prensibi kullanılarak elde edilmiştir. Kirişlerin eksenel hareketleri göz ardı edilerek denklemler basitleştirilmiştir; hesaplamalarda sadece enine hareketler dikkate alınmıştır. Galerkin Yöntemi, elde edilen doğrusal olmayan kısmi diferansiyel denklemleri bir dizi doğrusal olmayan adi diferansiyel denkleme ayırmak için kullanılmıştır. Bu denklemler, Harmonik Denge Yöntemi ile bir dizi doğrusal olmayan cebirsel denkleme dönüştürülmüştür ve daha sonra yay uzunluğu sürekliliği ile Newton'un yöntemi kullanılarak sayısal olarak çözülümüştür.

Anahtar Kelimeler: Doğrusal Olmayan Kirişler, Doğrusal Olmayan L-Şekilli Kirişler, Yapısal Dinamik, Euler Bernoulli Kiriş Teorisi

To my family

ACKNOWLEDGMENTS

I would like to express my deepest gratitude to my supervisor Prof. Dr. Ender Ciğeroğlu, and my co-supervisor Yiğit Yazıcıoğlu, for their guidance and support throughout my graduate education and thesis period.

I would like to thank my friends Aykut Çardak and Hümeyra Beyan for their friendship, technical and motivational support.

I would like to thank my coworkers in Control Systems Development Department in Roketsan Inc. for their support and trust in me.

Lastly, I am extremely thankful to my family for their endless love, support, and patience throughout my life.

TABLE OF CONTENTS

LIST OF TABLES

TABLES

LIST OF FIGURES

FIGURES

LIST OF ABBREVIATIONS

ABBREVIATIONS

ALCM	Arc-Length Continuation Method
BC	Boundary Condition
DOF	Degree of Freedom
FE	Finite Element
FRF	Frequency Response Function
HBM	Harmonic Balance Method
HCM	Homotopy Continuation Method
IBP	Integration by Parts
NLAE	Nonlinear Algebraic Equation
ODE	Ordinary Differential Equation
PDE	Partial Differential Equation
SDOF	Single Degree of Freedom
TMD	Tuned Mass Damper

LIST OF SYMBOLS

SYMBOLS

A	Cross Sectional Area of the Beam
δ	Dirac Delta Function
E	Young's Modulus of the Beam
$\mathbf{e}_j$	Unit Vector in the j^{th} Direction
$\mathbf{f}$	External Forcing Vector
$\mathbf{f_N}$	Nonlinear Forcing Vector
γ	Structural Damping Coefficient
$\mathbf{H}$	Structural Damping Matrix
h_j	Scaled Step Size in the j^{th} Direction
I	Second Moment of Area of the Beam
$\mathbf{J}$	Jacobian Matrix
$\mathbf{K}$	Stiffness Matrix
k_b	Stiffness of the Spring Attached to the Base Mass
L	Length of the Beam
L_{M_i}	Connection Point of the M_i w.r.t Its Axis Center
$\mathbf{M}$	Mass Matrix
M_b	Mass of the Base
M_i	Mass of the Concentrated Mass on the i^{th} Beam

ω	Frequency
$\mathbf{q}$	Response / Generalized Coordinate Vector
ρ	Density of the Beam
s	Arc-Length Parameter
T	Kinetic Energy
t	Temporal Independent Variable (Time)
U	Heaviside Step Function
u_i	Axial Motion of the i^{th} Beam
V	Potential Energy
W_{nc}	Virtual Work Done by Nonconservative Forces
w_b	Motion of the Base Mass
w_i	Transverse Motion of the i^{th} Beam
x_i	Spatial Independent Variable of the Coordinate System Attached to the i^{th} Beam

CHAPTER 1

INTRODUCTION & LITERATURE REVIEW

L-shaped beams are considered one of the most important components among engineering structures [1]. These beams are a sub-class of the beams commonly used in many applications such as buildings, aerospace structures, naval structures, vehicles, etc. Because of this reason, they are investigated in many studies. Earlier papers studied L-shaped beams using linear Euler-Bernoulli beam models since it is easy to derive the governing differential equations and it is possible to obtain the analytical solution. However, the linear Euler-Bernoulli beam model is valid only for small deflections. In later studies, nonlinear Euler-Bernoulli models are considered to obtain an accurate solution for large deflections. In addition, many studies experimentally observed the response of the beams. Some of these studies observed the dynamical behaviors of these beams both mathematically and experimentally for the comparison and validation of mathematical models.

Figure 1.1 Picture of an L-Shaped Beam

1.1 Literature Survey

Besides analytical and finite element modeling methods, many numerical methods exist to discretize the Euler-Bernoulli beam equation in spatial domain and turn it into an ordinary differential equation. The most common ones are the Galerkin method, the Collocation method, and the Assumed Modes method [2], [3]. Alongside these methods, Samandari and Cigeroglu [1] employed Differential Quadrature Method [4], [5] to discretize the nonlinear equations of motion of an L-shaped beam. Apart from these, Morales [6] applied the Rayleigh-Ritz-Meirovitch Substructure Synthesis method (RRMSSM) [7] to discretize the linear equation of motion of the L-shaped beam and compared the results with the results obtained using analytical and FEM solutions. In his later work [8], generic expressions of RRMSSM mass and stiffness matrices of the L-shaped beam were presented.

Some studies focus on the analytical solution of L-shaped beams. Bang's study [9] is one of the most prominent ones among these studies. In his study, an analytical solution for linearized equations of motion of the L-shaped beam is obtained. Gurgoze detected some mistakes in this study and corrected them [10] and later improved this study by obtaining an analytical solution of the linear L-shaped beam with a point mass attached to its end [11]. Oguamanam et al. [12] obtained linearized equations of motion for a two-member open frame structure with an arbitrary angle between them. They compared the natural frequencies obtained by the analytical and finite element methods. Georgiades et al. [13] studied in-plane and out-of-plane modal analysis of L-shaped beams. In this study, the analytical solutions are compared with the results of finite element analysis, and it is observed that for in-plane bending, the effects of shear and inertia are not significant, and for out-of-plane bending, the effects of shear and inertia are more critical, especially, for the second beam.

Since the linearized models for L-shaped beams are not valid for large deflections, many studies considered the nonlinear models for L-shaped beams. In [14], the nonlinear equation of motion of an L-shaped beam was formulated, and the global

mode approach was used to obtain mode shapes and natural frequencies of the system. The results were compared with FEM results to illustrate the validity of this approach. In the study of Georgiades, a nonlinear model for L-shaped beams was developed [15]. This study was the first to describe the out-of-plane motion of nonlinear L-shaped beams that had been neglected in the literature for many years.

Besides the studies that focus on analysis and mathematical modeling of L-shaped beams, many other studies were performed to observe the dynamical behaviors of these beams both mathematically and experimentally. Most of these studies consider L-shaped beams with two-to-one internal resonance to a primary resonance [16]–[21]. The study of Haddow et al. [16] is one of the first studies that compared the natural frequencies and planar dynamic responses of an L-shaped beam obtained by mathematical model and experiments. In addition, saturation, jump conditions, and the non-existence of a steady state response were also demonstrated experimentally. In [17]–[21], experimental responses of an L-shaped beam were compared to the results obtained by nonlinear mathematical modeling. Experimentally, it is observed that periodic, quasi-periodic, and chaotic responses occur when an L-shaped beam with quadratic nonlinearities is excited with minimal excitation levels, as predicted by the nonlinear theory.

Moreover, in literature, some papers studied the usage of L-shaped beams as piezoelectric energy harvesters. In [22], Erturk et al. developed a novel L-shaped beam piezoelectric energy harvester and analyzed its electromechanical behavior. The usage of this system in landing gears of UAVs was also suggested. Yao et al. [23] performed an experimental study using an L-shaped piezoelectric beam. The broadband energy harvesting and dynamic responses of this device were presented, and effects of the sizes of the beams and external excitation on the power generation behavior were studied.

1.2 Motivation and Scope

The main objective of this thesis is to analyze the behaviors of L-shaped beams by carrying out case studies and propose these beams to reduce the vibration amplitudes of certain structures as alternatives to tuned mass dampers (TMD) and investigate the nonlinear effects on the dynamic responses of these structures. The system is constructed as these beams are assumed to be connected from their ends to the vibratory systems. To investigate the response of the system, a nonlinear mathematical model for an L-shaped beam attached to a SDOF system is derived. The linearized mathematical model is verified using commercial finite element (FE) software. Case studies are performed to observe the effect of the structural parameters on the vibration characteristics on both one end fixed L-shaped beam and L-shaped beam attached to a SDOF system. Usage of these L-shaped beams as vibration absorbers is demonstrated using both linear and nonlinear L-shaped beams, and the effects of nonlinearities on the response of the linear L-shaped beams are investigated.

1.3 Outline

In Chapter 2, steady-state frequency response analysis of nonlinear vibratory systems under periodic excitation is explained. After that, Harmonic Balance Method (HBM), which is used to transform nonlinear ordinary differential equations (ODEs) into nonlinear algebraic equations (NLAEs), is explained. Finally, the numerical solution methods for these nonlinear algebraic equations are described.

In Chapter 3, the mathematical model of the L-shaped beam attached to a SDOF system is derived. Hamilton's Principle is carried out for the nonlinear Euler Bernoulli beam theory to obtain the mathematical model, and governing nonlinear partial differential equations (PDEs) are obtained. These PDEs are then transformed into nonlinear ODEs using Galerkin's Method.

In Chapter 4, mathematical models of both fixed L-shaped beam and L-shaped beam attached to a SDOF system are verified using FE software. Then, case studies are performed for both models to investigate the effect of the system parameters on the frequency responses of the beams.

In Chapter 5, nonlinear L-shaped beams are proposed as vibration absorbers as alternatives to tuned mass dampers (TMDs). Then, the nonlinear effects on the base response of the optimized linear L-shaped beam vibration absorbers and cantilever

In Chapter 6, a summary of the thesis is explained. The methodology, formulations, case studies, and their results are briefly mentioned and discussed. Critical remarks about the results are made.

CHAPTER 2

STEADY STATE PERIODIC RESPONSE ANALYSIS OF NONLINEAR STRUCTURES

2.1 Equation of Motion of a General Nonlinear System

The equation of motion of a nonlinear vibratory spring-mass system with viscous and structural damping is given as,

$$\mathbf{M}\ddot{\mathbf{q}} + \mathbf{C}\dot{\mathbf{q}} + \left(\mathbf{K} + i\mathbf{H}\right)\mathbf{q} + \mathbf{f}_N = \mathbf{f} \,. \tag{2.1}$$

$\mathbf{M}$, $\mathbf{C}$, $\mathbf{K}$ and $\mathbf{H}$ terms in Equation (2.1) represent mass, viscous damping, stiffness, and structural damping matrices, respectively. $\mathbf{q}$, $\mathbf{f}_N$ and $\mathbf{f}$ terms represent response, nonlinear forcing, and external forcing vectors, respectively.

The response of the nonlinear system can be stationary, periodic, quasi-periodic, or chaotic. In this study, only periodic response of the system is considered for a periodic external forcing, which can be obtained by utilizing Harmonic Balance method.

2.2 Harmonic Balance Method

Harmonic Balance method (HBM) is used to calculate the steady-state responses of nonlinear systems by transforming nonlinear ordinary differential equations (ODEs) into nonlinear algebraic equations (NLAE) in the frequency domain. To apply HBM, external forcing and response must be periodic. In HBM, displacement, excitation force, and nonlinear internal forcing vectors are represented by the Fourier series as periodic functions, and similar terms are balanced to obtain the nonlinear algebraic equations. Therefore, the response vector is written as follows,

$$\mathbf{q}(\theta) = \mathbf{q}_0 + \sum_{h=1}^{N_h} \mathbf{q}_s^h \sin(h\theta) + \mathbf{q}_c^h \cos(h\theta),\ \theta = \omega t, \tag{2.2}$$

where $\mathbf{q}_0$ is the bias term, $\mathbf{q}_s^h$ and $\mathbf{q}_c^h$ are the coefficients of sine and cosine for the h^{th} harmonic, respectively, and N_h is the number of harmonics used in the representation. For the exact representation of a periodic function, N_h should be selected as infinity. However, in practice, choosing a certain number of harmonics should be satisfactory to obtain an approximate representation since the contribution of the higher harmonics to the representation will be negligible. To reduce the harmonics in order to reduce the computational efforts, it is important to select a smaller N_h number such that it will still represent the function with negligible error. Similarly, the excitation force vector and nonlinear internal forcing vector can be written as follows

$$\mathbf{f}(\theta) = \mathbf{f}_0 + \sum_{h=1}^{N_h} \mathbf{f}_s^h \sin(h\theta) + \mathbf{f}_c^h \cos(h\theta), \tag{2.3}$$

$$\mathbf{f}_N(\theta) = \mathbf{f}_{N0} + \sum_{h=1}^{N_h} \mathbf{f}_{Ns}^h \sin(h\theta) + \mathbf{f}_{Nc}^h \cos(h\theta). \tag{2.4}$$

In order to write the excitation force vector and nonlinear internal forcing vectors in Fourier series representation, sine and cosine coefficients for each harmonic should be obtained. These coefficients are obtained using Fourier integrals as follows,

$$\mathbf{f}_0 = \frac{1}{T}\int_0^T \mathbf{f}(t)\,dt, \tag{2.5}$$

$$\mathbf{f}_s^h = \frac{2}{T}\int_0^T \mathbf{f}(t)\sin(h\cdot\omega\cdot t)\,dt, \tag{2.6}$$

$$\mathbf{f}_c^h = \frac{2}{T}\int_0^T \mathbf{f}(t)\cos(h\cdot\omega\cdot t)\,dt, \tag{2.7}$$

$$\mathbf{f}_{N0} = \frac{1}{T}\int_0^T \mathbf{f}_N(t)\,dt, \tag{2.8}$$

$$\mathbf{f}_{Ns}^{h} = \frac{2}{T}\int_0^T \mathbf{f}_N(t)\sin(h\cdot\omega\cdot t)\,dt\,, \tag{2.9}$$

$$\mathbf{f}_{Nc}^{h} = \frac{2}{T}\int_0^T \mathbf{f}_N(t)\cos(h\cdot\omega\cdot t)\,dt\,, \tag{2.10}$$

where T is the period ($T = 2\pi/\omega$). By substituting Equations (2.2), (2.3) and (2.4) into Equation (2.1) and rewriting it in terms of real values, nonlinear ODE is transformed into a system of NLAEs as follows,

$$\begin{aligned}
&\mathbf{K}\mathbf{q}_0 + \mathbf{f}_{N0} - \mathbf{f}_0 = 0,\\
&\begin{bmatrix} \mathbf{K} - (h\omega)^2\mathbf{M} & -\mathbf{H} \\ \mathbf{H} & \mathbf{K} - (h\omega)^2\mathbf{M} \end{bmatrix}\begin{bmatrix} \mathbf{q}_s^h \\ \mathbf{q}_c^h \end{bmatrix} + \begin{bmatrix} \mathbf{f}_{Ns}^h \\ \mathbf{f}_{Nc}^h \end{bmatrix} - \begin{bmatrix} \mathbf{f}_s^h \\ \mathbf{f}_s^h \end{bmatrix} = 0,\\
&h = 1, 2..N_h.
\end{aligned} \tag{2.11}$$

2.3 Numerical Solution of Nonlinear Algebraic Equation System

Steady-state response of the linear ODEs with periodic excitation can be obtained using analytical methods. Additionally, an analytical solution exists for the ODEs with simple nonlinearities. For complex nonlinearities, the ODE system can be solved only by applying numerical methods. Newton's method is a popular iterative solution method to solve any linear or nonlinear algebraic equation system. In this thesis, Newton's method is employed to solve the NLAEs obtained by transforming the nonlinear ODEs by using HBM. However, by only using Newton's method, steady-state response can be obtained for a specific frequency value, not for the desired frequency range. In addition, depending on the initial guess, Newton's method may not converge. Even if Newton's method converges, if multiple response values correspond to a specific frequency, the response obtained will depend on the selected initial guess. It could be either one of the maximum amplitude, minimum amplitude, or an amplitude value between them. Homotopy Continuation or Arc-Length Continuation with Newton's method could be used to overcome these

mentioned problems or obtain the system's frequency response for a frequency range.

2.3.1 Newton's Method

NLAEs written in Equation (2.11) can be expressed as follows,

$$\mathbf{r}(\mathbf{q},\omega)=\begin{bmatrix}\mathbf{K} & & & & \\ & \mathbf{K}-\omega^2\mathbf{M} & -\omega\mathbf{C}-\mathbf{H} & & \\ & \omega\mathbf{C}+\mathbf{H} & \mathbf{K}-\omega^2\mathbf{M} & & \\ & & & \ddots & \\ & & & \mathbf{K}-(N_h\omega)^2\mathbf{M} & -N_h\omega\mathbf{C}-\mathbf{H} \\ & & & N_h\omega\mathbf{C}+\mathbf{H} & \mathbf{K}-(N_h\omega)^2\mathbf{M}\end{bmatrix}\mathbf{q}+\begin{bmatrix}\mathbf{f}_{N0}\\ \mathbf{f}_{Ns}^{h}\\ \mathbf{f}_{Nc}^{h}\\ \vdots\\ \mathbf{f}_{Ns}^{N_h}\\ \mathbf{f}_{Nc}^{N_h}\end{bmatrix}-\begin{bmatrix}\mathbf{f}_{0}\\ \mathbf{f}_{s}^{h}\\ \mathbf{f}_{c}^{h}\\ \vdots\\ \mathbf{f}_{s}^{N_h}\\ \mathbf{f}_{c}^{N_h}\end{bmatrix}=\mathbf{0} \tag{2.12}$$

Expanding Equation (2.12) in Taylor Series around $\mathbf{q}$,

$$\mathbf{r}(\mathbf{q}+\Delta\mathbf{q},\omega)=\mathbf{r}(\mathbf{q},\omega)+\mathbf{J}(\mathbf{q},\omega)\Delta\mathbf{q}+O(\Delta\mathbf{q}^2), \tag{2.13}$$

where $\mathbf{J}(\mathbf{q},\omega)$ is

$$J(\mathbf{q},\omega)_{i,j}=\frac{\partial r_i}{\partial q_j}. \tag{2.14}$$

Neglecting higher order terms, i.e., $O(\Delta\mathbf{q}^2)=0$ in Equation (2.13) and considering it to be zero, it can be rewritten as,

$$\Delta\mathbf{q}=-\mathbf{J}(\mathbf{q},\omega)^{-1}\mathbf{r}(\mathbf{q},\omega). \tag{2.15}$$

New $\mathbf{q}$ value can be found by iterating it as,

$$\mathbf{q}_{i+1}=\mathbf{q}_i+\Delta\mathbf{q}. \tag{2.16}$$

Inserting Equation (2.15) into Equation (2.16),

$$\mathbf{q}_{i+1} = \mathbf{q}_i - \mathbf{J}\left(\mathbf{q}_i, \omega\right)^{-1} \mathbf{r}\left(\mathbf{q}_i, \omega\right). \tag{2.17}$$

Steady state response of the system at frequency ω could be obtained by iterating Equation (2.17) until it converges.

Jacobian matrix in Equation (2.14) could be calculated using numerical differentiation using Forward Difference Formula as

$$\mathbf{J}\left(\mathbf{q}, \omega\right)^{<j>} = \frac{\mathbf{r}\left(\mathbf{q} + h_j \mathbf{e}_j, \omega\right) - \mathbf{r}\left(\mathbf{q}, \omega\right)}{\mathbf{q}_j}, \tag{2.18}$$

where h_j is the scaled step size and $\mathbf{e}_j$ is the unit vector in the j^{th} direction.

2.3.2 Homotopy Continuation with Newton's Method

Homotopy Continuation (HCM) is a method to obtain the solution of an NLAE system for a specific frequency range. It obtains the solution by following the solution path. Because of that, it is considered a path-following method. It uses the solution of the linear system at the starting frequency as an initial guess and solves the nonlinear system by increasing or decreasing the frequency step by step, using the previous solution as an initial guess. For Newton's Method to converge at the starting point, starting frequency should be selected, such as solutions of linear and nonlinear systems are close to each other. These solutions are usually close at frequencies away from resonance points. The reason for that is that nonlinear forces are usually large around resonance points, which makes the linear and nonlinear solutions distant. In addition, the step size of the frequency should be selected appropriately so that solutions between previous and current steps do not vary too much for Newton's method to converge. However, choosing a too small step size will increase the computation time.

2.3.3 Arc-Length Continuation with Newton's Method

HCM with Newton's method may encounter convergence problems. It usually happens when the path of the solution turns back. Mathematically, this means that the determinant of the Jacobian matrix is either zero or too close to zero, i.e., the Jacobian matrix is singular that the inverse of it cannot be calculated. Moreover, for the case of multiple response values corresponding to a specific frequency point in the solution path, obtaining all of these solutions with HBM is impossible since frequency only goes in one direction, i.e., it either increases or decreases and doesn't turn back., The direction of the frequency needs to be changed to overcome these problems and obtain all solutions in the solution path.

In ALCM, a new parameter which is the arc-length parameter, is added to the NLAEs to make the Jacobian matrix non-singular at the turning points. By adding this, path following parameter becomes the new arc-length parameter instead of the frequency. This parameter is the radius of a hypothetical multi-dimensional sphere whose dimension is equal to the number of NLAEs plus one. In this sphere, the next solution point is searched.

For this new modified system, the frequency will be an unknown in the NLAEs as well as the Fourier coefficients of the steady-state response of the system. Then, the unknown vector of the system becomes,

$$\mathbf{a} = \begin{bmatrix} \mathbf{q} \\ \omega \end{bmatrix}. \tag{2.19}$$

A new equation is required since the unknown vector is increased by one. It is the equation of the hypothetical multi-dimensional sphere whose center is the previous solution point, and its radius is the arc-length parameter. This equation is written as,

$$\left(\mathbf{q}_k - \mathbf{q}_{k-1}\right)^T \cdot \left(\mathbf{q}_k - \mathbf{q}_{k-1}\right) + \left(\omega_k + \omega_{k-1}\right) = s^2, \tag{2.20}$$

where s is the mentioned arc-length parameter and k is the index number of the solution. Equation (2.20) can be rewritten as,

$$h(\mathbf{q}_k, \omega_k) = \Delta\mathbf{a}_k{}^T \cdot \Delta\mathbf{a}_k - s^2 = \mathbf{0}, \tag{2.21}$$

where,

$$\Delta\mathbf{a}_k = \begin{bmatrix} \Delta\mathbf{q}_k \\ \Delta\omega_k \end{bmatrix} = \begin{bmatrix} \mathbf{q}_k - \mathbf{q}_{k-1} \\ \omega_k + \omega_{k-1} \end{bmatrix}. \tag{2.22}$$

With this additional equation and unknown, Equation (2.17), which is the iteration equation in Newton's method, can be rewritten as,

$$\mathbf{a}_k^{i+1} = \mathbf{a}_k^i - \left[\begin{matrix} \frac{\partial \mathbf{r}(\mathbf{q},\omega)}{\partial \mathbf{q}} & \frac{\partial \mathbf{r}(\mathbf{q},\omega)}{\partial \omega} \\ \frac{\partial h(\mathbf{q},\omega)}{\partial \mathbf{q}} & \frac{\partial h(\mathbf{q},\omega)}{\partial \omega} \end{matrix} \right]^{-1}_{\substack{\mathbf{q}=\mathbf{q}_k^i \\ \omega=\omega_k^i}} \cdot \begin{bmatrix} \mathbf{r}(\mathbf{q}_k^i, \omega_k^i) \\ h(\mathbf{q}_k^i, \omega_k^i) \end{bmatrix}, \tag{2.23}$$

where,

$$\left[\begin{matrix} \frac{\partial h(\mathbf{q},\omega)}{\partial \mathbf{q}} & \frac{\partial h(\mathbf{q},\omega)}{\partial \omega} \end{matrix} \right]_{\substack{\mathbf{q}=\mathbf{q}_k^i \\ \omega=\omega_k^i}} = \left[2\Delta\mathbf{a}_k^{i\,T} \right]. \tag{2.24}$$

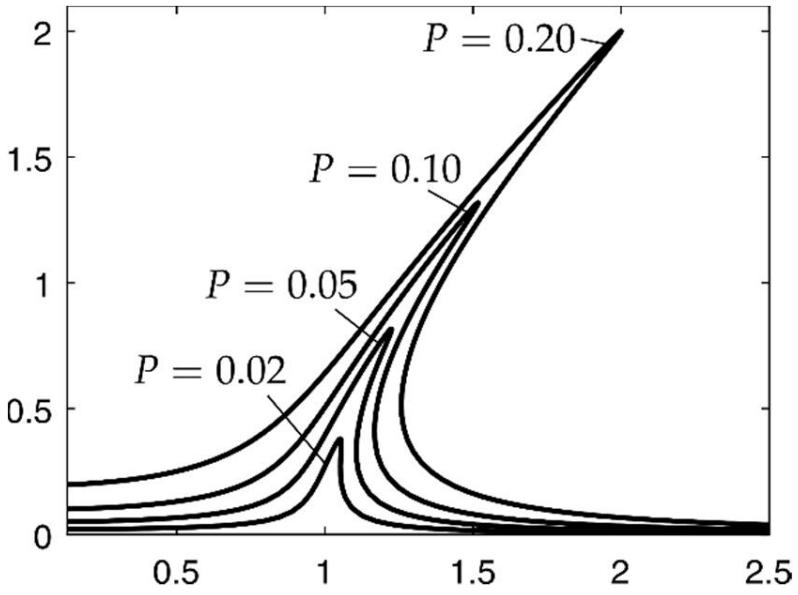

Figure 2.1. Frequency Response of a System with Cubic Nonlinearity [24]

CHAPTER 3

MATHEMATICAL MODEL OF L-SHAPED BEAM ATTACHED TO A SDOF SYSTEM

In this chapter, the nonlinear partial differential equations of motion of an L-shaped beam attached to a SDOF system are derived. The system is constructed as an L-shaped beam attached to a base mass-spring system with structural damping. The equations of motions are derived for a beam, transversally excited at the base with symmetric cross sections with respect to the respective longitudinal directions. Moreover, the motion of the base mass is constrained such that it can only make a translational motion in y_1 direction. Because of that, only the in-plane axial and transverse motion of the beam are considered, torsional and out-of-plane motion are neglected. The beam is modeled as two beams with different coordinate frames attached to their respective ends, as shown in Figure 3.1. In addition, point masses are connected to each beam to study the effects of such masses on the dynamic response of the L-shaped beam.

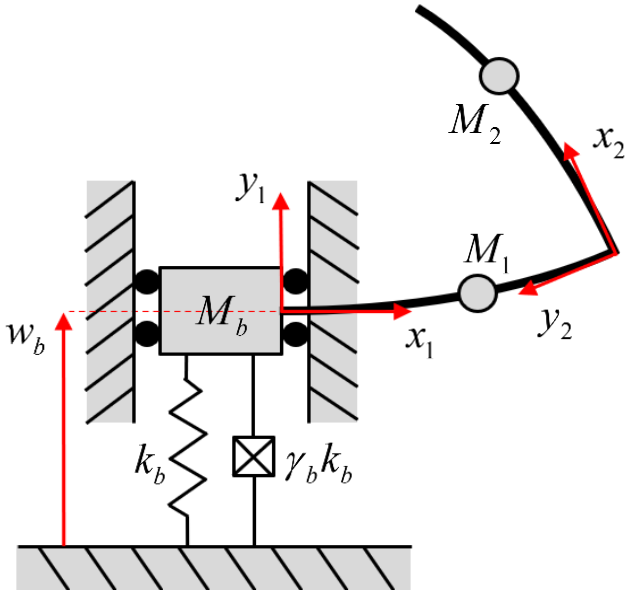

Figure 3.1. Schematic of the L-Shaped Beam Attached to a SDOF System

3.1 Derivation of the Governing Nonlinear PDEs of the System

Using Von Karman displacement field and strain relationship based on Euler-Bernoulli Beam theory [25], the nonlinear strain equation can be written as,

$$\varepsilon_r\left(x_r, z_r\right) = \frac{\partial u_r}{\partial x_r} + \frac{1}{2}\left(\frac{\partial w_r}{\partial x_r}\right)^2 - z_r \frac{\partial^2 w_r}{\partial {x_r}^2}, \tag{3.1}$$

where subscript r stands for beam 1 and 2, u_r and w_r represent the axial and transverse deflection of the r^{th} beam, respectively, and z_r is the out-of-plane coordinate axis of the r^{th} beam. These deflections are functions of both spatial (x_r) and temporal (t) independent variables.

The potential energy of the spring attached to the base mass can be written as,

$$V_b = \frac{1}{2} k_b {w_b}^2 \tag{3.2}$$

where k_b and w_b represent the spring stiffness attached to the base mass and motion of the base mass, respectively. The potential energy of the beams can be written as,

$$V_r = \frac{1}{2}\int_0^{L_r}\int_{A_r} \sigma_r \varepsilon_r \, dA_r \, dx_r , \tag{3.3}$$

where σ_r, A_r and L_r are stress, cross-sectional area, and length of the r^{th} beam, respectively. Using Hooke's law, the relation between stress and strain can be written as,

$$\sigma_r = E_r \varepsilon_r , \tag{3.4}$$

where E_r is the Young's Modulus of the r^{th} beam.

Using Equations (3.1) and (3.4), Equation (3.3) can be rewritten as,

$$V_r = \frac{1}{2}\int_0^{L_r}\int_{A_r} E_r\left(\frac{\partial u_r}{\partial x_r} + \frac{1}{2}\left(\frac{\partial w_r}{\partial x_r}\right)^2 - z_r\frac{\partial^2 w_r}{\partial x_r{}^2}\right)^2 dA_r dx_r \,. \tag{3.5}$$

For symmetric cross-section with respect to an axis normal to the beam plane, integrating Equation (3.5) with respect to the area term, equation becomes,

$$V_r = \frac{E_r}{2}\int_0^{L_r}\left(A_r\left(\frac{\partial u_r}{\partial x_r} + \frac{1}{2}\left(\frac{\partial w_r}{\partial x_r}\right)^2\right)^2 + I_r\left(\frac{\partial^2 w_r}{\partial x_r{}^2}\right)^2\right)dx_r \,. \tag{3.6}$$

Since the equation of the kinetic energy for the total system is too long, it is broken into five equations. Kinetic energy for the base mass is written as,

$$T_b = \frac{1}{2}M_b\dot{w}_b{}^2, \tag{3.7}$$

where M_b represents the mass of the base. For the first beam, kinetic energy is written as,

$$T_1 = \frac{1}{2}\int_0^{L_1}\rho_1 A_1\dot{u}_1{}^2 dx_1 + \frac{1}{2}\int_0^{L_1}\rho_1 A_1\left(\dot{w}_1{}^2 + \dot{w}_b{}^2\right)dx_1 \,, \tag{3.8}$$

where ρ_1 represents the density of the first beam. For the second beam, kinetic energy is written as,

$$\begin{aligned} T_2 = {} & \frac{1}{2}\int_0^{L_2}\rho_2 A_2\left(\dot{u}_2 + \dot{w}_1\big|_{x_1=L_1} + \dot{w}_b\right)^2 dx_2 \\ & + \frac{1}{2}\int_0^{L_2}\rho_2 A_2\left(\dot{w}_2 + x_2\left.\frac{\partial\dot{w}_1}{\partial x_1}\right|_{x_1=L_1} - \dot{u}_1\big|_{x_1=L_1}\right)^2 dx_2 \end{aligned}, \tag{3.9}$$

where ρ_2 represents the density of the second beam. For the concentrated mass on the first beam, kinetic energy is written as,

$$T_3 = \frac{1}{2}\int_0^{L_1} M_1\dot{u}_1{}^2\delta\left(x_1 - L_{M_1}\right)dx_1 + \frac{1}{2}\int_0^{L_1} M_1\left(\dot{w}_1{}^2 + \dot{w}_b{}^2\right)\delta\left(x_1 - L_{M_1}\right)dx_1 \,, \tag{3.10}$$

where M_1 and L_{M_1} represents the mass of the concentrated mass on the first beam and its connection point w.r.t its axis center, respectively. δ is the Dirac delta function. For the concentrated mass on the second beam, kinetic energy is written as,

$$\begin{aligned} T_4 = & \frac{1}{2}\int_0^{L_2} M_2 \left(\dot{u}_2 + \dot{w}_1\big|_{x_1=L_1} + \dot{w}_b\right)^2 \delta\left(x_2 - L_{M_2}\right) dx_2 \\ & + \frac{1}{2}\int_0^{L_2} M_2 \left(\dot{w}_2 + x_2 \left.\frac{\partial \dot{w}_1}{\partial x_1}\right|_{x_1=L_1} - \dot{u}_1\big|_{x_1=L_1} \right)^2 \delta\left(x_2 - L_{M_2}\right) dx_2 \end{aligned}, \tag{3.11}$$

where M_2 and L_{M_2} represents the mass of the concentrated mass on the second beam and its connection point w.r.t its axis center, respectively.

Virtual work done by base excitation can be written as,

$$W_{nc} = F_b w_b, \tag{3.12}$$

where F_b is the force applied to the base mass.

Since, coordinate frames attached to both beams are moving frames, the motion of the base mass is included in the kinetic energy of the both beams, and the motion of the point at the end of the first beam is included in the kinetic energy of the second beam.

Hamilton's principle can be written as follows,

$$\int_{t_1}^{t_2} \left(\delta L + \delta W_{nc}\right) dt = \int_{t_1}^{t_2} \delta T dt - \int_{t_1}^{t_2} \delta V dt + \int_{t_1}^{t_2} \delta W_{nc} dt = 0, \tag{3.13}$$

where

$$V = V_b + V_1 + V_2, \tag{3.14}$$

$$T = T_b + T_1 + T_2 + T_3 + T_4. \tag{3.15}$$

Inserting Equations (3.2) and (3.6) into the Equation (3.13), applying integration by parts (IBP) to the potential energy part of it, and rearranging the terms, the following equations are obtained.

$$\int_{t_1}^{t_2} \delta V_b dt = \int_{t_1}^{t_2} k_b w_b \delta w_b dt \tag{3.16}$$

$$\begin{aligned}\int_{t_1}^{t_2} \delta V_1 dt = \int_{t_1}^{t_2}\int_0^{L_1} & \left(\begin{array}{l} -\frac{\partial}{\partial x_1}\left(E_1 A_1 \left(\frac{\partial u_1}{\partial x_1} + \frac{1}{2}\left(\frac{\partial w_1}{\partial x_1} \right)^2 \right) \right) \delta u_1 \\ + \left(E_1 I_1 \frac{\partial^4 w_1}{\partial x_1^4} - \frac{\partial}{\partial x_1}\left(E_1 A_1 \left(\frac{\partial u_1}{\partial x_1} + \frac{1}{2}\left(\frac{\partial w_1}{\partial x_1} \right)^2 \right) \frac{\partial w_1}{\partial x_1} \right) \right) \delta w_1 \end{array} \right) dx_1 dt \\ + \int_{t_1}^{t_2} & \left(\begin{array}{l} \left(E_1 A_1 \left(\frac{\partial u_1}{\partial x_1} + \frac{1}{2}\left(\frac{\partial w_1}{\partial x_1} \right)^2 \right) \delta u_1 \right)\Big|_0^{L_1} \\ + \left(\left(E_1 A_1 \left(\frac{\partial u_1}{\partial x_1} + \frac{1}{2}\left(\frac{\partial w_1}{\partial x_1} \right)^2 \right) \frac{\partial w_1}{\partial x_1} - \frac{\partial}{\partial x_1}\left(E_1 I_1 \frac{\partial^2 w_1}{\partial x_1^2} \right) \right) \delta w_1 \right)\Big|_0^{L_1} \\ + \left(E_1 I_1 \frac{\partial^2 w_1}{\partial x_1^2} \delta\left(\frac{\partial w_1}{\partial x_1} \right) \right)\Big|_0^{L_1} \end{array} \right) dt \end{aligned} \tag{3.17}$$

.

$$\int_{t_1}^{t_2}\delta V_2 dt=\int_{t_1}^{t_2}\int_0^{L_2}\left(\begin{array}{l}-\dfrac{\partial}{\partial x_2}\left(E_2A_2\left(\dfrac{\partial u_2}{\partial x_2}+\dfrac{1}{2}\left(\dfrac{\partial w_2}{\partial x_2}\right)^2\right)\right)\delta u_2\\ +\left(E_2I_2\dfrac{\partial^4 w_2}{\partial {x_2}^4}-\dfrac{\partial}{\partial x_2}\left(E_2A_2\left(\dfrac{\partial u_2}{\partial x_2}+\dfrac{1}{2}\left(\dfrac{\partial w_2}{\partial x_2}\right)^2\right)\dfrac{\partial w_2}{\partial x_2}\right)\right)\delta w_2\end{array}\right)dx_2dt$$
$$+\int_{t_1}^{t_2}\left(\begin{array}{l}\left(E_2A_2\left(\dfrac{\partial u_2}{\partial x_2}+\dfrac{1}{2}\left(\dfrac{\partial w_2}{\partial x_2}\right)^2\right)\delta u_2\right)\Big|_0^{L_2}\\ +\left(\left(E_2A_2\left(\dfrac{\partial u_2}{\partial x_2}+\dfrac{1}{2}\left(\dfrac{\partial w_2}{\partial x_2}\right)^2\right)\dfrac{\partial w_2}{\partial x_2}-\dfrac{\partial}{\partial x_2}\left(E_2I_2\dfrac{\partial^2 w_2}{\partial {x_2}^2}\right)\right)\delta w_2\right)\Big|_0^{L_2}\\ +\left(E_2I_2\dfrac{\partial^2 w_2}{\partial {x_2}^2}\delta\left(\dfrac{\partial w_2}{\partial x_2}\right)\right)\Big|_0^{L_2}\end{array}\right)dt \quad . \tag{3.18}$$

Inserting Equations (3.7)-(3.11) into the Equation (3.13), applying integration by parts (IBP) to the kinetic energy part of it and assuming u_1, u_2, w_1, w_2 and w_b are prescribed at t_1 and t_2 so that $\delta u_1=0$, $\delta u_2=0$, $\delta w_b=0$, $\delta w_1=0$, $\delta w_2=0$, $\delta u_1(L_1)=0$, $\delta w_1(L_1)=0$, $\delta\left(\left.\dfrac{\partial w_1}{\partial x_1}\right|_{x_1=L_1}\right)=0$ at t_1 and t_2, following equations are obtained.

$$\int_{t_1}^{t_2}\delta T_b dt=-\int_{t_1}^{t_2}\frac{\partial}{\partial t}\left(M_b\frac{\partial w_b}{\partial t}\right)\delta w_b dt\,. \tag{3.19}$$

$$\int_{t_1}^{t_2}\delta T_1 dt = -\int_0^{L_1}\int_{t_1}^{t_2}\begin{pmatrix}\frac{\partial}{\partial t}\left(\rho_1 A_1\left(\frac{\partial w_b}{\partial t}+\frac{\partial w_1}{\partial t}\right)\right)\delta w_b \\ +\frac{\partial}{\partial t}\left(\rho_1 A_1\frac{\partial u_1}{\partial t}\right)\delta u_1 dt \\ +\frac{\partial}{\partial t}\left(\rho_1 A_1\left(\frac{\partial w_b}{\partial t}+\frac{\partial w_1}{\partial t}\right)\right)\delta w_1\end{pmatrix} dt dx_1 . \qquad (3.20)$$

$$\int_{t_1}^{t_2}\delta T_2 dt = -\int_0^{L_2}\int_{t_1}^{t_2}\begin{pmatrix}\frac{\partial}{\partial t}\left(\rho_2 A_2\left(\frac{\partial u_2}{\partial t}+\frac{\partial w_b}{\partial t}+\frac{\partial w_1(L_1)}{\partial t}\right)\right)\delta w_b \\ +\frac{\partial}{\partial t}\left(\rho_2 A_2\left(\frac{\partial u_2}{\partial t}+\frac{\partial w_b}{\partial t}+\frac{\partial w_1(L_1)}{\partial t}\right)\right)\delta u_2 \\ +\frac{\partial}{\partial t}\left(\rho_2 A_2\left(\frac{\partial w_2}{\partial t}+x_2\frac{\partial^2 w_1}{\partial t\partial x_1}\bigg|_{x_1=L_1}-\frac{\partial u_1(L_1)}{\partial t}\right)\right)\delta w_2 \\ -\frac{\partial}{\partial t}\left(\rho_2 A_2\left(\frac{\partial w_2}{\partial t}+x_2\frac{\partial^2 w_1}{\partial t\partial x_1}\bigg|_{x_1=L_1}-\frac{\partial u_1(L_1)}{\partial t}\right)\right)\delta u_1(L_1) \\ +\frac{\partial}{\partial t}\left(\rho_2 A_2\left(\frac{\partial u_2}{\partial t}+\frac{\partial w_b}{\partial t}+\frac{\partial w_1(L_1)}{\partial t}\right)\right)\delta w_1(L_1) \\ +\frac{\partial}{\partial t}\left(\rho_2 A_2\left(\frac{\partial w_2}{\partial t}+x_2\frac{\partial^2 w_1}{\partial t\partial x_1}\bigg|_{x_1=L_1}-\frac{\partial u_1(L_1)}{\partial t}\right)x_2\right)\delta\left(\frac{\partial w_1}{\partial x_1}\bigg|_{x_1=L_1}\right)\end{pmatrix} dt dx_2$$

(3.21)

$$\int_{t_1}^{t_2}\delta T_3 dt = -\int_0^{L_1}\int_{t_1}^{t_2}\begin{pmatrix}\frac{\partial}{\partial t}\left(M_1\delta\left(x_1-L_{M_1}\right)\left(\frac{\partial w_b}{\partial t}+\frac{\partial w_1}{\partial t}\right)\right)\delta w_b \\ +\frac{\partial}{\partial t}\left(M_1\delta\left(x_1-L_{M_1}\right)\frac{\partial u_1}{\partial t}\right)\delta u_1 dt \\ +\frac{\partial}{\partial t}\left(M_1\delta\left(x_1-L_{M_1}\right)\left(\frac{\partial w_b}{\partial t}+\frac{\partial w_1}{\partial t}\right)\right)\delta w_1\end{pmatrix} dx_1 . \qquad (3.22)$$

$$\int_{t_1}^{t_2}\delta T_4 dt = -\int_0^{L_2}\int_{t_1}^{t_2}\left(\begin{array}{l}
\dfrac{\partial}{\partial t}\left(M_2\delta\left(x_2-L_{M_2}\right)\left(\dfrac{\partial u_2}{\partial t}+\dfrac{\partial w_b}{\partial t}+\dfrac{\partial w_1\left(L_1\right)}{\partial t}\right)\right)\delta w_b \\
+\dfrac{\partial}{\partial t}\left(M_2\delta\left(x_2-L_{M_2}\right)\left(\dfrac{\partial u_2}{\partial t}+\dfrac{\partial w_b}{\partial t}+\dfrac{\partial w_1\left(L_1\right)}{\partial t}\right)\right)\delta u_2 \\
+\dfrac{\partial}{\partial t}\left(M_2\delta\left(x_2-L_{M_2}\right)\left(\dfrac{\partial w_2}{\partial t}+x_2\left.\dfrac{\partial^2 w_1}{\partial t\partial x_1}\right|_{x_1=L_1}-\dfrac{\partial u_1\left(L_1\right)}{\partial t}\right)\right)\delta w_2 \\
-\dfrac{\partial}{\partial t}\left(M_2\delta\left(x_2-L_{M_2}\right)\left(\begin{array}{l}\dfrac{\partial w_2}{\partial t}+x_2\left.\dfrac{\partial^2 w_1}{\partial t\partial x_1}\right|_{x_1=L_1} \\ -\dfrac{\partial u_1\left(L_1\right)}{\partial t}\end{array}\right)\right)\delta u_1\left(L_1\right) \\
+\dfrac{\partial}{\partial t}\left(M_2\delta\left(x_2-L_{M_2}\right)\left(\dfrac{\partial u_2}{\partial t}+\dfrac{\partial w_b}{\partial t}+\dfrac{\partial w_1\left(L_1\right)}{\partial t}\right)\right)\delta w_1\left(L_1\right) \\
+\dfrac{\partial}{\partial t}\left(M_2\delta\left(x_2-L_{M_2}\right)\left(\begin{array}{l}\dfrac{\partial w_2}{\partial t}+x_2\left.\dfrac{\partial^2 w_1}{\partial t\partial x_1}\right|_{x_1=L_1} \\ -\dfrac{\partial u_1\left(L_1\right)}{\partial t}\end{array}\right)x_2\right)\delta\left(\left.\dfrac{\partial w_1}{\partial x_1}\right|_{x_1=L_1}\right)
\end{array}\right)dtdx_2 \tag{3.23}$$

The Virtual work part of the Equation (3.13) can be written as,

$$\int_{t_1}^{t_2}\delta W_{nc}dt = \int_{t_1}^{t_2}F_b\delta w_b dt\,, \tag{3.24}$$

Inserting Equations (3.16)-(3.24) into Equation (3.13), simplifying and rearranging it, the following equation could be written as,

$$\int_{t_1}^{t_2}\int_0^{L_1}\left(C_{u_1}\delta u_1 + C_{w_1}\delta w_1\right)dx_1dt + \int_{t_1}^{t_2}\int_0^{L_2}\left(C_{u_2}\delta u_2 + C_{w_2}\delta w_2\right)dx_2dt$$
$$+\int_{t_1}^{t_2}\begin{pmatrix} C_{w_b}\delta w_b + C_{u_1(0)} + C_{u_1(L_1)} + C_{w_1(0)} + C_{w_1(L_1)} + C_{u_2(0)} + C_{u_2(L_2)} \\ +C_{w_2(0)} + C_{w_2(L_2)} + C_{\frac{\partial w_1(0)}{\partial x_1}} + C_{\frac{\partial w_1(L_1)}{\partial x_1}} + C_{\frac{\partial w_2(0)}{\partial x_2}} + C_{\frac{\partial w_2(L_2)}{\partial x_2}} \end{pmatrix}dt = 0 \tag{3.25}$$

The coefficients C_{w_b}, C_{u_1}, C_{w_1}, C_{u_2} and C_{w_2} in the Equation (3.25) will give the five governing nonlinear partial differential equations (PDEs), and the coefficients $C_{u_1(0)}$, $C_{u_1(L_1)}$, $C_{w_1(0)}$, $C_{w_1(L_1)}$, $C_{u_2(0)}$, $C_{u_2(L_2)}$, $C_{w_2(0)}$, $C_{w_2(L_2)}$, $C_{\frac{\partial w_1(0)}{\partial x_1}}$, $C_{\frac{\partial w_1(L_1)}{\partial x_1}}$, $C_{\frac{\partial w_2(0)}{\partial x_2}}$ and $C_{\frac{\partial w_2(L_2)}{\partial x_2}}$ which are the byproducts of the IBP, will give the twelve boundary condition (BC) equations of the system by setting all these coefficients to 0 in order to satisfy the Equation (3.25). The equations for these coefficients are written as,

$$\begin{aligned} C_{w_b} = 0 = &-\int_0^{L_1}\left(\rho_1 A_1 + M_1\delta\left(x_1 - L_{M_1}\right)\right)\left(\ddot{w}_b + \ddot{w}_1\right)dx_1 \\ &-\int_0^{L_1}\left(\rho_2 A_2 + M_2\delta\left(x_2 - L_{M_2}\right)\right)\left(\ddot{w}_b + \ddot{w}_1\left(L_1\right) + \ddot{u}_2\right)dx_2, \\ &-M_b\ddot{w}_b - k_b w_b + F_b \end{aligned} \tag{3.26}$$

$$C_{u_1} = 0 = -\left(\rho_1 A_1 + M_1\delta\left(x_1 - L_{M_1}\right)\right)\ddot{u}_1 + \frac{\partial}{\partial x_1}\left(E_1 A_1\left(\frac{\partial u_1}{\partial x_1} + \frac{1}{2}\left(\frac{\partial w_1}{\partial x_1}\right)^2\right)\right), \tag{3.27}$$

$$\begin{aligned} C_{w_1} = 0 = &-\left(\rho_1 A_1 + M_1\delta\left(x_1 - L_{M_1}\right)\right)\left(\ddot{w}_1 + \ddot{w}_b\right) - E_1 I_1\frac{\partial^4 w_1}{\partial {x_1}^4} \\ &+\frac{\partial}{\partial x_1}\left(E_1 A_1\left(\frac{\partial u_1}{\partial x_1} + \frac{1}{2}\left(\frac{\partial w_1}{\partial x_1}\right)^2\right)\frac{\partial w_1}{\partial x_1}\right) \end{aligned}, \tag{3.28}$$

$$\begin{aligned} C_{u_2} = 0 = &-\left(\rho_2 A_2 + M_2\delta\left(x_2 - L_{M_2}\right)\right)\left(\ddot{u}_2 + \ddot{w}_1\left(L_1\right) + \ddot{w}_b\right) \\ &+\frac{\partial}{\partial x_2}\left(E_2 A_2\left(\frac{\partial u_2}{\partial x_2} + \frac{1}{2}\left(\frac{\partial w_2}{\partial x_2}\right)^2\right)\right) \end{aligned}, \tag{3.29}$$

$$C_{w_2} = 0 = -\left(\rho_2 A_2 + M_2 \delta\left(x_2 - L_{M_2}\right)\right)\left(\ddot{w}_2 + x_2 \frac{\partial \ddot{w}_1\left(L_1\right)}{\partial x_1} - \ddot{u}_1\left(L_1\right)\right) \\ -E_2 I_2 \frac{\partial^4 w_2}{\partial {x_2}^4} + \frac{\partial}{\partial x_2}\left(E_2 A_2\left(\frac{\partial u_2}{\partial x_2} + \frac{1}{2}\left(\frac{\partial w_2}{\partial x_2}\right)^2\right)\frac{\partial w_2}{\partial x_2}\right) \quad , \qquad (3.30)$$

$$C_{u_1(0)} = 0 = \left(E_1 A_1\left(\left.\frac{\partial u_1}{\partial x_1}\right|_{x_1=0} + \frac{1}{2}\left(\left.\frac{\partial w_1}{\partial x_1}\right|_{x_1=0}\right)^2\right)\right)\delta u_1\left(0\right), \qquad (3.31)$$

$$C_{u_1(L_1)} = 0 = \left(\begin{array}{l} -E_1 A_1\left(\left.\frac{\partial u_1}{\partial x_1}\right|_{x_1=L_1} + \frac{1}{2}\left(\left.\frac{\partial w_1}{\partial x_1}\right|_{x_1=L_1}\right)^2\right) \\ +\int_0^{L_2}\left(\begin{array}{l}\left(\rho_2 A_2 + M_2 \delta\left(x_2 - L_{M_2}\right)\right) \\ \left(\ddot{w}_2 + x_2 \left.\frac{\partial \ddot{w}_1}{\partial x_1}\right|_{x_1=L_1} - \ddot{u}_1\left(L_1\right)\right)\end{array}\right)dx_2 \end{array}\right)\delta u_1\left(L_1\right), \qquad (3.32)$$

$$C_{w_1(0)} = 0 = \left(\begin{array}{l} E_1 A_1\left(\left.\frac{\partial u_1}{\partial x_1}\right|_{x_1=0} + \frac{1}{2}\left(\left.\frac{\partial w_1}{\partial x_1}\right|_{x_1=0}\right)^2\right)\left.\frac{\partial w_1}{\partial x_1}\right|_{x_1=0} \\ -\left(\frac{\partial}{\partial x_1}\left(E_1 I_1 \frac{\partial^2 w_1}{\partial {x_1}^2}\right)\right)\Bigg|_{x_1=0} \end{array}\right)\delta w_1\left(0\right), \qquad (3.33)$$

$$C_{w_1(L_1)} = 0 = \left(\begin{array}{l} -E_1 A_1\left(\left.\frac{\partial u_1}{\partial x_1}\right|_{x_1=L_1} + \frac{1}{2}\left(\left.\frac{\partial w_1}{\partial x_1}\right|_{x_1=L_1}\right)^2\right)\left.\frac{\partial w_1}{\partial x_1}\right|_{x_1=L_1} \\ +\left(\frac{\partial}{\partial x_1}\left(E_1 I_1 \frac{\partial^2 w_1}{\partial {x_1}^2}\right)\right)\Bigg|_{x_1=L_1} \\ -\int_0^{L_2}\left(\begin{array}{l}\left(\rho_2 A_2 + M_2 \delta\left(x_2 - L_{M_2}\right)\right) \\ \left(\ddot{u}_2 + \ddot{w}_1\left(L_1\right) + \ddot{w}_b\right)\end{array}\right)dx_2 \end{array}\right)\delta w_1\left(L_1\right), \qquad (3.34)$$

$$C_{u_2(0)} = 0 = \left(E_2 A_2 \left(\left. \frac{\partial u_2}{\partial x_2} \right|_{x_2=0} + \frac{1}{2} \left(\left. \frac{\partial w_2}{\partial x_2} \right|_{x_2=0} \right)^2 \right) \right) \delta u_2(0), \tag{3.35}$$

$$C_{u_2(L_2)} = 0 = -\left(E_2 A_2 \left(\left. \frac{\partial u_2}{\partial x_2} \right|_{x_2=L_2} + \frac{1}{2} \left(\left. \frac{\partial w_2}{\partial x_2} \right|_{x_2=L_2} \right)^2 \right) \right) \delta u_2(L_2), \tag{3.36}$$

$$C_{w_2(0)} = 0 = \begin{pmatrix} E_2 A_2 \left(\left. \frac{\partial u_2}{\partial x_2} \right|_{x_2=0} + \frac{1}{2} \left(\left. \frac{\partial w_2}{\partial x_2} \right|_{x_2=0} \right)^2 \right) \left. \frac{\partial w_2}{\partial x_2} \right|_{x_2=0} \\ -\left(\frac{\partial}{\partial x_2} \left(E_2 I_2 \frac{\partial^2 w_2}{\partial {x_2}^2} \right) \right) \Bigg|_{x_2=0} \end{pmatrix} \delta w_2(0), \tag{3.37}$$

$$C_{w_2(L_2)} = 0 = -\begin{pmatrix} E_2 A_2 \left(\left. \frac{\partial u_2}{\partial x_2} \right|_{L_2} + \frac{1}{2} \left(\left. \frac{\partial w_2}{\partial x_2} \right|_{L_2} \right)^2 \right) \left. \frac{\partial w_2}{\partial x_2} \right|_{L_2} \\ -\left(\frac{\partial}{\partial x_2} \left(E_2 I_2 \frac{\partial^2 w_2}{\partial {x_2}^2} \right) \right) \Bigg|_{x_2=L_2} \end{pmatrix} \delta w_2(L_2), \tag{3.38}$$

$$C_{\frac{\partial w_1(0)}{\partial x_1}} = 0 = E_1 I_1 \left. \frac{\partial^2 w_1}{\partial {x_1}^2} \right|_{x_1=0} \delta \left. \frac{\partial w_1}{\partial x_1} \right|_{x_1=0}, \tag{3.39}$$

$$C_{\frac{\partial w_1(L_1)}{\partial x_1}} = 0 = \begin{pmatrix} -E_1 I_1 \left. \frac{\partial^2 w_1}{\partial {x_1}^2} \right|_{x_1=L_1} \\ -\int_0^{L_2} \left(\begin{pmatrix} \left(\rho_2 A_2 + M_2 \delta\left(x_2 - L_{M_2} \right) \right) \\ \left(\ddot{w}_2 + x_2 \left. \frac{\partial \ddot{w}_1}{\partial x_1} \right|_{x_1=L_1} - \ddot{u}_1(L_1) \right) x_2 dx_2 \end{pmatrix} \right) \end{pmatrix} \delta \left. \frac{\partial w_1}{\partial x_1} \right|_{x_1=L_1}, \tag{3.40}$$

$$C_{\frac{\partial w_2(0)}{\partial x_2}} = 0 = E_2 I_2 \left. \frac{\partial^2 w_2}{\partial {x_2}^2} \right|_{x_2=0} \delta \left. \frac{\partial w_2}{\partial x_2} \right|_{x_2=0}, \tag{3.41}$$

$$C_{\frac{\partial w_2(L_2)}{\partial x_2}} = 0 = -E_2 I_2 \left.\frac{\partial^2 w_2}{\partial {x_2}^2}\right|_{x_2=L_2} \delta \left.\frac{\partial w_2}{\partial x_2}\right|_{x_2=L_2} . \quad (3.42)$$

Since the kinetic energy of the transverse motion is more dominant than the axial one, accelerations due to the axial motion of the beams are neglected, i.e., $\ddot{u}_i = 0$ in Equations (3.26)-(3.42). Then, Equations (3.27) and (3.29) can be rewritten respectively as,

$$\frac{\partial}{\partial x_1}\left(E_1 A_1 \left(\frac{\partial u_1}{\partial x_1} + \frac{1}{2}\left(\frac{\partial w_1}{\partial x_1} \right)^2 \right) \right) = 0 , \quad (3.43)$$

$$\frac{\partial}{\partial x_2}\left(E_2 A_2 \left(\frac{\partial u_2}{\partial x_2} + \frac{1}{2}\left(\frac{\partial w_2}{\partial x_2} \right)^2 \right) \right) = \left(\rho_2 A_2 + M_2 \delta\left(x_2 - L_{M_2} \right) \right)\left(\ddot{w}_1(L_1) + \ddot{w}_b \right) . \quad (3.44)$$

Integrating Equations (3.43) and (3.44) along their respective lengths and simplifying them, the following equations are obtained as,

$$E_1 A_1 \left(\frac{\partial u_1}{\partial x_1} + \frac{1}{2}\left(\frac{\partial w_1}{\partial x_1} \right)^2 \right) = \frac{E_1 A_1}{2L_1} \int_0^{L_1} \left(\frac{\partial w_1}{\partial x_1} \right)^2 dx_1 , \quad (3.45)$$

$$E_2 A_2 \left(\frac{\partial u_2}{\partial x_2} + \frac{1}{2}\left(\frac{\partial w_2}{\partial x_2} \right)^2 \right) = \begin{pmatrix} \rho_2 A_2 x_2 + M_2 U\left(x_2 - L_{M_2} \right) \\ -\frac{\rho_2 A_2 L_2}{2} - M_2 \frac{L_2 - L_{M_2}}{L_2} \end{pmatrix} \left(\ddot{w}_1(L_1) + \ddot{w}_b \right) + \frac{E_2 A_2}{2L_2} \int_0^{L_2} \left(\frac{\partial w_2}{\partial x_2} \right)^2 dx_2 , \quad (3.46)$$

where U represents the Heaviside step function. By disregarding the acceleration due to axial motion of the beams, Equation (3.26) becomes,

$$\begin{aligned} &-\int_0^{L_1} \left(\rho_1 A_1 + M_1 \delta\left(x_1 - L_{M_1} \right) \right)\left(\ddot{w}_b + \ddot{w}_1 \right) dx_1 \\ &-\int_0^{L_2} \left(\rho_2 A_2 + M_2 \delta\left(x_2 - L_{M_2} \right) \right)\left(\ddot{w}_b + \ddot{w}_1(L_1) \right) dx_2 . \\ &-M_b \ddot{w}_b - k_b w_b = 0 \end{aligned} \quad (3.47)$$

Substituting Equations (3.43) and (3.45) into the modified Equation (3.28) where accelerations due to axial motion of the beams are disregarded, it becomes,

$$\begin{aligned} &-\left(\rho_1 A_1 + M_1 \delta\left(x_1 - L_{M_1}\right)\right)\left(\ddot{w}_1 + \ddot{w}_b\right) - E_1 I_1 \frac{\partial^4 w_1}{\partial {x_1}^4} \\ &+ \frac{E_1 A_1}{2L_1} \int_0^{L_1} \left(\frac{\partial w_1}{\partial x_1}\right)^2 dx_1 \frac{\partial^2 w_1}{\partial {x_1}^2} = 0 \end{aligned} \quad . \tag{3.48}$$

Substituting Equations (3.44) and (3.46) into the modified Equation (3.30) where accelerations due to axial motion of the beams are disregarded and rearranging it, it becomes,

$$\begin{aligned} &-\left(\rho_2 A_2 + M_2 \delta\left(x_2 - L_{M_2}\right)\right)\left(\ddot{w}_2 + x_2 \left.\frac{\partial \ddot{w}_1}{\partial x_1}\right|_{x_1 = L_1} - \left(\ddot{w}_1\left(L_1\right) + w_b\right)\frac{\partial w_2}{\partial x_2}\right) \\ &-E_2 I_2 \frac{\partial^4 w_2}{\partial {x_2}^4} + \begin{pmatrix} \rho_2 A_2 x_2 + M_2 U\left(x_2 - L_{M_2}\right) \\ -\frac{\rho_2 A_2 L_2}{2} - M_2 \frac{L_2 - L_{M_2}}{L_2} \end{pmatrix}\left(\ddot{w}_1\left(L_1\right) + \ddot{w}_b\right)\frac{\partial^2 w_2}{\partial {x_2}^2} \\ &+ \frac{E_2 A_2}{2L_2} \int_0^{L_2} \left(\frac{\partial w_2}{\partial x_2}\right)^2 dx_2 \frac{\partial^2 w_2}{\partial {x_2}^2} = 0 \end{aligned} \tag{3.49}$$

Using Equations (3.45), (3.46) and modified boundary condition Equations (3.31)-(3.42) where accelerations due to axial motion of the beams are disregarded, BCs are obtained as,

$$w_1(0) = 0\,, \tag{3.50}$$

$$\frac{\partial w_1(0)}{\partial x_1} = 0\,, \tag{3.51}$$

$$\begin{aligned} &\frac{E_1 A_1}{2L_1}\left(\int_0^{L_1}\left(\frac{\partial w_1}{\partial x_1}\right)^2 dx_1\right)\left.\frac{\partial w_1}{\partial x_1}\right|_{x_1 = L_1} - E_1 I_1 \left.\frac{\partial^3 w_1}{\partial {x_1}^3}\right|_{x_1 = L_1} \\ &+ \int_0^{L_2}\left(\rho_2 A_2 + M_2 \delta\left(x_2 - L_{M_2}\right)\right) dx_2 \left(\ddot{w}_1\left(L_1\right) + \ddot{w}_b\right) = 0 \end{aligned} \quad , \tag{3.52}$$

$$\int_0^{L_2}\left(\rho_2 A_2 + M_2\delta\left(x_2 - L_{M_2}\right)\right)\left(\ddot{w}_2 + x_2\left.\frac{\partial\ddot{w}_1}{\partial x_1}\right|_{x_1=L_1}\right)x_2 dx_2 + E_1 I_1\left.\frac{\partial^2 w_1}{\partial x_1^{\,2}}\right|_{x_1=L_1} = 0\,, \quad (3.53)$$

$$w_2\left(0\right) = 0\,, \quad (3.54)$$

$$\frac{\partial w_2\left(0\right)}{\partial x_2} = 0\,, \quad (3.55)$$

$$\begin{aligned}&\left(\frac{\rho_2 A_2 L_2}{2} + \frac{M_2 L_{M_2}}{L_2}\right)\left(\ddot{w}_1\left(L_1\right) + \ddot{w}_b\right) - E_2 I_2\left.\frac{\partial^3 w_2}{\partial x_2^{\,3}}\right|_{x_2=L_2} \\ &+ \frac{E_2 A_2}{2L_2}\left(\int_0^{L_2}\left(\frac{\partial w_2}{\partial x_2}\right)^2 dx_2\right)\left.\frac{\partial w_2}{\partial x_2}\right|_{x_2=L_2} = 0\end{aligned}\,, \quad (3.56)$$

$$E_2 I_2\left.\frac{\partial^2 w_2}{\partial x_2^{\,2}}\right|_{x_2=L_2} = 0\,. \quad (3.57)$$

3.2 Discretization of the Nonlinear PDEs Using Galerkin's Method

3.2.1 Galerkin's Method

Galerkin's method is a variational method used to discretize PDEs into ordinary differential equations (ODEs). This method turns PDEs into residual forms, then multiply with weight functions and integrate over their respective domain. These weight functions need to be selected such that they satisfy all geometric BCs; however, they don't have to satisfy natural BCs. Assuming a residual form represented as $r\left(x,t\right)$, the mathematical representation of the above equation is

$$\int_D w(x)\, r\left(x,t\right) dx = 0 \quad , (3.58)$$

where $w(x)$ represents the weight function and D represent the domain of the equation. Applying IBP to Equation (3.58), this equation is transformed into its weak form. This form has two advantages, which are:

- The dependent variables are required to be p times differentiable in weak form, whereas they needed to be 2p times differentiable before.
- BCs can be relaxed by implementing natural BCs into the weak form using the byproducts of IBP.

Then, using the weight functions as trial functions for the dependent variable, the weak form is transformed into ODE.

3.2.2 Discretization of the Nonlinear PDEs into ODEs

Assuming an approximate solution for the transverse motion of the beams as,

$$w_{r,n}(x_r,t)=\sum_{i=1}^{n_r}\left(\phi_{r,i}(x_r)q_{r,i}(t)\right), \tag{3.59}$$

where $\phi_{r,i}(x)$ is a trial function, $q_{r,i}(t)$ is generalized coordinate, and n_r is the number of admissible functions used for r^{th} beam. The following admissible functions are considered as trial functions since they satisfy all geometric BCs and are differentiable at least two times.

$$\phi_{r,i}(x_r)=\left(\frac{x_r}{L_r}\right)^{i+1}. \tag{3.60}$$

Equation (3.60) is also a weight function since trial functions are the weight functions in Galerkin's Method.

Since w_b is a function of only time, the relationship between w_b and generalized coordinate of it can be written as,

$$w_b(t)=q_b(t). \tag{3.61}$$

Substituting Equations (3.59) and (3.61) into Equation (3.47), it can be written as,

$$\begin{aligned}
&-\int_0^{L_1}\left(\rho_1 A_1+M_1\delta\left(x_1-L_{M_1}\right)\right)\left(\ddot{q}_b+\sum_{i=1}^{n_1}\left(\phi_{1,i}\ddot{q}_{1,i}\right)\right)dx_1\\
&-\int_0^{L_2}\left(\rho_2 A_2+M_2\delta\left(x_2-L_{M_2}\right)\right)\left(\ddot{q}_b+\sum_{i=1}^{n_1}\left(\phi_{1,i}\left(L_1\right)\ddot{q}_{1,i}\right)\right)dx_2 .\\
&-M_b\ddot{q}_b-k_b q_b+F_b=0
\end{aligned} \tag{3.62}$$

Substituting Equation (3.60) into Equation (3.62) and solving the integrals, it can be transformed into a nonlinear ODE as,

$$\begin{aligned}
&-\ddot{q}_b\left(\rho_1 A_1 L_1+M_1+\rho_2 A_2 L_2+M_2+M_b\right)\\
&-\sum_{i=1}^{n_1}\left(\ddot{q}_{1,i}\left(\rho_1 A_1 L_1\frac{1}{i+2}\right)+M_1\left(\frac{L_{M_1}}{L_1}\right)^{i+1}+\rho_2 A_2 L_2+M_2\right)-k_b q_b=0
\end{aligned} . \tag{3.63}$$

Applying Galerkin's method to Equation (3.48) by multiplying it with Equation (3.60), applying IBP, integrating it along its respective beam length, and substituting Equations (3.59) and (3.61) into it, it can be written as,

$$\begin{aligned}
&\int_0^{L_1}\phi_{1,i}\left(\begin{array}{l}
-\left(\rho_1 A_1+M_1\delta\left(x_1-L_{M_1}\right)\right)\left(\ddot{q}_b+\sum_{i=1}^{n_1}\left(\phi_{1,i}\ddot{q}_{1,i}\right)\right)\\
-\sum_{i=1}^{n_1}\left(\frac{\partial^2\phi_{1,i}}{\partial x_1^{\,2}}q_{1,i}\right)E_1I_1\sum_{i=1}^{n_1}\left(\frac{\partial^2\phi_{1,i}}{\partial x_1^{\,2}}q_{1,i}\right)\\
+\frac{E_1A_1}{2L_1}\int_0^{L_1}\left(\sum_{i=1}^{n_1}\left(\frac{\partial\phi_{1,i}}{\partial x_1}q_{1,i}\right)\right)^2dx_1\sum_{i=1}^{n_1}\left(\frac{\partial^2\phi_{1,i}}{\partial x_1^{\,2}}q_{1,i}\right)
\end{array}\right)dx_1\\
&-\phi_{1,i}\left(L_1\right)E_1I_1\sum_{i=1}^{n_1}\left(\left.\frac{\partial^3\phi_{1,i}}{\partial x_1^{\,3}}\right|_{x_1=L_1}q_{1,i}\right)+\phi_{1,i}\left(0\right)E_1I_1\sum_{i=1}^{n_1}\left(\left.\frac{\partial^3\phi_{1,i}}{\partial x_1^{\,3}}\right|_{x_1=0}q_{1,i}\right)\\
&+\left.\frac{\partial\phi_{1,i}}{\partial x_1}\right|_{x_1=L_1}E_1I_1\sum_{i=1}^{n_1}\left(\left.\frac{\partial^2\phi_{1,i}}{\partial x_1^{\,2}}\right|_{x_1=L_1}q_{1,i}\right)-\left.\frac{\partial\phi_{1,i}}{\partial x_1}\right|_{x_1=0}E_1I_1\sum_{i=1}^{n_1}\left(\left.\frac{\partial^2\phi_{1,i}}{\partial x_1^{\,2}}\right|_{x_1=0}q_{1,i}\right)=0
\end{aligned} . \tag{3.64}$$

Applying relaxation of BCs by substituting BC Equations (3.50)-(3.53) into Equation (3.64), solving the integrals, and simplifying the equation further, the following equation is obtained as,

$$
\begin{aligned}
&-\ddot{w}_b\left(\rho_1 A_1 L_1\frac{1}{i+2}+M_1\left(\frac{L_{M_1}}{L_1}\right)^{i+1}+\rho_2 A_2 L_2+M_2\right)\\
&-\sum_{j=1}^{n_1}\left(\ddot{q}_{1,j}\left(\begin{array}{l}\rho_1 A_1 L_1\dfrac{1}{i+j+3}+M_1\left(\dfrac{L_{M_1}}{L_1}\right)^{i+j+2}+\rho_2 A_2 L_2+M_2\\ +(i+1)(j+1)\left(\dfrac{L_2}{L_1}\right)^2\left(\dfrac{\rho_2 A_2 L_2}{3}+M_2\left(\dfrac{L_{M_2}}{L_2}\right)^2\right)\end{array}\right)\right)\\
&-\sum_{j=1}^{n_2}\left(\ddot{q}_{2,j}(i+1)\frac{L_2}{L_1}\left(\rho_2 A_2 L_2\frac{1}{j+3}+M_2\left(\frac{L_{M_2}}{L_2}\right)^{j+2}\right)\right) \qquad \text{.(3.65)}\\
&-\sum_{j=1}^{n_1}\left(q_{1,j}\frac{E_1 I_1}{L_1^{\,3}}\frac{(i+1)i(j+1)j}{i+j-1}\right)\\
&-\sum_{j=1}^{n_1}\sum_{k=1}^{n_1}\sum_{l=1}^{n_1}\left(q_{1,j}q_{1,k}q_{1,l}\frac{E_1 A_1}{2L_1^{\,3}}\frac{(i+1)(j+1)(k+1)(l+1)}{(i+l+1)(j+k+1)}\right)=0
\end{aligned}
$$

Applying Galerkin's method to Equation (3.49) by multiplying it with Equation (3.60), applying IBP, integrating it along its respective beam length, and substituting Equations (3.59) and (3.61) into it, it can be written as,

$$\int_0^{L_2}\phi_{2,i}\left(\begin{array}{l}
-\begin{pmatrix}\rho_2 A_2\\ +M_2\delta\left(x_2-L_{M_2}\right)\end{pmatrix}\left(\begin{array}{l}\sum_{i=1}^{n_2}\left(\phi_{2,i}\ddot{q}_{2,i}\right)+x_2\sum_{i=1}^{n_1}\left(\left.\frac{\partial\phi_{1,i}}{\partial x_1}\right|_{x_1=L_1}\ddot{q}_{1,i}\right)\\ -\left(\sum_{i=1}^{n_1}\left(\phi_{1,i}\left(L_1\right)\ddot{q}_{1,i}\right)+w_b\right)\sum_{i=1}^{n_2}\left(\frac{\partial\phi_{2,i}}{\partial x_2}q_{2,i}\right)\end{array}\right)\\
-E_2I_2\sum_{i=1}^{n_2}\left(\frac{\partial^4\phi_{2,i}}{\partial {x_2}^4}q_{2,i}\right)\\
+\begin{pmatrix}\rho_2A_2x_2+M_2U\left(x_2-L_{M_2}\right)\\ -\frac{\rho_2A_2L_2}{2}-M_2\frac{L_2-L_{M_2}}{L_2}\end{pmatrix}\left(\ddot{w}_1\left(L_1\right)+\ddot{w}_b\right)\sum_{i=1}^{n_2}\left(\frac{\partial^2\phi_{2,i}}{\partial {x_2}^2}q_{2,i}\right)\\
+\frac{E_2A_2}{2L_2}\int_0^{L_2}\left(\sum_{i=1}^{n_2}\left(\frac{\partial\phi_{2,i}}{\partial x_2}q_{2,i}\right)\right)^2dx_2\sum_{i=1}^{n_2}\left(\frac{\partial^2\phi_{2,i}}{\partial {x_2}^2}q_{2,i}\right)
\end{array}\right)dx_2$$

$$-\phi_{2,i}\left(L_2\right)E_2I_2\sum_{i=1}^{n_2}\left(\left.\frac{\partial^3\phi_{2,i}}{\partial {x_2}^3}\right|_{x_2=L_2}q_{2,i}\right)+\phi_{2,i}\left(0\right)E_2I_2\sum_{i=1}^{n_2}\left(\left.\frac{\partial^3\phi_{2,i}}{\partial {x_2}^3}\right|_{x_2=0}q_{2,i}\right)$$

$$+\left.\frac{\partial\phi_{2,i}}{\partial x_2}\right|_{x_2=L_2}E_2I_2\sum_{i=1}^{n_2}\left(\left.\frac{\partial^2\phi_{2,i}}{\partial {x_2}^2}\right|_{x_2=L_2}q_{2,i}\right)-\left.\frac{\partial\phi_{2,i}}{\partial x_2}\right|_{x_2=0}E_2I_2\sum_{i=1}^{n_2}\left(\left.\frac{\partial^2\phi_{2,i}}{\partial {x_2}^2}\right|_{x_2=0}q_{2,i}\right)=0 \quad (3.66)$$

Applying relaxation of BCs by substituting BC Equations (3.54)-(3.57) into Equation (3.66), solving the integrals, and simplifying the equation further, the following equation is obtained as,

$$
\begin{aligned}
&-\sum_{j=1}^{n_2}\left(\ddot{q}_{2,j}\left(\rho_2 A_2 L_2\frac{1}{i+j+3}+M_2\left(\frac{L_{M_2}}{L_2}\right)^{i+j+2}\right)\right)\\
&-\sum_{j=1}^{n_1}\left(\ddot{q}_{1,j}\,(j+1)\frac{L_2}{L_1}\left(\rho_2 A_2 L_2\frac{1}{i+3}+M_2\left(\frac{L_{M_2}}{L_2}\right)^{i+2}\right)\right)\\
&-\sum_{j=1}^{n_2}\left(q_{2,j}\frac{E_2 I_2}{{L_2}^3}\frac{(i+1)i(j+1)j}{i+j-1}\right)\\
&-\ddot{w}_b\sum_{j=1}^{n_2}\left(q_{2,j}\frac{E_2 A_2}{2{L_2}^3}\frac{(i+1)(j+1)}{(i+j+1)}\frac{1}{L_2}\left(\begin{array}{l}\rho_2 A_2 L_2\dfrac{(i+j)}{2(i+j+2)}\\ +M_2\dfrac{L_{M_2}}{L_2}\left(1-\left(\dfrac{L_{M_2}}{L_2}\right)^{i+j}\right)\end{array}\right)\right)\\
&-\sum_{j=1}^{n_2}\sum_{k=1}^{n_1}\left(q_{2,j}\ddot{q}_{1,k}\frac{E_2 A_2}{2{L_2}^3}\frac{(i+1)(j+1)}{(i+j+1)}\frac{1}{L_2}\left(\begin{array}{l}\rho_2 A_2 L_2\dfrac{(i+j)}{2(i+j+2)}\\ +M_2\dfrac{L_{M_2}}{L_2}\left(1-\left(\dfrac{L_{M_2}}{L_2}\right)^{i+j}\right)\end{array}\right)\right)\\
&-\sum_{j=1}^{n_2}\sum_{k=1}^{n_2}\sum_{l=1}^{n_2}\left(q_{2,j}q_{2,k}q_{2,l}\frac{E_2 A_2}{2{L_2}^3}\frac{(i+1)(j+1)(k+1)(l+1)}{(i+l+1)(j+k+1)}\right)=0
\end{aligned}
\qquad (3.67)
$$

3.3 Representation of Nonlinear ODEs in Matrix Form

After obtaining governing nonlinear ODEs, these obtained Equations (3.63), (3.65), (3.67) are transformed into matrix form. In addition, structural damping is introduced to add damping to the system. The mass matrix $\mathbf{M}$ can be written as,

$$
\mathbf{M}=\left[\begin{array}{c|ccc|ccc}
Mbb & M1b_1 & \cdots & M1b_{n_1} & 0 & \cdots & 0\\
\hline
Mb1_1 & M11_{1,1} & \cdots & M11_{1,n_1} & M12_{1,1} & \cdots & M12_{1,n_2}\\
\vdots & \vdots & \ddots & \vdots & \vdots & \ddots & \vdots\\
Mb1_{n_1} & M11_{n_1,1} & \cdots & M11_{n_1,n_1} & M12_{n_1,1} & \cdots & M12_{n_1,n_2}\\
\hline
0 & M21_{1,1} & \cdots & M21_{1,n_1} & M22_{1,1} & \cdots & M22_{1,n_2}\\
\vdots & \vdots & \ddots & \vdots & \vdots & \ddots & \vdots\\
0 & M21_{n_2,1} & \cdots & M21_{n_2,n_1} & M22_{n_2,1} & \cdots & M22_{n_2,n_2}
\end{array}\right], \qquad (3.68)
$$

where,

$$Mbb = M_b + \rho_1 A_1 L_1 + M_1 + \rho_2 A_2 L_2 + M_2, \tag{3.69}$$

$$M1b_i = \rho_1 A_1 L_1 \frac{1}{i+2} + M_1 \left(\frac{L_{M_1}}{L_1} \right)^{i+1} + \rho_2 A_2 L_2 + M_2, \tag{3.70}$$

$$Mb1_i = \rho_1 A_1 L_1 \frac{1}{i+2} + M_1 \left(\frac{L_{M_1}}{L_1} \right)^{i+1} + \rho_2 A_2 L_2 + M_2, \tag{3.71}$$

$$\begin{aligned} M11_{i,j} = {} & \rho_1 A_1 L_1 \frac{1}{i+j+3} + M_1 \left(\frac{L_{M_1}}{L_1} \right)^{i+j+2} + \rho_2 A_2 L_2 + M_2 \\ & + (i+1)(j+1) \left(\frac{L_2}{L_1} \right)^2 \left(\frac{\rho_2 A_2 L_2}{3} + M_2 \left(\frac{L_{M_2}}{L_2} \right)^2 \right) \end{aligned}, \tag{3.72}$$

$$M22_{i,j} = \rho_2 A_2 L_2 \frac{1}{i+j+3} + M_2 \left(\frac{L_{M_2}}{L_2} \right)^{i+j+2}, \tag{3.73}$$

$$M12_{i,j} = (i+1) \frac{L_2}{L_1} \left(\rho_2 A_2 L_2 \frac{1}{j+3} + M_2 \left(\frac{L_{M_2}}{L_2} \right)^{j+2} \right), \tag{3.74}$$

$$M21_{i,j} = (j+1) \frac{L_2}{L_1} \left(\rho_2 A_2 L_2 \frac{1}{i+3} + M_2 \left(\frac{L_{M_2}}{L_2} \right)^{i+2} \right). \tag{3.75}$$

The stiffness matrix $\mathbf{K}$ can be written as,

$$\mathbf{K} = \begin{bmatrix} k_b & & \\ & \begin{matrix} K_{11_{1,1}} & \cdots & K_{11_{1,n_1}} \\ \vdots & \ddots & \vdots \\ K_{11_{n_1,1}} & \cdots & K_{11_{n_1,n_1}} \end{matrix} & \\ & & \begin{matrix} K_{22_{1,1}} & \cdots & K_{22_{1,n_2}} \\ \vdots & \ddots & \vdots \\ K_{22_{n_2,1}} & \cdots & K_{22_{n_2,n_2}} \end{matrix} \end{bmatrix}, \tag{3.76}$$

where,

$$K11_{i,j} = \frac{E_1 I_1}{L_1^{\,3}} \frac{(i+1)i(j+1)j}{i+j-1}, \tag{3.77}$$

$$K22_{i,j} = \frac{E_2 I_2}{L_2^{\,3}} \frac{(i+1)i(j+1)j}{i+j-1}. \tag{3.78}$$

The structural damping matrix $\mathbf{H}$ can be written as,

$$\mathbf{H} = \left[\begin{array}{c|ccc|ccc} \gamma_b k_b & & & & & & \\ \hline & \gamma_1 K_{11_{1,1}} & \cdots & \gamma_1 K_{11_{1,n_1}} & & & \\ & \vdots & \ddots & \vdots & & & \\ & \gamma_1 K_{11_{n_1,1}} & \cdots & \gamma_1 K_{11_{n_1,n_1}} & & & \\ \hline & & & & \gamma_2 K_{22_{1,1}} & \cdots & \gamma_2 K_{22_{1,n_2}} \\ & & & & \vdots & \ddots & \vdots \\ & & & & \gamma_2 K_{22_{n_2,1}} & \cdots & \gamma_2 K_{22_{n_2,n_2}} \end{array}\right], \tag{3.79}$$

where γ_b represents the structural damping coefficient of the spring attached to the base mass, γ_1 and γ_2 represent the structural damping coefficients of the first and second beams, respectively.

The generalized coordinate vector $\mathbf{q}$ can be written as,

$$\mathbf{q} = \left[\begin{array}{c|ccc|ccc} q_b & q_{1,1} & \cdots & q_{1,n_1} & q_{2,1} & \cdots & q_{2,n_2} \end{array}\right]^T. \tag{3.80}$$

Nonlinear forcing vector $\mathbf{f}_N$ can be written as,

$$\mathbf{f}_N = \left[\begin{array}{c|ccc|ccc} 0 & f_{N1_1} & \cdots & f_{N1_{n_1}} & f_{N2_1} & \cdots & f_{N2_{n_2}} \end{array}\right]^T, \tag{3.81}$$

where,

$$f_{N1_i} = \sum_{j=1}^{n_1}\sum_{k=1}^{n_1}\sum_{l=1}^{n_1}\left(q_{1,j} q_{1,k} q_{1,l} \frac{E_1 A_1}{2L_1^{\,3}} \frac{(i+1)(j+1)(k+1)(l+1)}{(i+l+1)(j+k+1)} \right), \tag{3.82}$$

$$f_{N2_i} = \ddot{q}_b \sum_{j=1}^{n_2} \left(q_{2,j} \frac{(i+1)(j+1)}{(i+j+1)} \frac{1}{L_2} \left(\begin{array}{l} \rho_2 A_2 L_2 \dfrac{(i+j)}{2(i+j+2)} \\ +M_2 \dfrac{L_{M_2}}{L_2} \left(1 - \left(\dfrac{L_{M_2}}{L_2} \right)^{i+j} \right) \end{array} \right) \right)$$

$$- \sum_{j=1}^{n_2} \sum_{k=1}^{n_1} \left(q_{2,j} \ddot{q}_{1,k} \frac{(i+1)(j+1)}{(i+j+1)} \frac{1}{L_2} \left(\begin{array}{l} \rho_2 A_2 L_2 \dfrac{(i+j)}{2(i+j+2)} \\ +M_2 \dfrac{L_{M_2}}{L_2} \left(1 - \left(\dfrac{L_{M_2}}{L_2} \right)^{i+j} \right) \end{array} \right) \right) \quad (3.83)$$

$$+ \sum_{j=1}^{n_2} \sum_{k=1}^{n_2} \sum_{l=1}^{n_2} \left(q_{2,j} q_{2,k} q_{2,l} \frac{E_2 A_2}{2 L_2^{\,3}} \frac{(i+1)(j+1)(k+1)(l+1)}{(i+l+1)(j+k+1)} \right)$$

As it can be understood from Equations (3.82) and (3.83), there is only a cubic nonlinearity which is called a cubic stiffness, acting on the first beam; however, both cubic and quadratic nonlinearities act on the second beam.

External forcing vector $\mathbf{f}$ can be written as,

$$\mathbf{f} = \left[F_b \;\vdots\; 0 \quad \cdots \quad 0 \;\vdots\; 0 \quad \cdots \quad 0 \right]^T . \quad (3.84)$$

By assembling these matrices, the matrix representation of the system can be written as,

$$\mathbf{M}\ddot{\mathbf{q}} + \left(\mathbf{K} + i\mathbf{H} \right) \mathbf{q} + \mathbf{f}_N = \mathbf{f} . \quad (3.85)$$

CHAPTER 4

CASE STUDIES

In this chapter, several case studies are carried out to see the effects of system parameters on the vibration characteristics of the one-end fixed L-shaped beam and L-shaped beam attached to a SDOF system.

4.1 Case Study: One End Fixed L-Shaped Beam

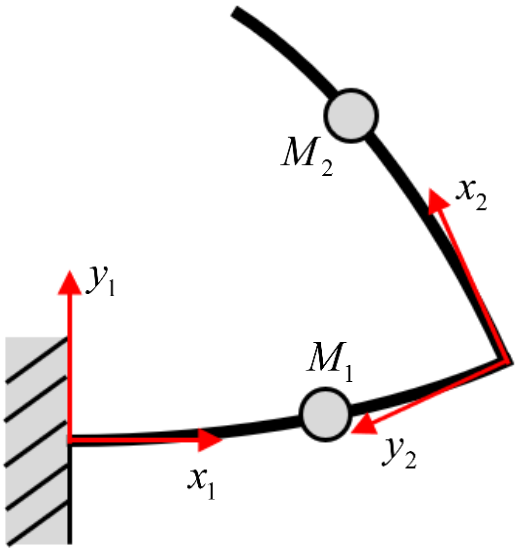

Figure 4.1. Schematic of the Fixed L-Shaped Beam

This section covers several case studies of the one-end fixed L-shaped beam to observe the effects of the system parameters. Comparisons between linear and nonlinear systems are carried out, and it is observed that as the excitation amplitude increases, it is necessary to consider the nonlinear effects to capture the dynamics of the L-shaped beam accurately. Additionally, the effect of the number of harmonics used on the response is demonstrated to choose the optimum number of harmonics for further calculations.

4.1.1 Mathematical Model of the Fixed L-Shaped Beam

In Section 3, a mathematical model is derived for an L-shaped beam attached to a SDOF system. Likewise, a mathematical model is needed for this case study to carry out case studies for the fixed L-shaped beam. The mathematical model for this system can be derived using the equations of motion of the L-shaped beam attached to a SDOF system by ignoring the motion of the base mass. By doing that, the first rows and columns of matrix Equations (3.68), (3.76), (3.79) and the first rows of vector Equations (3.80), (3.81) which are related to the motion of the base mass are discarded as,

$$\mathbf{M} = \left[\begin{array}{ccc:ccc} M11_{1,1} & \cdots & M11_{1,n_1} & M12_{1,1} & \cdots & M12_{1,n_2} \\ \vdots & \ddots & \vdots & \vdots & \ddots & \vdots \\ M11_{n_1,1} & \cdots & M11_{n_1,n_1} & M12_{n_1,1} & \cdots & M12_{n_1,n_2} \\ \hdashline M21_{1,1} & \cdots & M21_{1,n_1} & M22_{1,1} & \cdots & M22_{1,n_2} \\ \vdots & \ddots & \vdots & \vdots & \ddots & \vdots \\ M21_{n_2,1} & \cdots & M21_{n_2,n_1} & M22_{n_2,1} & \cdots & M22_{n_2,n_2} \end{array}\right], \tag{4.1}$$

$$\mathbf{K} = \left[\begin{array}{ccc:ccc} K_{11_{1,1}} & \cdots & K_{11_{1,n_1}} & & & \\ \vdots & \ddots & \vdots & & & \\ K_{11_{n_1,1}} & \cdots & K_{11_{n_1,n_1}} & & & \\ \hdashline & & & K_{22_{1,1}} & \cdots & K_{22_{1,n_2}} \\ & & & \vdots & \ddots & \vdots \\ & & & K_{22_{n_2,1}} & \cdots & K_{22_{n_2,n_2}} \end{array}\right], \tag{4.2}$$

$$\mathbf{H} = \left[\begin{array}{ccc:ccc} \gamma_1 H_{11_{1,1}} & \cdots & \gamma_1 H_{11_{1,n_1}} & & & \\ \vdots & \ddots & \vdots & & & \\ \gamma_1 H_{11_{n_1,1}} & \cdots & \gamma_1 H_{11_{n_1,n_1}} & & & \\ \hdashline & & & \gamma_2 H_{22_{1,1}} & \cdots & \gamma_2 H_{22_{1,n_2}} \\ & & & \vdots & \ddots & \vdots \\ & & & \gamma_2 H_{22_{n_2,1}} & \cdots & \gamma_2 H_{22_{n_2,n_2}} \end{array}\right], \tag{4.3}$$

$$\mathbf{q} = \left[q_{1,1} \quad \cdots \quad q_{1,n_1} \;\vdots\; q_{2,1} \quad \cdots \quad q_{2,n_2} \right]^T, \tag{4.4}$$

$$\mathbf{f}_N = \left[f_{N1_1} \quad \cdots \quad f_{N1_{n_1}} \;\vdots\; f_{N2_1} \quad \cdots \quad f_{N2_{n_2}} \right]^T. \tag{4.5}$$

Since the forcing vector derived in Section 3 is for the base excitation, a new forcing vector should be derived for the fixed L-beam case.

A sinusoidal force is assumed to be applied on the r^{th} beam at the location x_f as,

$$F_r\left(x_f, t\right) = F_0 \delta\left(x_f\right) \sin\left(\omega t\right), \tag{4.6}$$

where F_0 represents the amplitude of the forcing.

Galerkin's method explained in Section 3.2.1 is applied to Equation (4.6) to discretize it as,

$$f_{r_i} = F_0 \sin\left(\omega t\right) \left(\frac{x_f}{L_r} \right)^{i+1}, i = 1, 2, ... n_r. \tag{4.7}$$

Depending on which beam force is applied, the forcing vector can be written as,

$$\mathbf{f} = \begin{cases} \left[f_{1_1} \quad \cdots \quad f_{1_{n_1}} \;\vdots\; 0 \quad \cdots \quad 0 \right]^T \; if \; r = 1 \\ \left[0 \quad \cdots \quad 0 \;\vdots\; f_{2_1} \qquad f_{2_{n_1}} \right]^T \; if \; r = 2 \end{cases}. \tag{4.8}$$

Inserting Equations (4.1)-(4.5) and (4.8) into Equation (3.85), matrix representation of the nonlinear ODE system can be obtained. Then the nonlinear ODE system is transformed into NLAEs using HBM explained in Section 2.2, and these NLAEs are solved using both HCM and ALCM explained in Sections 2.3.2 and 2.3.3, respectively. After solving it for generalized coordinates, responses of the beams can be obtained as,

$$w_r\left(x_r, t\right) = \sum_{i=1}^{n_r} \left(\left(\frac{x_r}{L_r} \right)^{i+1} q_{r,i}\left(t\right) \right). \tag{4.9}$$

Moreover, since the coordinate frame attached to the second beam is non-inertial, its response w.r.t a fixed point represented in an inertial frame (i.e., coordinate frame attached to the first beam) can be obtained as,

$$w_2^{(1)}(x_2,t)=\sum_{i=1}^{n_2}\left(\left(\frac{x_2}{L_2}\right)^{i+1}q_{2,i}(t)\right)+\frac{x_2}{L_2}\frac{L_2}{L_1}\sum_{i=1}^{n_2}\left((i+1)q_{1,i}(t)\right). \tag{4.10}$$

4.1.2 Results

To reduce the number of system parameters, it is assumed that the materials, the cross sections, and the structural damping coefficients of the first and the second beams are the same, i.e. $\rho=\rho_1=\rho_2$, $E=E_1=E_2$, $A=A_1=A_2$, $I=I_1=I_2$, $\gamma=\gamma_1=\gamma_2$.

4.1.2.1 Linear Model Results

First, the validity of the linear model is checked by comparing the results obtained with results obtained by commercial finite element (FE) software ANSYS. Responses w.r.t the coordinate frame of the first beam, i.e., $w_r^{(1)}$ are compared with the ANSYS FRF results since ANSYS gives deformation results only w.r.t inertial frames. BEAM189 elements are used in the model. Moreover, in order to perform only in-plane motion, other translational and rotational DOFs are fixed. This study is performed for the system parameters given in Table 4.1. Using these parameters, other system parameters could be obtained as,

$$\frac{L_2}{L_1}=\frac{\rho AL_2}{\rho AL_1}, \tag{4.11}$$

$$\frac{EI}{L_2^{\,3}}=\frac{EI}{L_1^{\,3}}\cdot\left(\frac{\rho AL_1}{\rho AL_2}\right)^3, \tag{4.12}$$

$$\frac{EA}{2L_2^{\,3}} = \frac{EA}{2L_1^{\,3}} \cdot \left(\frac{\rho A L_1}{\rho A L_2} \right)^3 . \tag{4.13}$$

Results of the linear system are compared to the FE software results in Figure 4.3 and Figure 4.4.

Table 4.1. Selected System Parameters for Case 1

System Parameters	**Case 1**	**System Parameters**	**Case 1**
$\rho A L_1$	$0.3925\,kg$	$\frac{EI}{L_1^{\,3}}$	$1333.3\frac{N}{m}$
$\rho A L_2$	$0.3925\,kg$	$\frac{EA}{2L_1^{\,3}}$	$8\cdot 10^7\,\frac{N}{m^3}$
M_1	$0.1kg$	L_2	$0.5m$
M_2	$0.1kg$	F_0	$1N$
L_{M_1} / L_1	0.5	γ	0.01
L_{M_2} / L_2	1	x_f / L_r	$x_f / L_1 = 1$

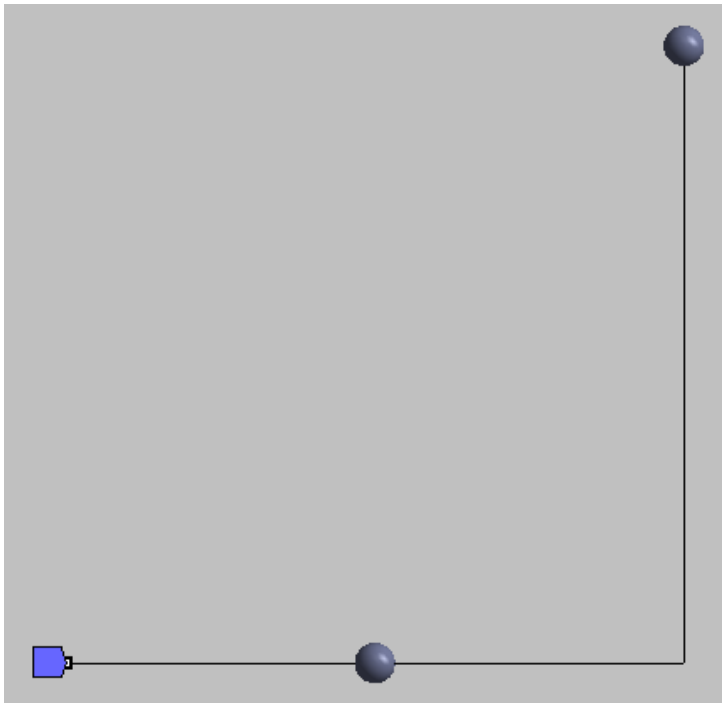

Figure 4.2. ANSYS Model of the Fixed L-Shaped Beam

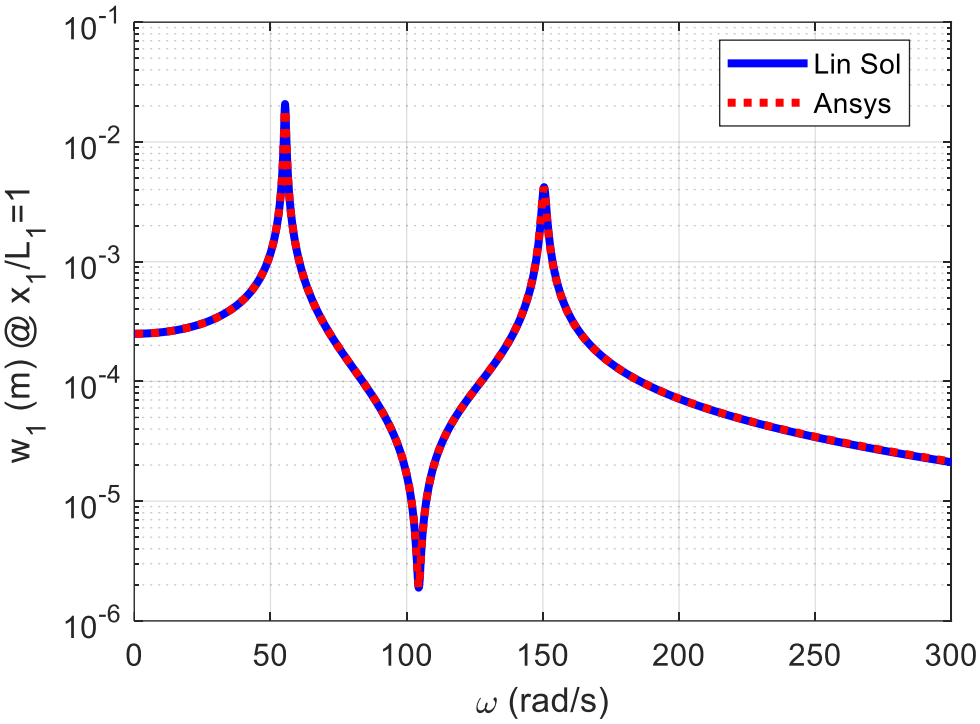

Figure 4.3. Comparison of the Linear Model with ANSYS at $x_1 / L_1 = 1$ for Case 1

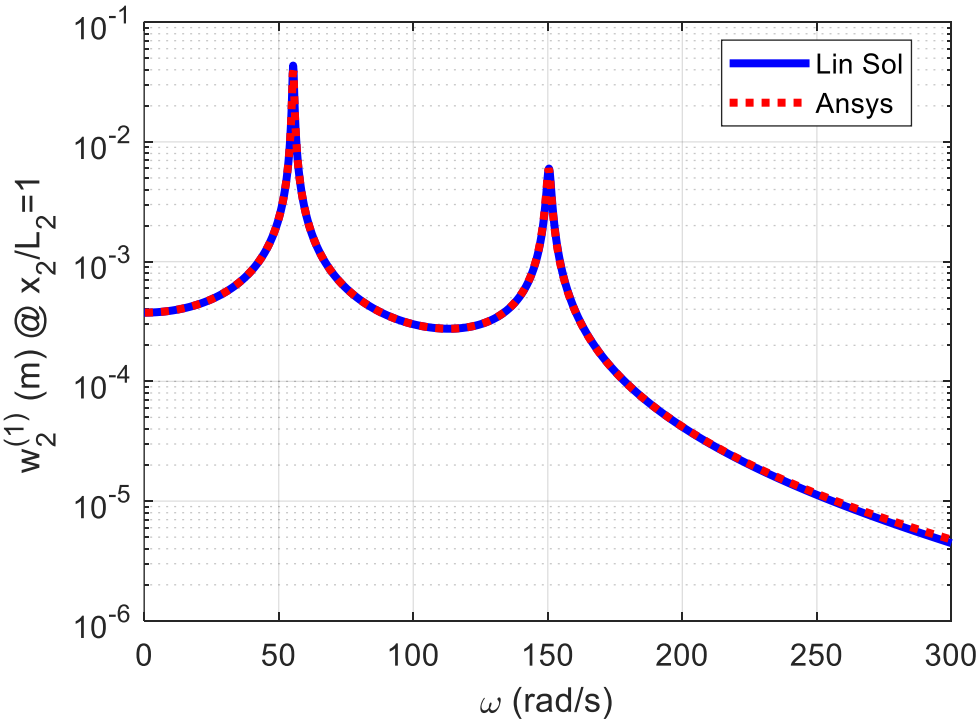

Figure 4.4. Comparison of the Linear Model with ANSYS at $x_2 / L_2 = 1$ for Case 1

It can be seen that the results obtained in Figure 4.3 and Figure 4.4 are identical to each other, which verifies the linear model developed.

After verifying the model, the first two mode shapes of the fixed L-shaped beam for Case 1 are obtained as in Figure 4.5.

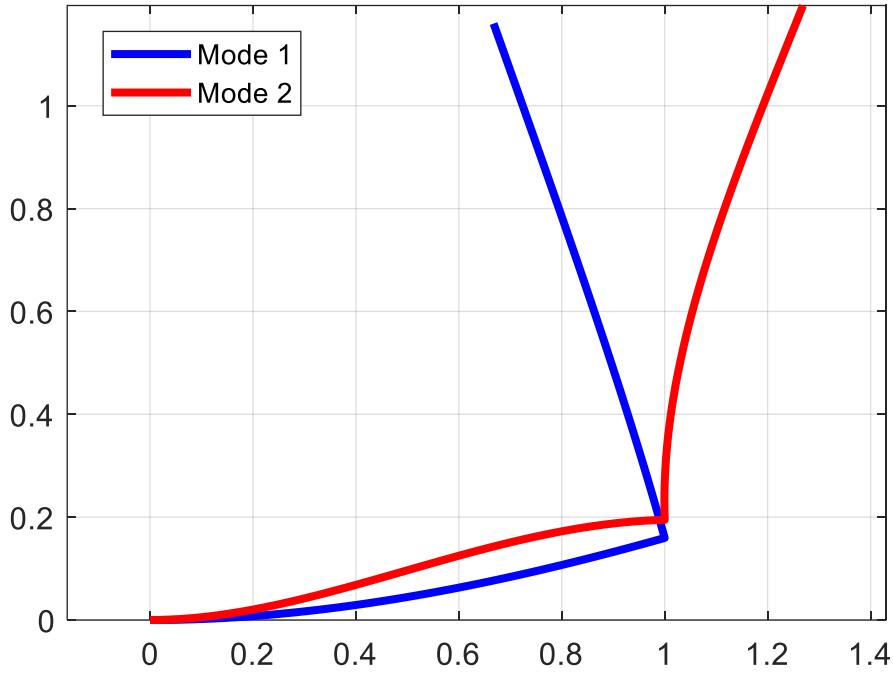

Figure 4.5. Mode Shapes of the Fixed L-Shaped Beam for Case 1

4.1.2.2 Investigation of the Effect of the Harmonics

To investigate the effect of the number of harmonics used, HBM is utilized for one, two, and three harmonics with bias terms. The investigation is performed using case 1 parameters. Moreover, in order to see the effect of the forcing amplitude on the number of harmonics used, results are obtained for $F_0 = 1N$ and $F_0 = 2N$.

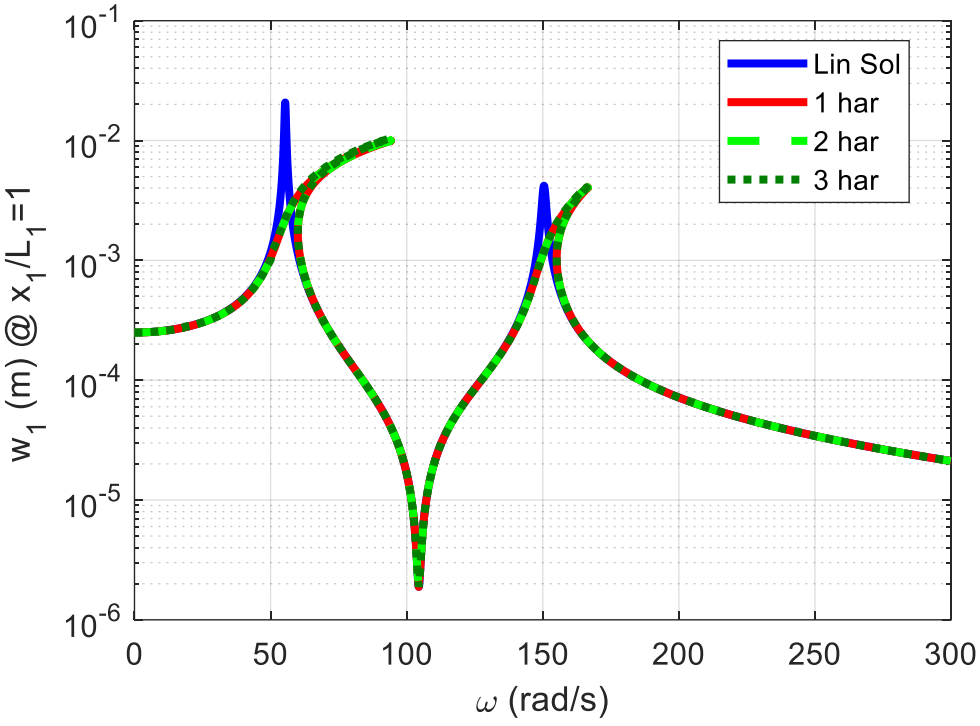

Figure 4.6. Comparison of the Harmonics Used at $x_1 / L_1 = 1$ for $F_0 = 1N$

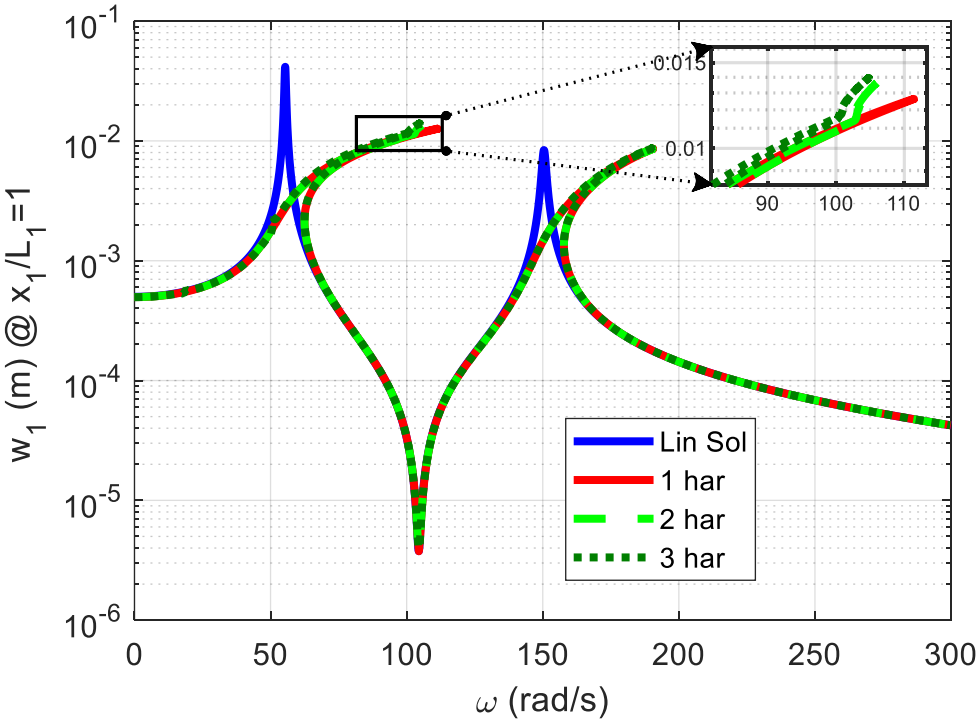

Figure 4.7. Comparison of the Harmonics Used at $x_1 / L_1 = 1$ for $F_0 = 2N$

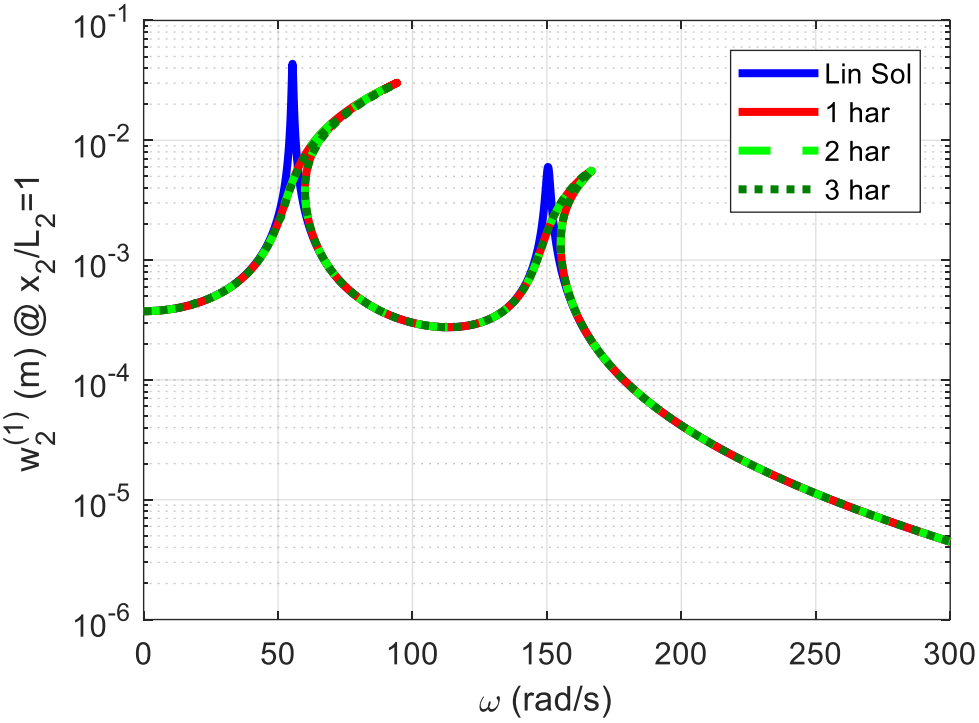

Figure 4.8. Comparison of the Harmonics Used at $x_2 / L_2 = 1$ for $F_0 = 1N$

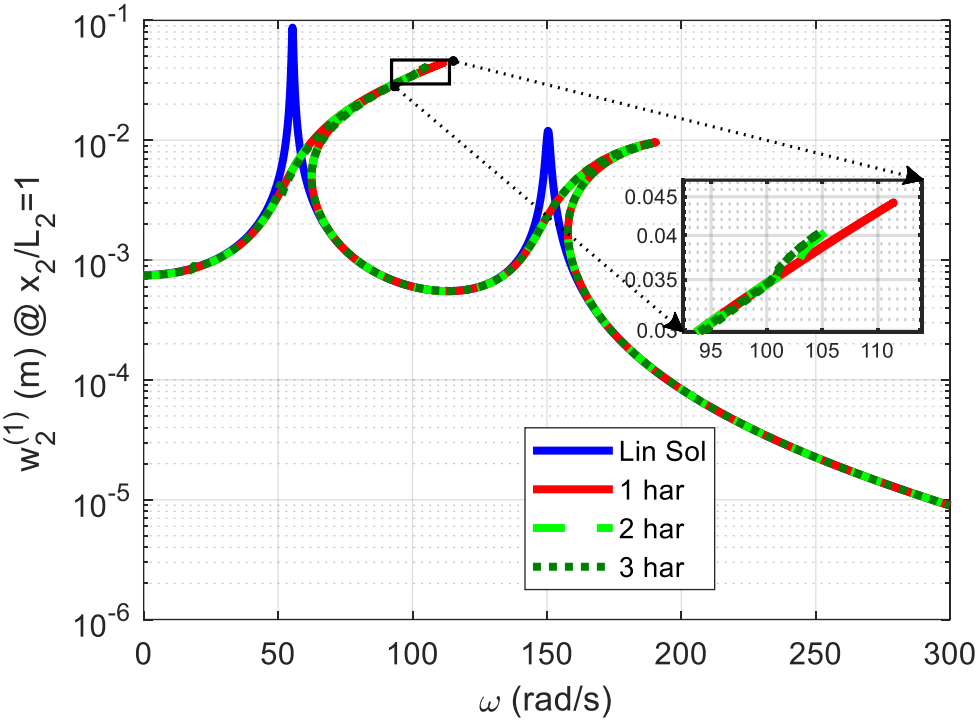

Figure 4.9. Comparison of the Harmonics Used at $x_2 / L_2 = 1$ for $F_0 = 2N$

The responses in Figure 4.6 and Figure 4.8 are identical to each other; however, in Figure 4.7 and Figure 4.9, the difference near the resonance points becomes clear. The effect of the squared nonlinearity can be seen from the notches in the responses obtained using higher harmonics. It can be understood from these figures that this nonlinearity takes into effect under high forcing. Moreover, two harmonics and three harmonics solutions are nearly identical. They only differ from each other slightly around resonance points. However, this difference can be disregarded, and two harmonic solution could be preferred since three harmonic solution takes much more time than the two harmonics solution.

4.1.2.3 Case Study Results

After verifying the linear model and observing the effect of the harmonics, several case studies are performed. Case 1 is used as the basis for the system parameters, and for each study, one of the parameters is selected as the controlled variable while others are kept constant to observe its effects on the nonlinear response of the system. The selected controlled variables and their values are given in Table 4.2. The natural frequencies of the linear system for each case are presented in Table 4.3.

In the first case study, to observe the effect of forcing amplitude on the nonlinear response of the model, different excitation forcing amplitudes are considered, and the normalized responses with respect to forcing amplitudes are compared with each other. It can be seen from Figure 4.10 and Figure 4.11 that, when the forcing is very small, the responses are very similar to the response of the linear system. When a forcing with an amplitude of 0.05 N is applied, cubic stiffness nonlinearity starts to take effect. As the forcing amplitude increases, the resonance frequency shifts to the right, which is the outcome of the cubic stiffness nonlinearity dominant in this system. Moreover, when the forcing amplitude is 2N, the squared nonlinearity becomes effective, as seen from the notch at the first resonance.

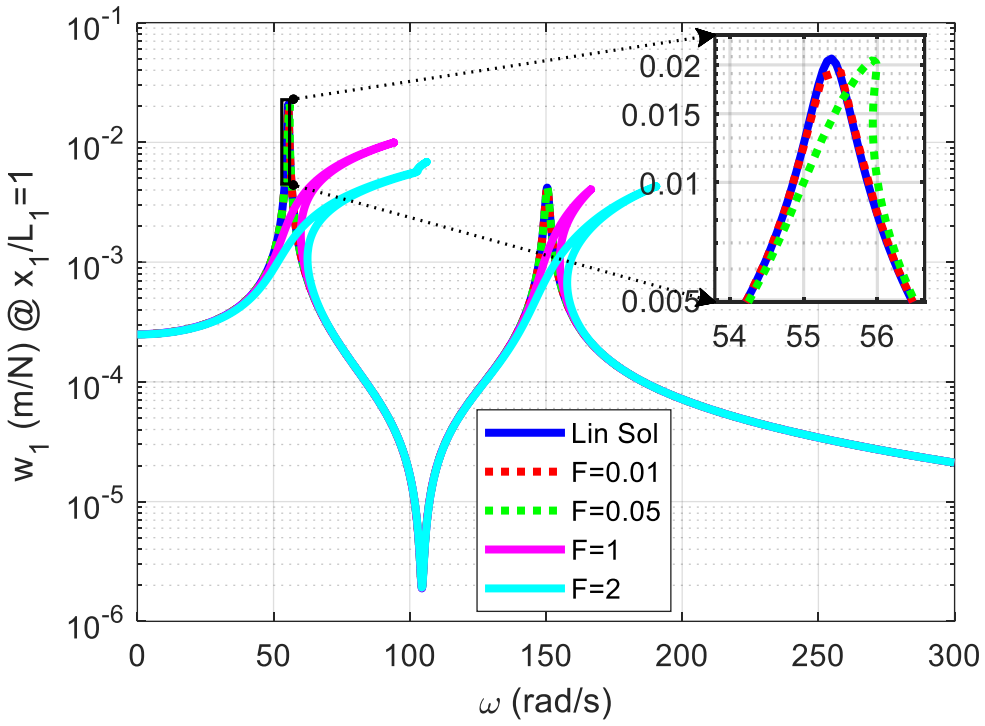

Figure 4.10. Effect of the Forcing Amplitude on the FRF at $x_1 / L_1 = 1$ for Case 1

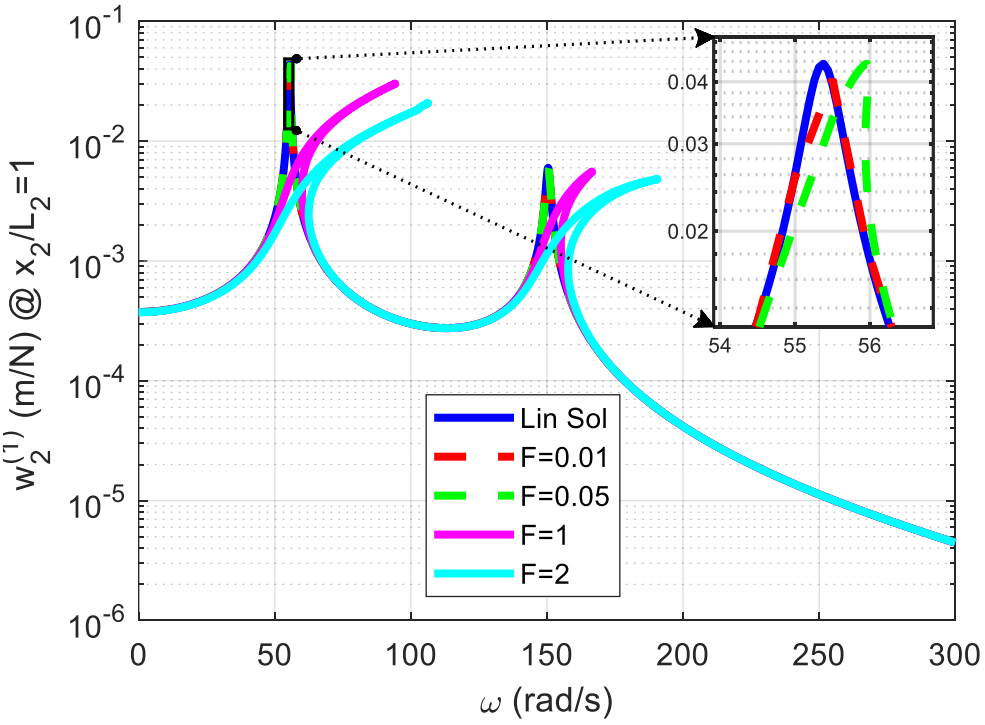

Figure 4.11. Effect of the Forcing Amplitude on the FRF at $x_2 / L_2 = 1$ for Case 1

Table 4.2. Controlled Variables and Their Values

	Controlled Variable and Its Value
Case 2	$\rho AL_1 = 0.19625 kg$
Case 3	$\rho AL_2 = 0.19625 kg$
Case 4	$M_1 = 0.5 kg$
Case 5	$M_2 = 0.5 kg$
Case 6	$L_{M_1} / L_1 = 1$
Case 7	$L_{M_2} / L_2 = 0.5$
Case 8	$\frac{EI}{L_1^3} = 666.67 \frac{N}{m}$
Case 9	$\frac{EA}{2L_1^3} = 4 \cdot 10^7 \frac{N}{m^3}$
Case 10	$L_2 = 0.1 m$

Table 4.3. Natural Frequencies for Each Case

	$\omega_1 (rad/s)$	$\omega_2 (rad/s)$
Ansys	55.365	150.36
Case 1	55.37	150.44
Case 2	29.57	118.25
Case 3	89.557	295.91
Case 4	54.812	143.77
Case 5	35.75	106.95
Case 6	53.796	145.64
Case 7	62.223	170.97
Case 8	39.152	106.38
Case 9	55.37	150.44
Case 10	55.37	150.44

In the second case study, the effect of the masses of the first and the second beams (ρAL_1 and ρAL_2) on the vibration characteristics are compared. These are labeled as Case 2 and Case 3, respectively. Since densities and areas of each beam are equal

to each other, changing these parameters result in a change in the ratio of the beam lengths. The steady-state frequency responses at $x_1 / L_1 = 1$ and $x_2 / L_2 = 1$ are given in Figure 4.12 and Figure 4.13, respectively.

It can be seen from the figures that a decrease in the mass of the first beam causes a decrease in the resonance frequencies, whereas decreasing the mass of the second beam causes an increase in the resonance frequencies in contrast to Case 2. Additionally, a decrease in the L_2 / L_1 ratio makes cubic stiffness more dominant at the first resonance frequency. Moreover, increasing the mass of the first beam amplifies the resonance response at the tip of the beam; similarly, an increase in the second beam's mass amplifies the response at the tip point of the second beam.

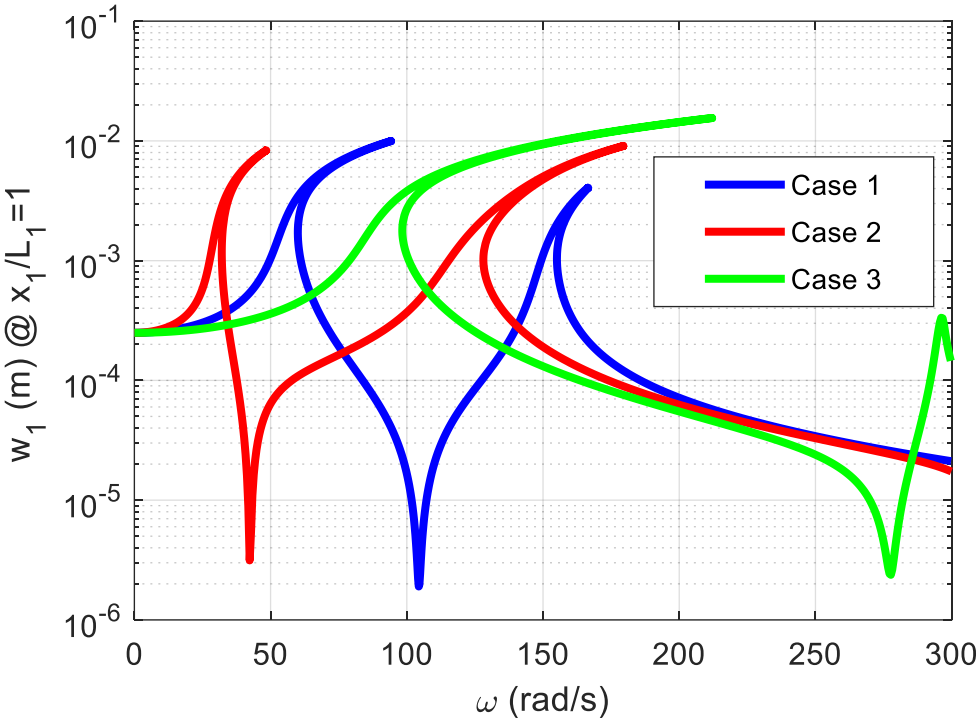

Figure 4.12. Comparison of the FRFs of the Cases 1, 2, and 3 at $x_1 / L_1 = 1$

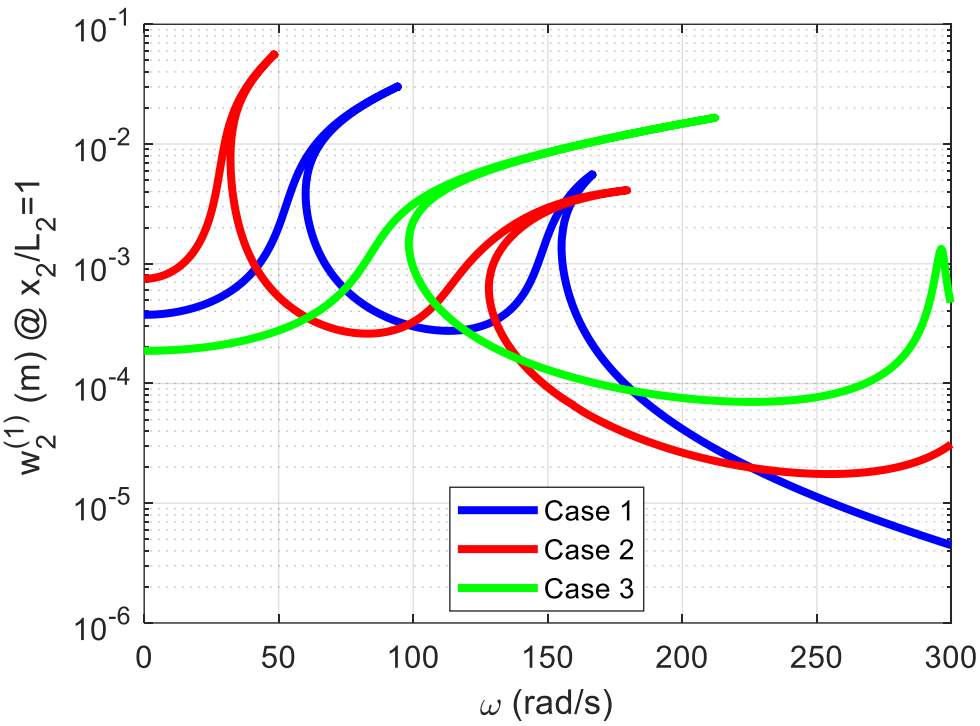

Figure 4.13. Comparison of the FRFs of the Cases 1, 2, and 3 at $x_2 / L_2 = 1$

The third case study investigates the effect of the concentrated masses connected to the first and second beams (M_1 and M_2) on the vibration characteristics. These are labeled as Case 4 and Case 5, respectively. The frequency responses at $x_1 / L_1 = 1$ and $x_2 / L_2 = 1$ are obtained and given in Figure 4.14 and Figure 4.15, respectively. It can be seen that increase in the mass of the concentrated mass attached to the first beam has a slight effect on the resonance frequencies and frequency responses compared to the concentrated mass attached to the second beam. The increase in the second concentrated mass causes a decrease in the resonance frequencies, which is an expected result. Moreover, an increase in the second concentrated mass decreases the resonance amplitude at the tip of the second beam significantly around the second resonance frequency of the L-shaped beam.

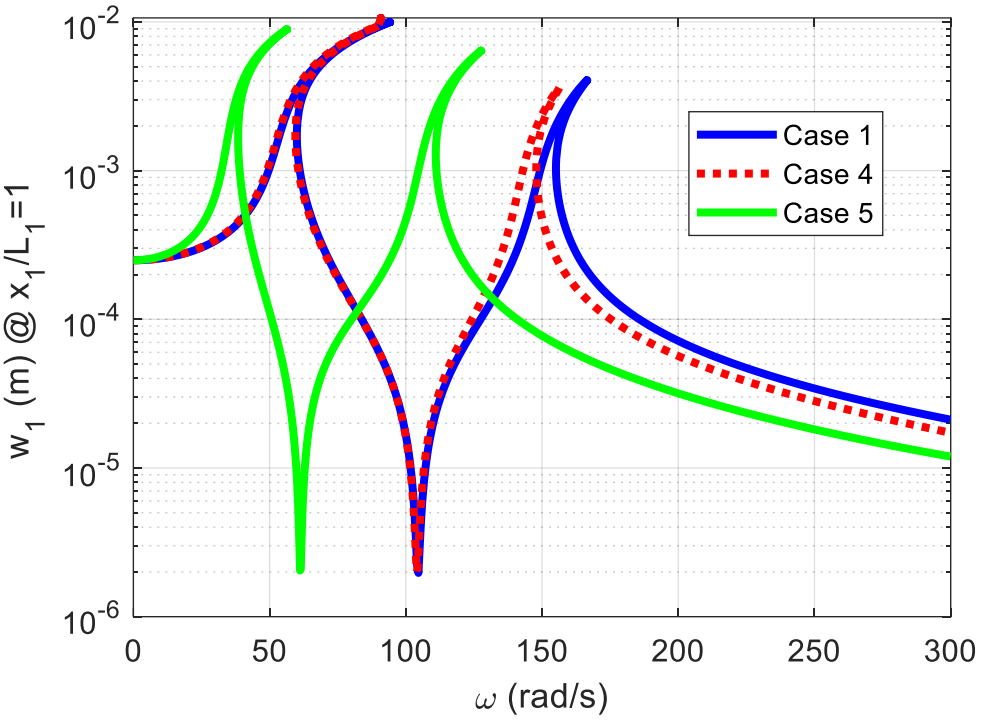

Figure 4.14. Comparison of the FRFs of the Cases 1, 4 and 5 at $x_1 / L_1 = 1$

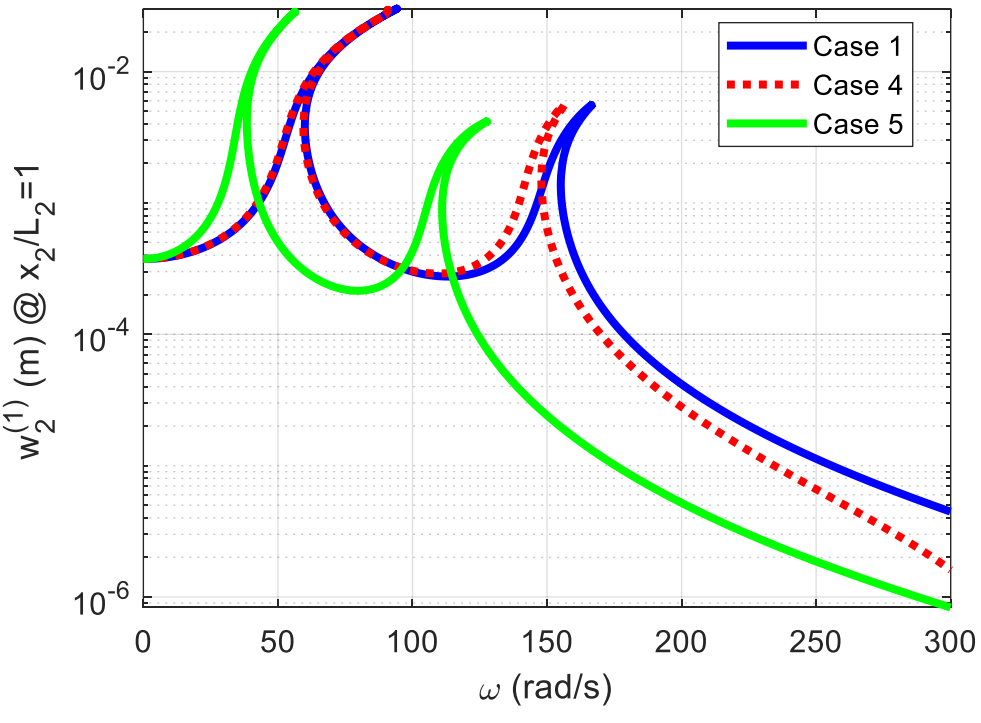

Figure 4.15. Comparison of the FRFs of the Cases 1, 4 and 5 at $x_2 / L_2 = 1$

The fourth case study investigates the effect of the locations of the first and the second concentrated masses (L_{M_1}/L_1 and L_{M_2}/L_2) on the vibration characteristics. These are labeled as Case 6 and Case 7, respectively. The steady-state frequency responses obtained at $x_1/L_1=1$ and $x_2/L_2=1$ are given in Figure 4.16 and Figure 4.17, respectively.

As seen from the results of Case 6, a change in the ratio of L_{M_1}/L_1 has a negligible effect on the system. On the other hand, a decrease in the L_{M_2}/L_2 ratio causes an increase in the resonance frequencies.

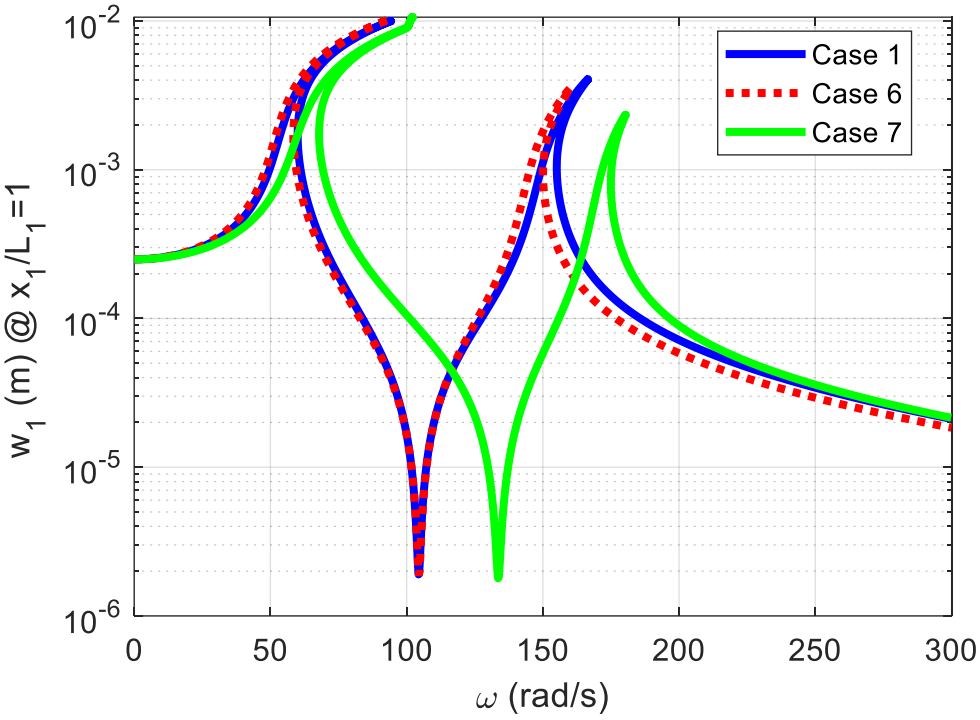

Figure 4.16. Comparison of the FRFs of the Cases 1, 6 and 7 at $x_1/L_1=1$

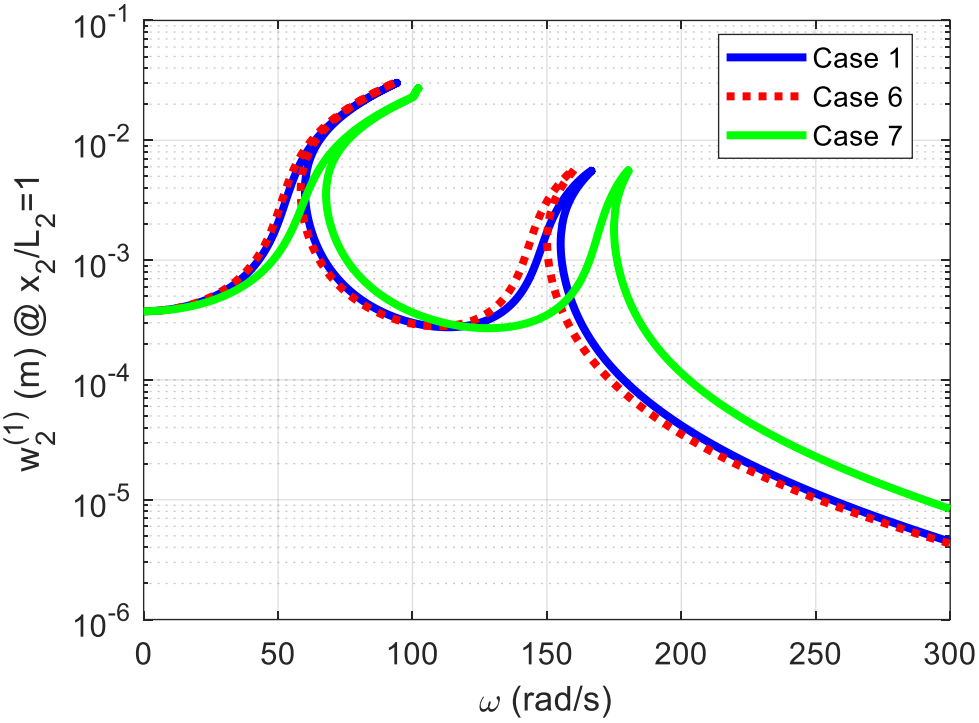

Figure 4.17. Comparison of the FRFs of the Cases 1, 6 and 7 at $x_2 / L_2 = 1$

In the fifth case study, the effect of the stiffness of the first beam (EI / L_1^3) is investigated. The stiffness parameter of the first beam is reduced by half in Case 8. Since the length ratio of the beams is 1.0 for Case 1, the stiffness parameter of the second beam is the same as the first beam, which means that this parameter affects the stiffness of both the first and the second beams. Responses of the L-shaped beam obtained at $x_1 / L_1 = 1$ and $x_2 / L_2 = 1$ are given in Figure 4.18 and Figure 4.19, respectively.

It is observed from the figures that when the stiffness is decreased, the resonance frequencies also decrease. Additionally, as the linear stiffness decreases, the effect of the nonlinear stiffness becomes more dominant. It should be noted that quadratic nonlinearity becomes more apparent in the results around the first resonance frequency. It is also observed that the responses at the tips of each beam at the resonance frequencies increase.

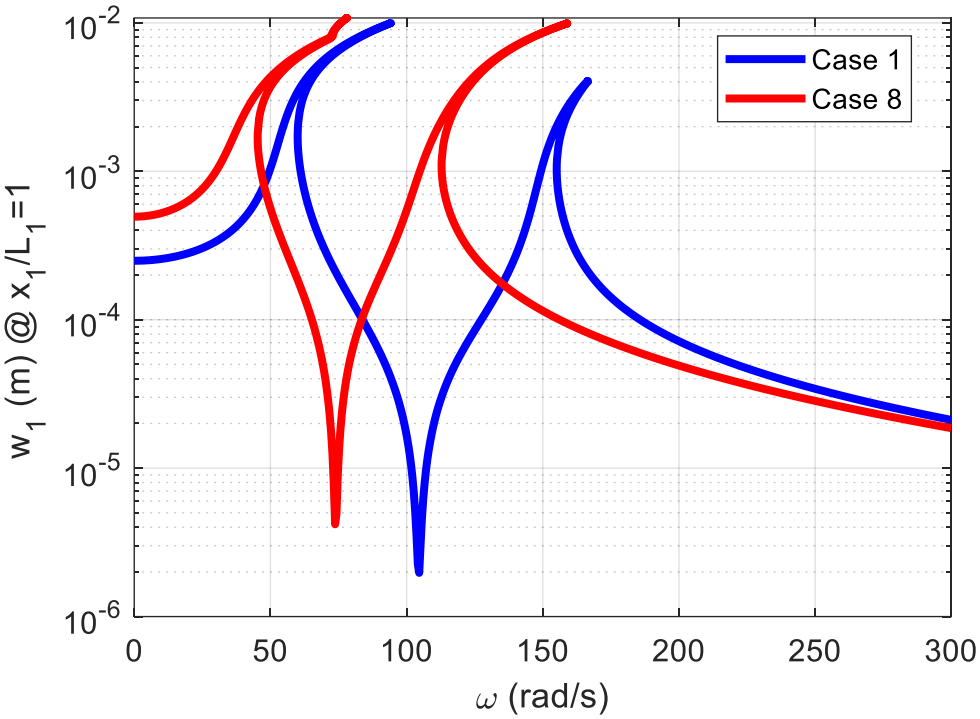

Figure 4.18. Comparison of the FRFs of the Cases 1 and 8 at $x_1 / L_1 = 1$

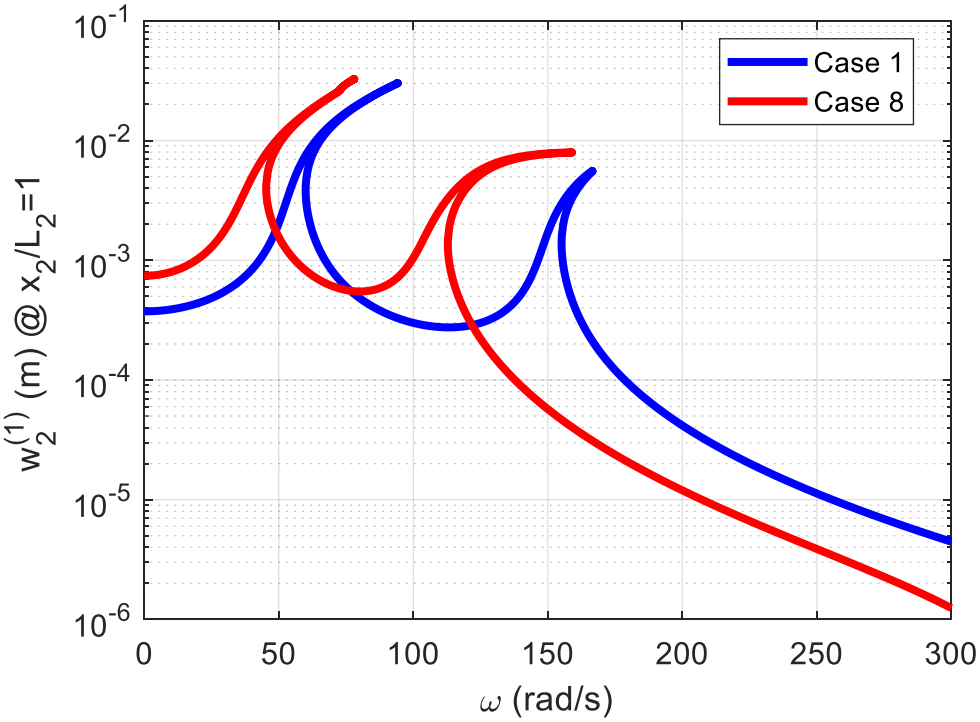

Figure 4.19. Comparison of the FRFs of the Cases 1 and 8 at $x_2 / L_2 = 1$

In the sixth case study, the effects of nonlinearity terms are investigated. These are cubic and quadratic nonlinearities that are proportional to $EA/\left(2L_1^3\right)$ and L_2 terms, respectively. Since the ratio of the lengths of the beams is equal to 1.0, the coefficient of the cubic nonlinearity for the second beam ($EA/\left(2L_2^3\right)$) is equal to the coefficient of the cubic nonlinearity for the first beam. Responses of the L-shaped beam obtained at $x_1/L_1=1$ and $x_2/L_2=1$ are given in Figure 4.20 and Figure 4.21, respectively. To demonstrate the effects of the nonlinearity, F_0 is selected as 2N instead of 1N.

As seen from the figures, a decrease in the cubic nonlinearity parameter in Case 9 decreases the cubic stiffness effect and shifts the resonance points to the right as expected. However, decreasing L_2 five times in Case 10 has no significant effect on the responses. This shows that the cubic nonlinearity is much more dominant than the quadratic one.

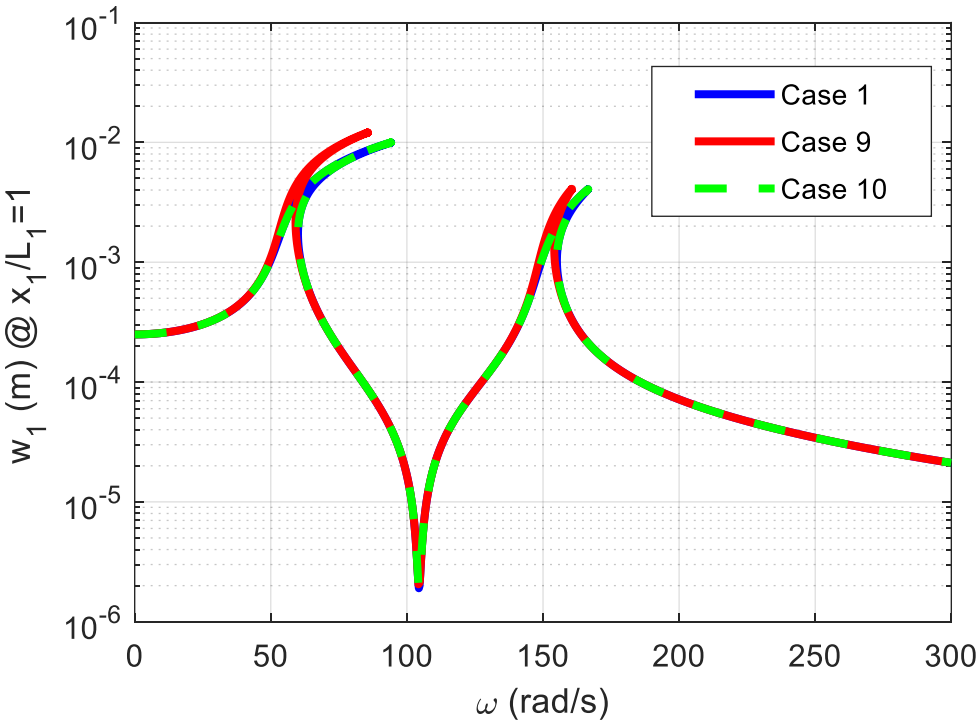

Figure 4.20. Comparison of the FRFs of the Cases 1, 9 and 10 at $x_1/L_1=1$

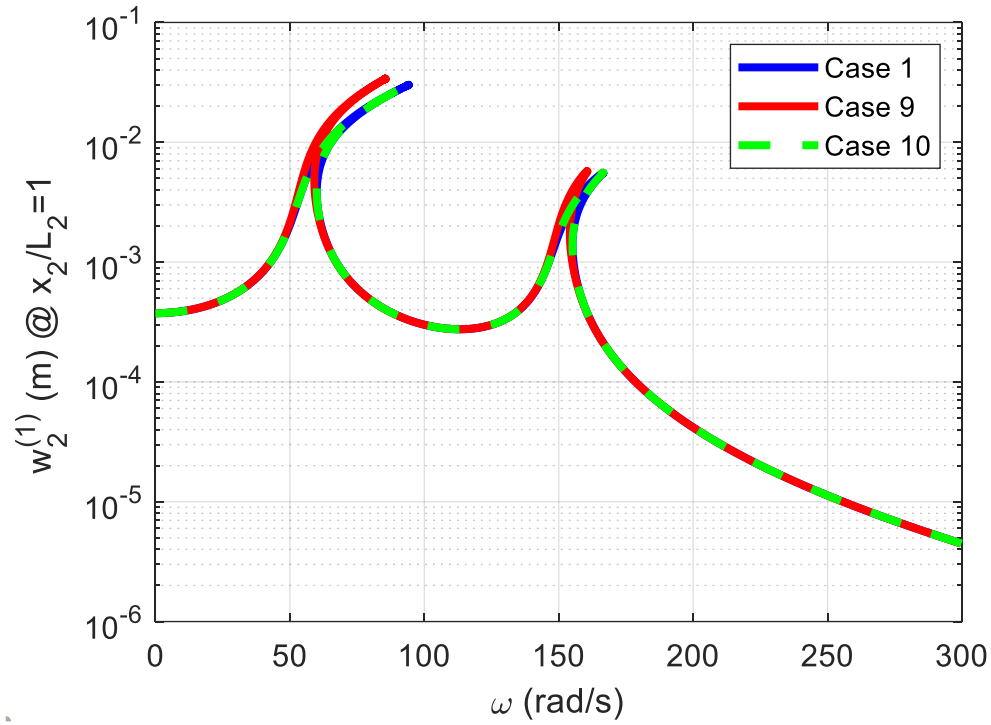

Figure 4.21. Comparison of the FRFs of the Cases 1, 9 and 10 at $x_2 / L_2 = 1$

4.2 Case Study: L-Shaped Beam Attached to a SDOF System

This section covers several case studies of the L-shaped beam attached to a SDOF system in order to observe the effects of the system parameters. Additionally, as in Section 4.1, comparisons between linear and nonlinear systems are carried out, and it is seen that it is necessary to consider the nonlinear effects as the excitation amplitude increases to capture the dynamics of the L-shaped beam attached to a SDOF system accurately. Additionally, the effect of the number of harmonics used on the response is demonstrated to choose the optimum number of harmonics for further calculations.

4.2.1 Mathematical Model

The mathematical model for the L-shaped beam attached to a SDOF system is derived in Chapter 3. The base excitation of the system is assumed to be a sinusoidal forcing as,

$$F_b = F_0 \sin(\omega t). \tag{4.14}$$

To obtain the responses of the beams in their own reference frames, Equation (4.9) is used.

$$w_r(x_r,t) = \sum_{i=1}^{n_r}\left(\left(\frac{x_r}{L_r}\right)^{i+1} q_{r,i}(t)\right). \tag{4.15}$$

To find the response of the second beam w.r.t the coordinate frame of the first beam, the following equation is used.

$$w_2^{(1)}(x_2,t) = \sum_{i=1}^{n_2}\left(\left(\frac{x_2}{L_2}\right)^{i+1} q_{2,i}(t)\right) + \frac{x_2}{L_2}\frac{L_2}{L_1}\sum_{i=1}^{n_2}\left((i+1)q_{1,i}(t)\right). \tag{4.16}$$

Equation (4.15) for $r=1$ and Equation (4.16) could be used to obtain the responses of the L-shaped beam without including the motion of the base mass. Using these equations, effects of the system parameters on the L-shaped beam could be examined. Moreover, the response of the L-shaped beam w.r.t an inertial frame, i.e., earth frame, could be obtained using the following equations as,

$$w_1^{(e)}(x_1,t) = w_b(t) + \sum_{i=1}^{n_r}\left(\left(\frac{x_1}{L_1}\right)^{i+1} q_{1,i}(t)\right), \tag{4.17}$$

$$w_2^{(e)}(x_2,t) = \sum_{i=1}^{n_2}\left(\left(\frac{x_2}{L_2}\right)^{i+1} q_{2,i}(t)\right) + \frac{x_2}{L_2}\frac{L_2}{L_1}\sum_{i=1}^{n_2}\left((i+1)q_{1,i}(t)\right). \tag{4.18}$$

4.2.2 Results

As in Section 4.1.2, the number of system parameters is reduced by assuming the materials, cross sections, and structural damping coefficients of the first and the second beams are the same, i.e. $\rho = \rho_1 = \rho_2$, $E = E_1 = E_2$, $A = A_1 = A_2$, $I = I_1 = I_2$, $\gamma = \gamma_1 = \gamma_2$.

4.2.2.1 Linear Model Results

Responses w.r.t the coordinate frame of the first beam, i.e., $w_r^{(e)}$ are compared with the ANSYS FRF results since ANSYS gives deformation results only w.r.t inertial frames.

Before carrying out case studies, the linear model is validated by comparing the results obtained with results obtained by ANSYS. BEAM189 elements are used in the model. Moreover, in order to perform only in-plane motion, other translational and rotational DOFs are fixed. This study is performed using the same system parameters given in Table 5.1. Additional parameters related to the base mass are given in Table 4.4. Using these parameters, other system parameters could be obtained using Equations (4.11)-(4.13). Results of the linear system are compared with the FE software results in Figure 4.23, Figure 4.24 and Figure 4.25. Moreover, the first three mode shapes of the system are shown in Figure 4.26.

Table 4.4. Additional System Parameters for Case 1

System Parameters	Case 1	System Parameters	Case 1
M_b	$10\,kg$	k_b	$10^5\,\frac{N}{m}$
γ_b	0.01	F_0	$7.5\,N$

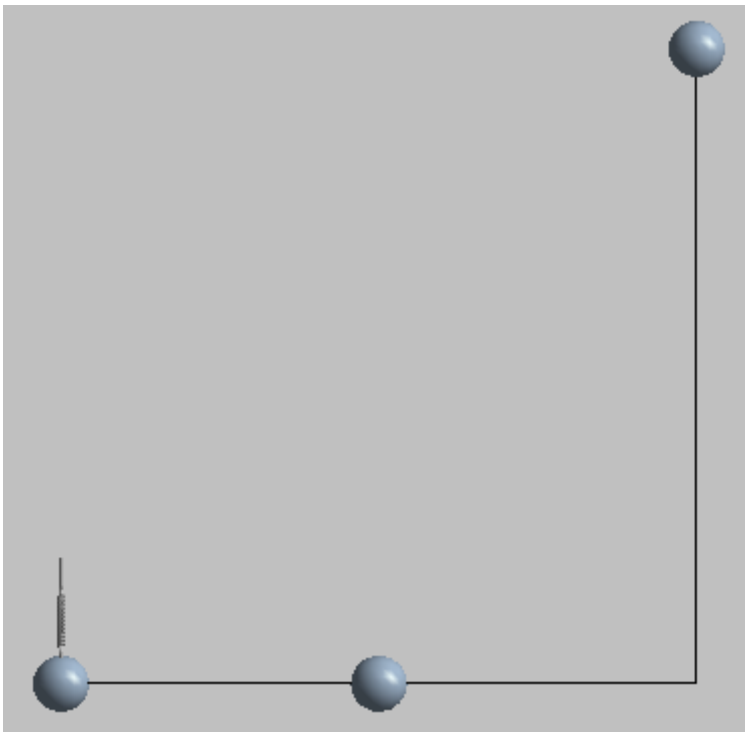

Figure 4.22. ANSYS Model of the L-Shaped Beam Attached to a SDOF System

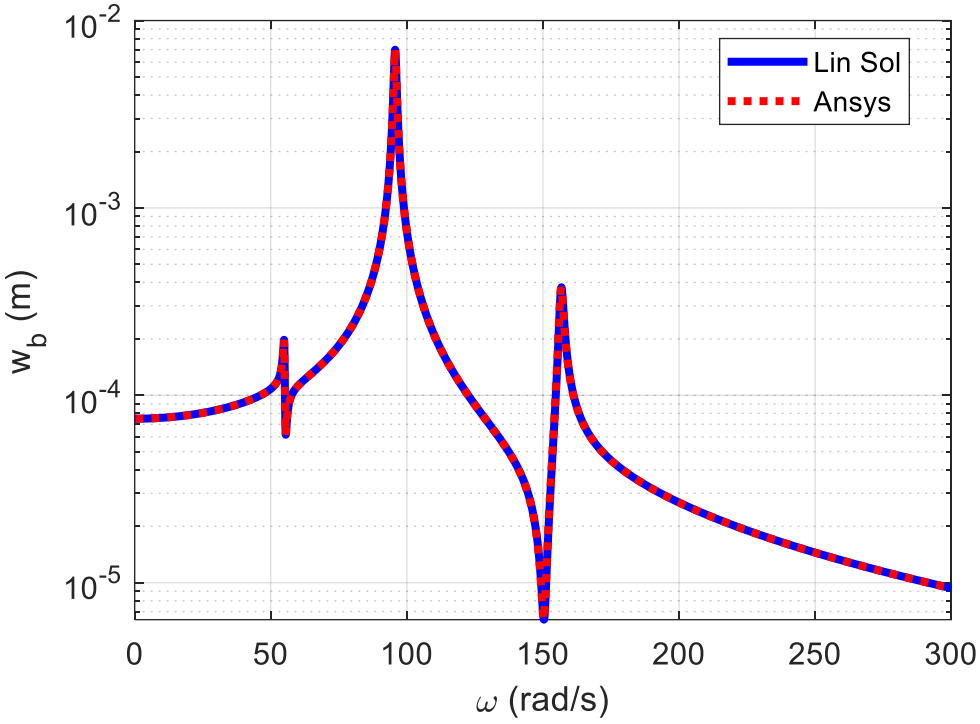

Figure 4.23. Comparison of w_b obtained by Linear Model and ANSYS for Case 1

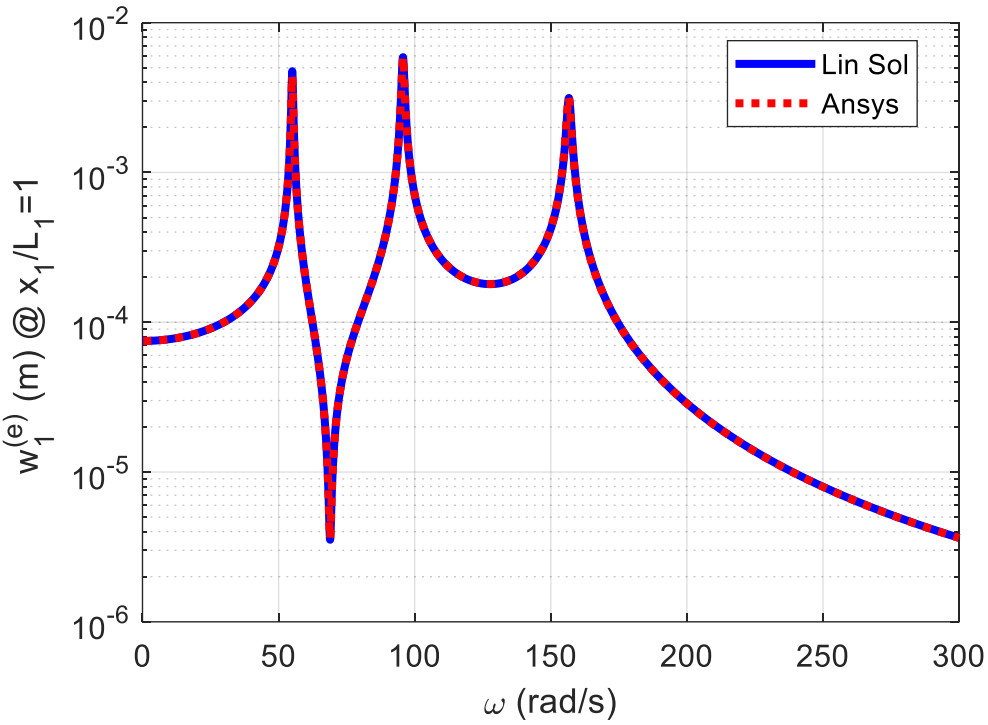

Figure 4.24. Comparison of the Linear Model with ANSYS at $x_1 / L_1 = 1$ for Case 1

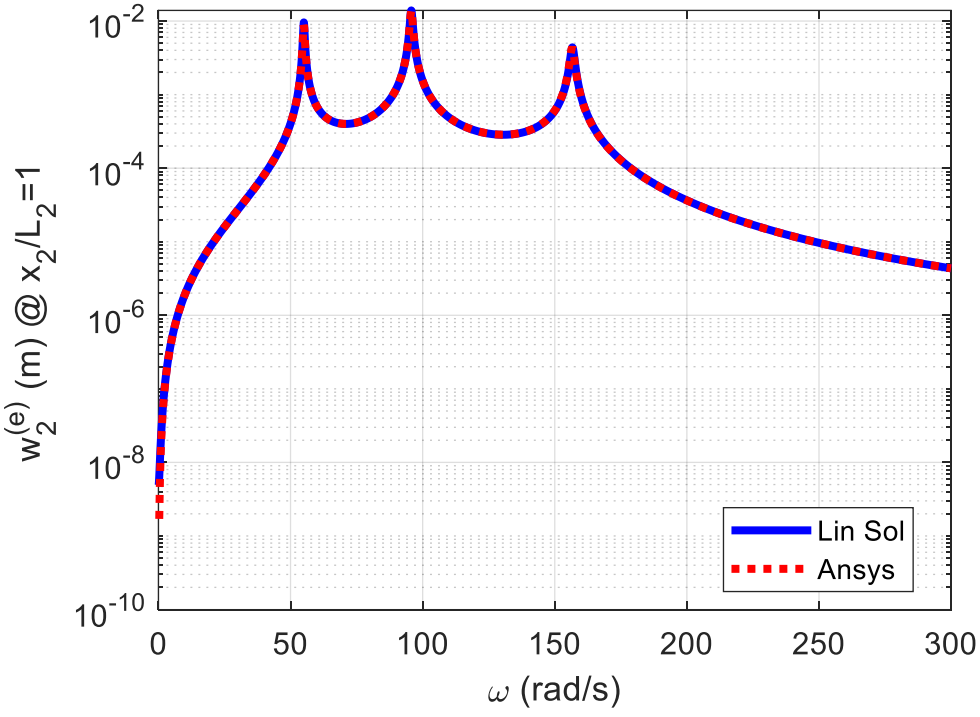

Figure 4.25. Comparison of the Linear Model with ANSYS at $x_2 / L_2 = 1$ for Case 1

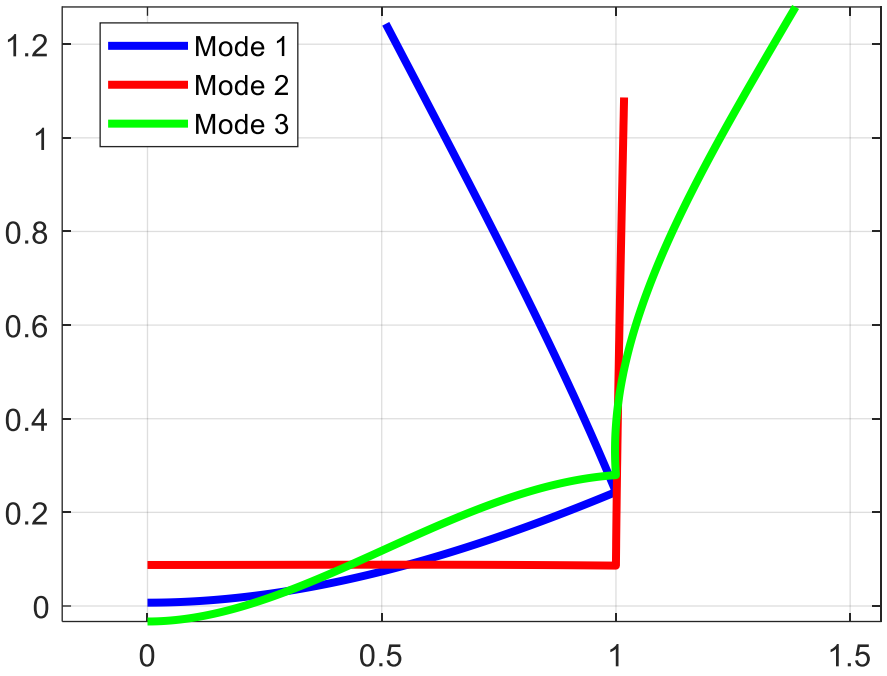

Figure 4.26. Mode Shapes for the L-Shaped Beam Attached to a SDOF System

Figure 4.23, Figure 4.24 and Figure 4.25 show that responses obtained using the ANSYS model and the linear model are nearly identical to each other, which verifies the linear model. Moreover, the first and third resonance points are close to the first two resonance points of the fixed L-shaped beam using Case 1 parameters and the second resonance point is nearly equal to the frequency of the system where the L-shaped beam moves as a rigid body. In addition, Figure 4.26 shows that the first and third resonances are related to the deformation of the L-shaped beam, whereas; the second resonance is related to the motion of the base mass. As it can be seen from the second mode shape, beam acts as like a rigid body.

4.2.2.2 Investigation of the Effect of the Harmonics

In this section, HBM is utilized for one, two, and three harmonics with bias terms in order to analyze the effect of the number of harmonics used. This analysis is performed using case 1 parameters.

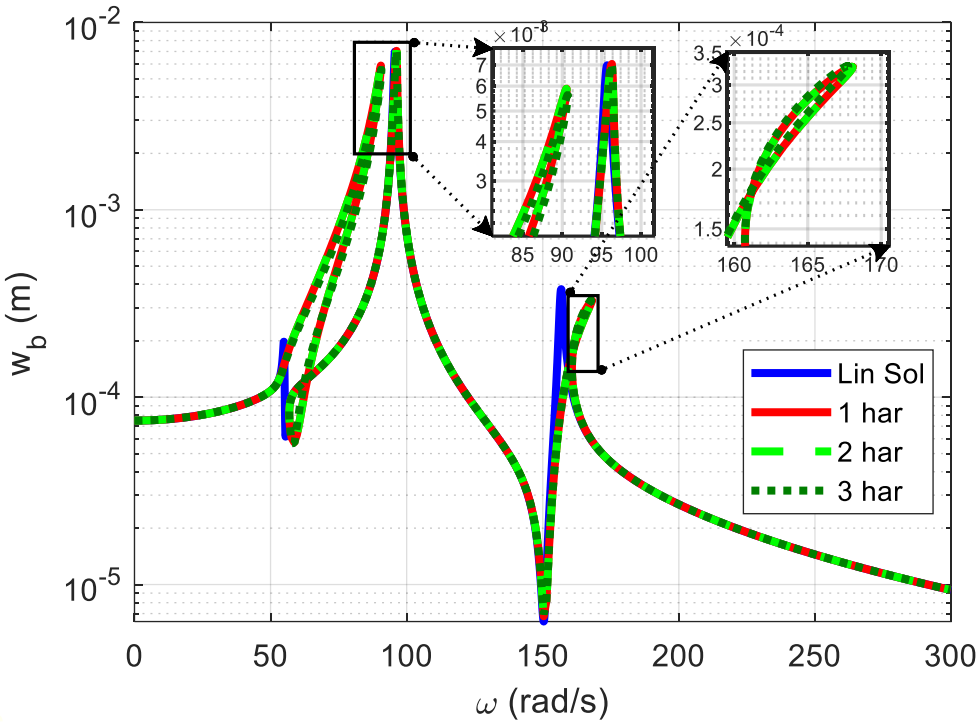

Figure 4.27. Comparison of the Harmonics Used for w_b

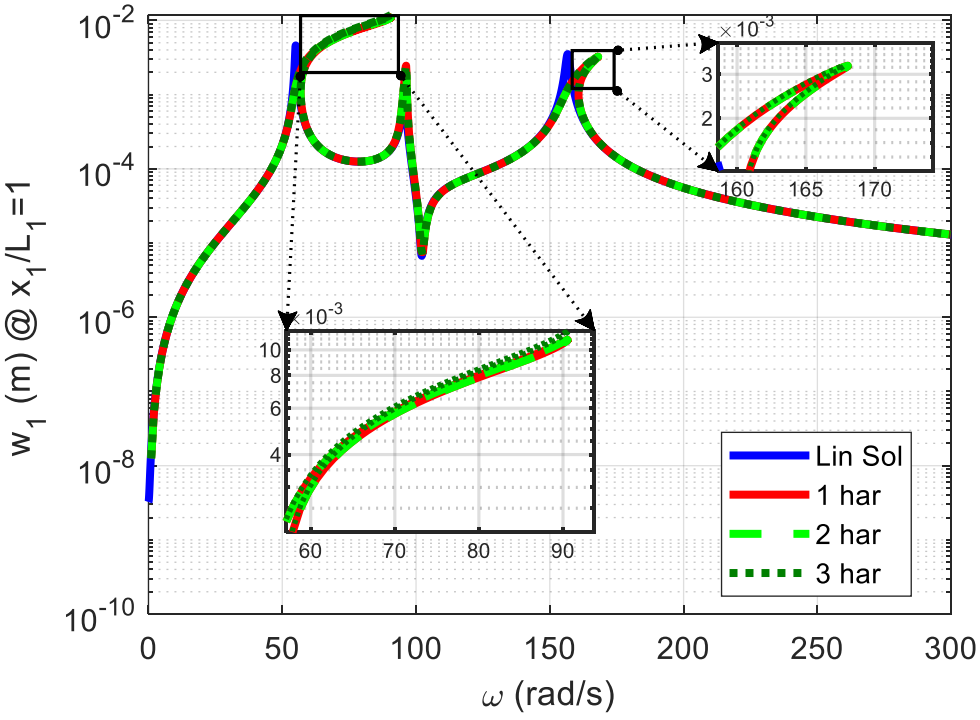

Figure 4.28. Comparison of the Harmonics Used at $x_1 / L_1 = 1$

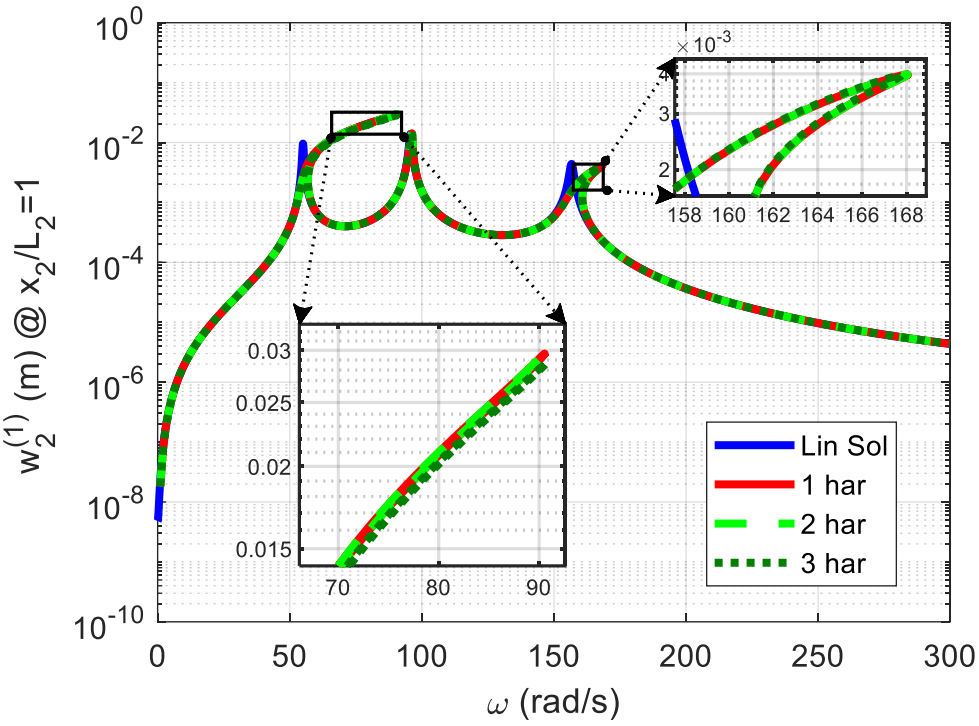

Figure 4.29. Comparison of the Harmonics Used at $x_2 / L_2 = 1$

The responses compared in Figure 4.27, Figure 4.28, and Figure 4.29 are identical. In the case of base excitation, the effect of the squared nonlinearity cannot be seen contrary to the fixed beam case since there are no notches in the responses obtained using higher harmonics. However, to obtain a more accurate response and observe whether notches start to form, two harmonic solution is used for the case studies.

4.2.2.3 Case Study Results

After verifying the linear model and observing the effect of the harmonics, several case studies are performed. As in Section 4.1.2.3, Case 1 is used as the basis for the system parameters, and one of the structural parameters is selected as the controlled variable while others are kept constant for each study to observe the effects of these parameters on the nonlinear response of the system. The controlled variables are selected the same as in Section 4.1.2.3, which are given in Table 4.2. The natural frequencies of the linear system for each case are presented in Table 4.5.

The first case study is carried out to observe the effect of the forcing amplitude on the nonlinear response of the model. Different excitation forcing amplitudes are considered, and the normalized responses with respect to forcing amplitudes are compared with each other. It can be seen from Figure 4.30, Figure 4.31, and Figure 4.32 that, when the forcing is very small, the responses are very similar to the response of the linear system. When the forcing is increased to 1N, the nonlinear response starts to differ from the linear one, and when forcing becomes 2N, cubic nonlinearity starts to take effect. As the forcing amplitude increases, the resonance frequency shifts to the right, which is the outcome of the cubic stiffness nonlinearity dominant in this system. Unlike Section 4.1.2.3, squared nonlinearity does not affect the nonlinear response since notches do not occur. Moreover, since the base mass is excited, resonance frequencies corresponding to the motion of the base mass, in this case, the second resonance, have greater amplitudes than the other frequencies. Additionally, as the effect of the nonlinearity increases, the first resonance tends to get closer to the second resonance, which increases its amplitude.

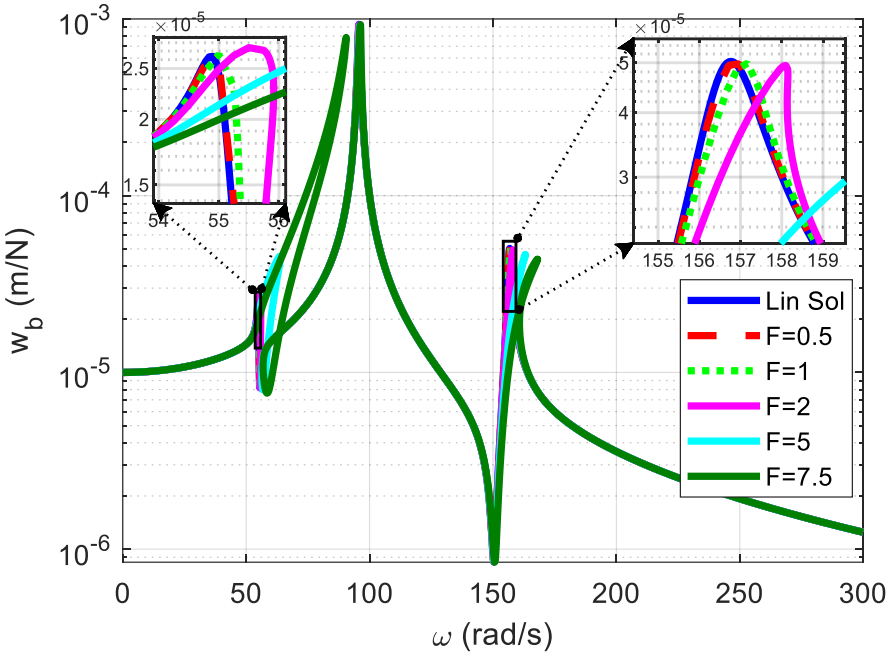

Figure 4.30. Effect of the Forcing Amplitude on the FRF of w_b for Case 1

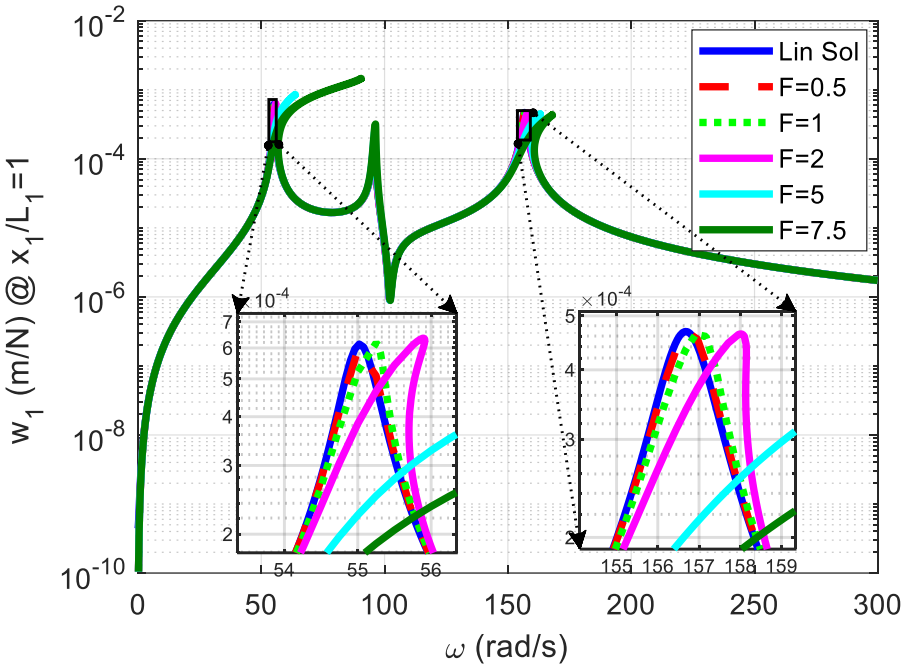

Figure 4.31. Effect of the Forcing Amplitude on the FRF at $x_1 / L_1 = 1$ for Case 1

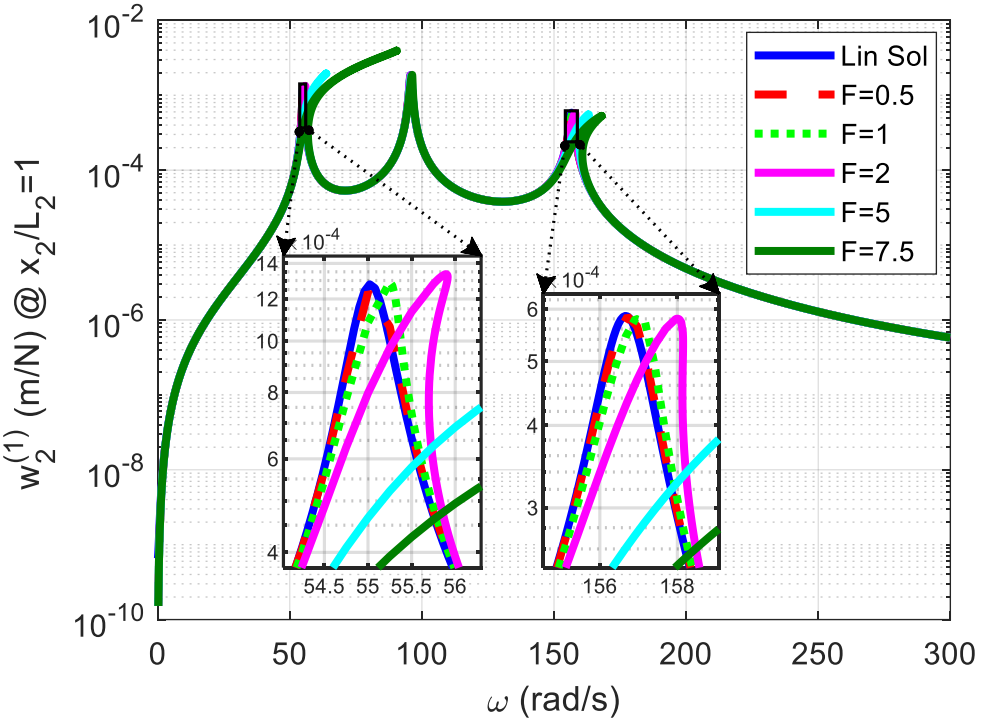

Figure 4.32. Effect of the Forcing Amplitude on the FRF at $x_2 / L_2 = 1$ for Case 1

In the second case study, by comparing Cases 2 and 3 in Figure 4.33, Figure 4.34, and Figure 4.35, the effect of the masses of the first and the second beams on the vibration characteristics and frequency responses are investigated. It can be understood that a decrease in the mass of the first beam causes the resonance frequencies to decrease; however, a decrease in the mass of the second beam causes the resonance frequencies to increase in contrast to Case 2. Moreover, the decrease in ρAL_2 causes the first resonance frequency and the second resonance frequency which are related to the first deformational mode of the beam and the mode of the base mass, respectively, to get closer to each other. Decreasing beyond a specific value causes these resonance frequencies to switch, as in Case 3. This amplifies the effect of the cubic nonlinearity on the second resonance as the curve leans to the right around that frequency. This effect also causes the second resonance of w_b to decrease significantly.

Table 4.5. Natural Frequencies for Each Case

	$\omega_1\,(rad/s)$	$\omega_2\,(rad/s)$	$\omega_3\,(rad/s)$
Ansys	55.019	95.693	156.60
Case 1	55.024	95.693	156.68
Case 2	29.567	92.518	126.82
Case 3	84.147	104.5	298.9
Case 4	54.352	93.865	152.26
Case 5	35.679	87.808	120.81
Case 6	53.429	95.873	151.69
Case 7	61.465	97.41	176.03
Case 8	39.053	91.056	115.99
Case 9	55.024	95.693	156.68
Case 10	55.024	95.693	156.68

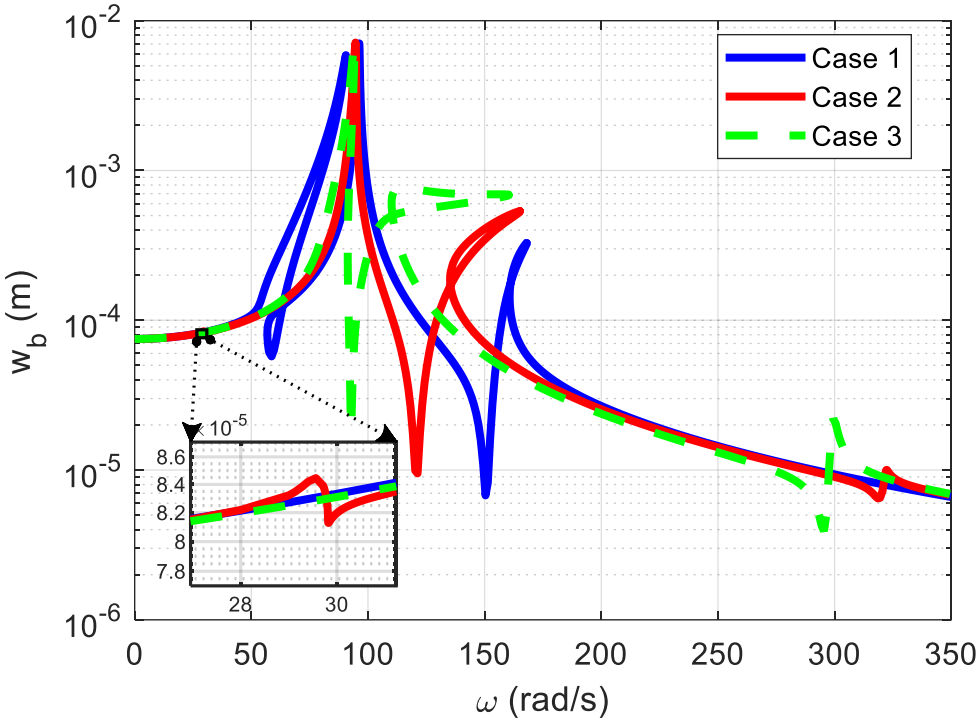

Figure 4.33. Comparison of the FRFs of w_b for the Cases 1, 2 and 3

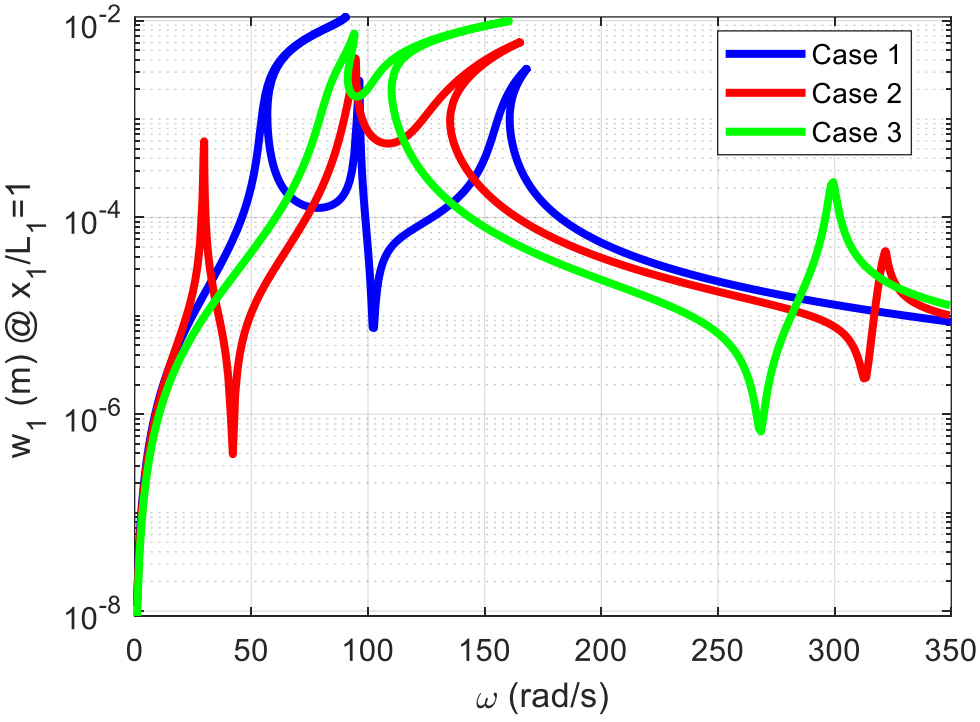

Figure 4.34. Comparison of the FRFs of the Cases 1, 2 and 3 at $x_1 / L_1 = 1$

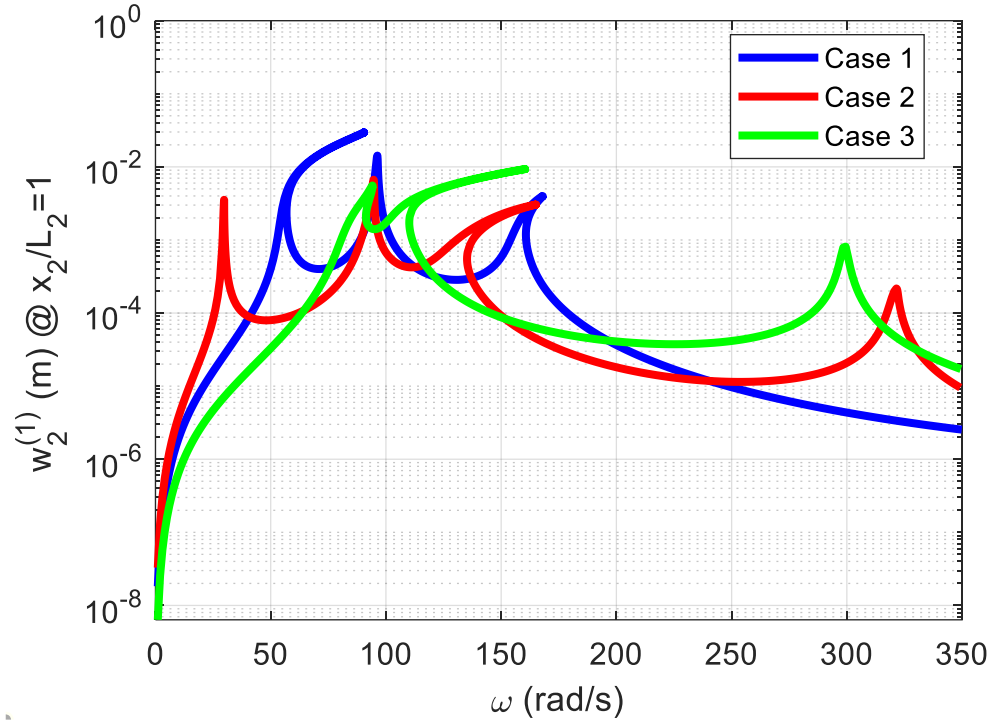

Figure 4.35. Comparison of the FRFs of the Cases 1, 2 and 3 at $x_2 / L_2 = 1$

In the third case study, the effect of the concentrated masses connected to the first and second beams on the vibration characteristics are studied by comparing Case 2 and 3 in Figure 4.36, Figure 4.37, and Figure 4.38. It is understood that the change in the mass of the concentrated mass attached to the first beam has a minor effect on the frequency responses compared to the change in the concentrated mass attached to the second beam. The increase in the second concentrated mass causes a decrease in the resonance frequencies. In addition, a decrease in the first resonance frequency causes a great decrease in the amplitude of w_b since it gets further away from the mode of w_b which decreases its effect on the first resonance.

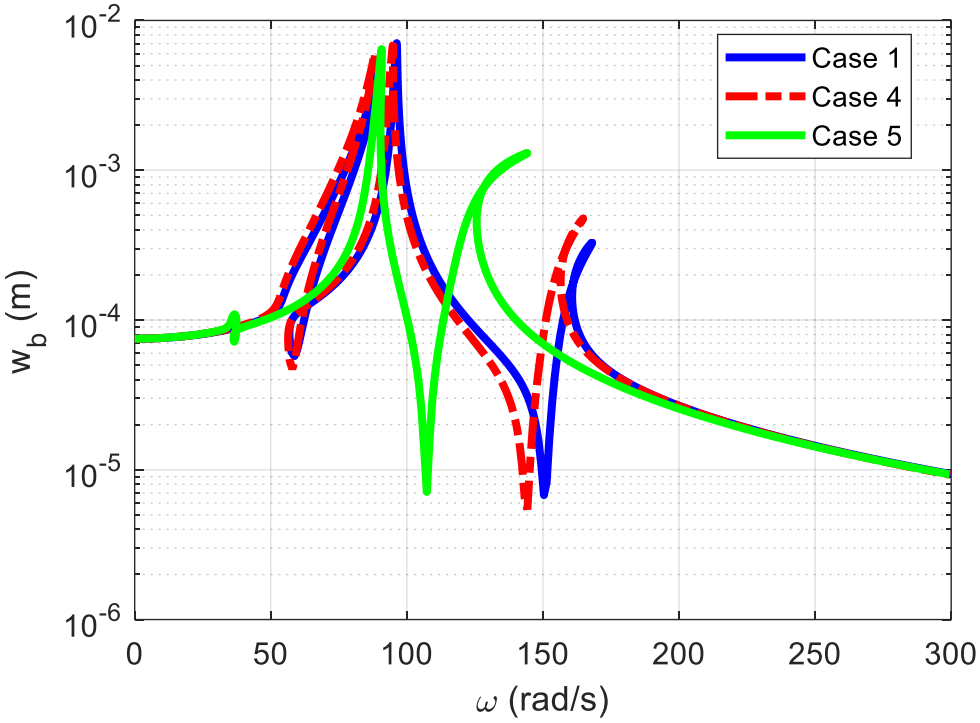

Figure 4.36. Comparison of the FRFs of w_b for the Cases 1, 4 and 5

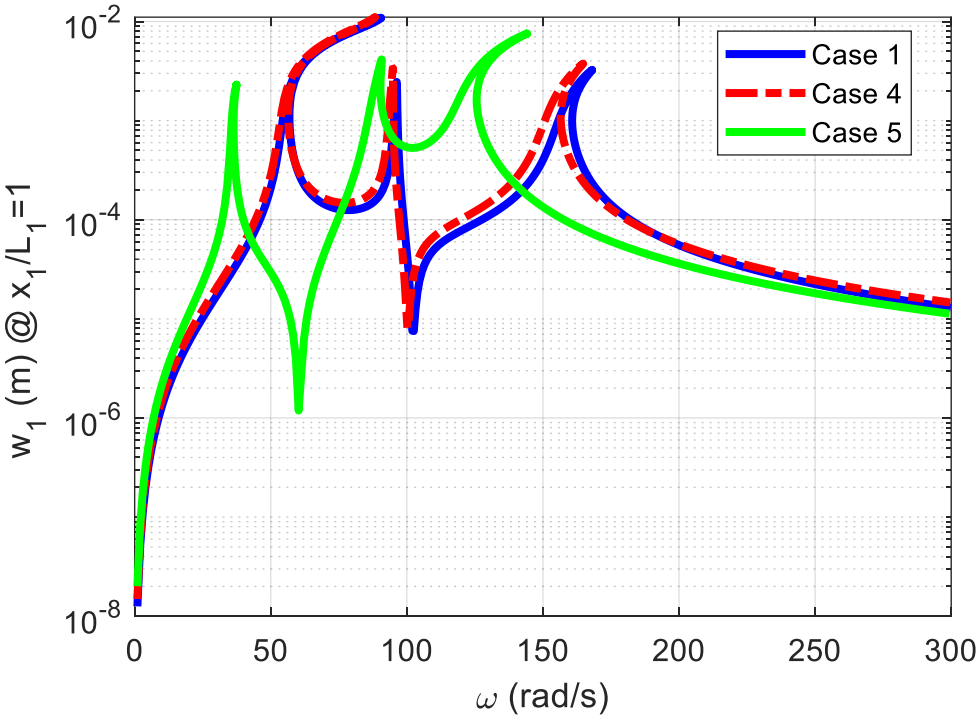

Figure 4.37. Comparison of the FRFs of the Cases 1, 4 and 5 at $x_1 / L_1 = 1$

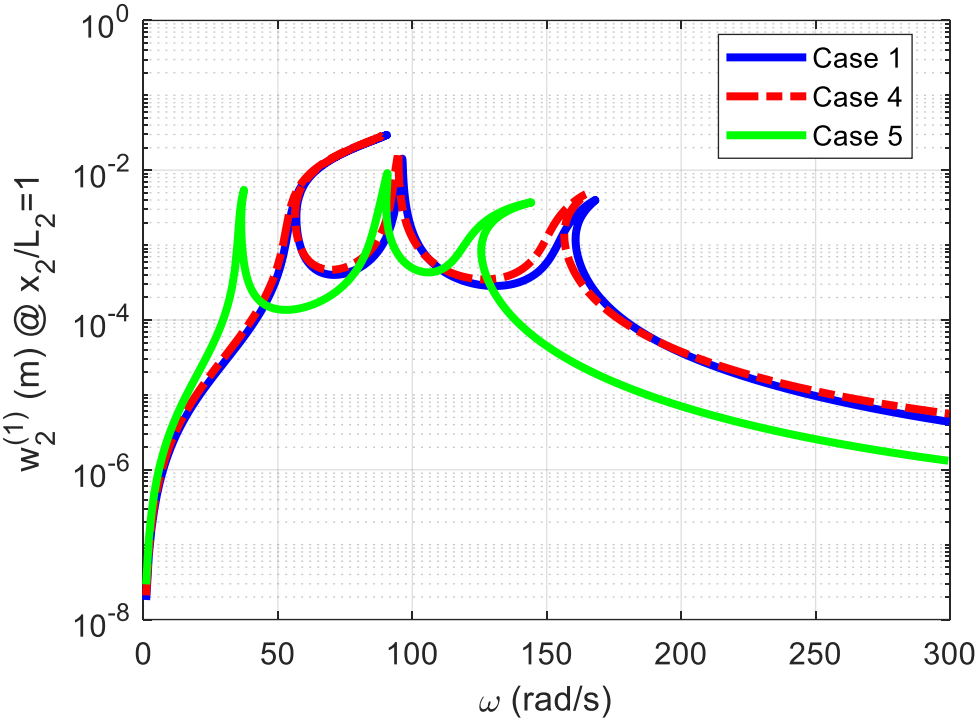

Figure 4.38. Comparison of the FRFs of the Cases 1, 4 and 5 at $x_2 / L_2 = 1$

The effect of the locations of the first and the second concentrated masses on the vibration characteristics is studied in the fourth case study. It is observed that the location of the first concentrated mass has little effect on the frequency responses and natural frequencies, as seen from the results of Case 6. On the other hand, the location of the second concentrated mass has a significant effect, especially on the second and third resonance points. Decreasing L_{M_2} / L_2 ratio causes an increase in the resonance frequencies, especially on the third one. Moreover, the amplitude of w_b at the second resonance decreases as L_{M_2} / L_2 decreases since nonlinearity starts to take greater effect.

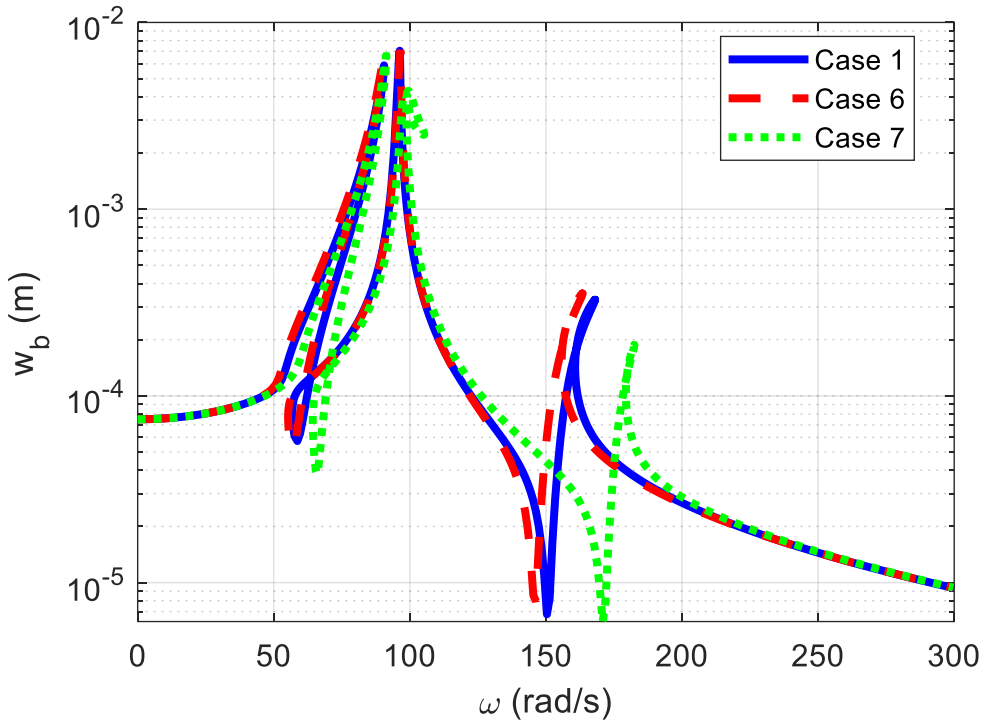

Figure 4.39. Comparison of the FRFs of w_b for the Cases 1, 6 and 7

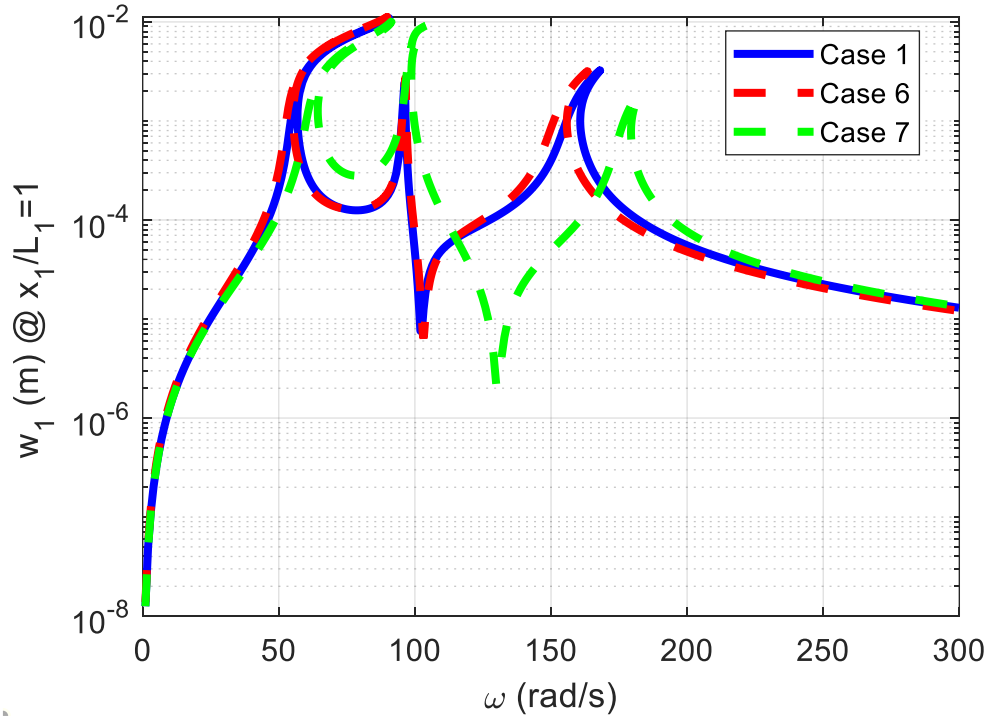

Figure 4.40. Comparison of the FRFs of the Cases 1, 6 and 7 at $x_1 / L_1 = 1$

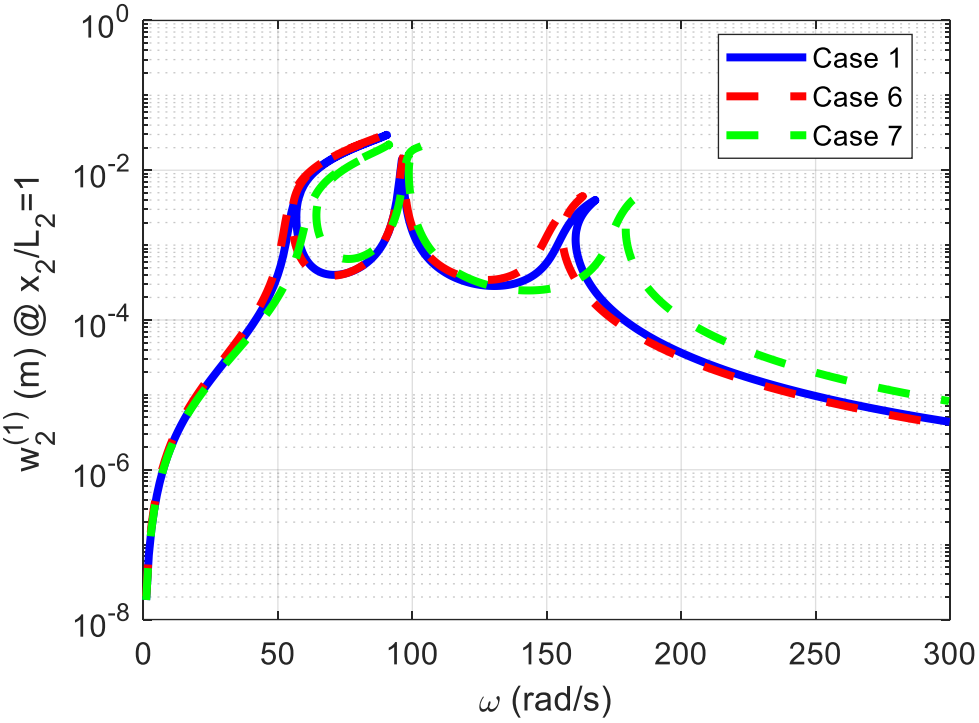

Figure 4.41. Comparison of the FRFs of the Cases 1, 6 and 7 at $x_2 / L_2 = 1$

The effect of the stiffness parameter of the first is investigated in the fifth case study. Since the stiffness parameter of the second beam is a dependent variable, its effect is not investigated. From Figure 4.42, Figure 4.43, and Figure 4.44, it is observed that a decrease in the stiffness causes the resonance frequencies to decrease also. Moreover, as the linear stiffness parameter decreases, the nonlinearities in the system become more dominant. Additionally, the effect of the quadratic nonlinearity becomes more apparent on the first beam around the first resonance, as seen in Figure 4.43.

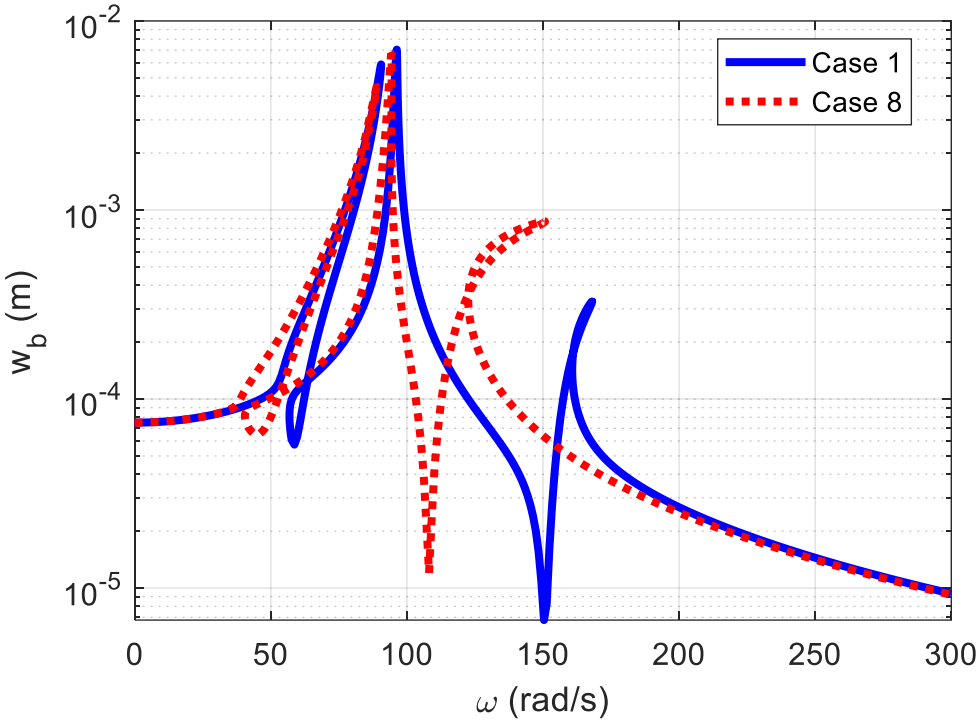

Figure 4.42. Comparison of the FRFs of w_b for the Cases 1 and 8

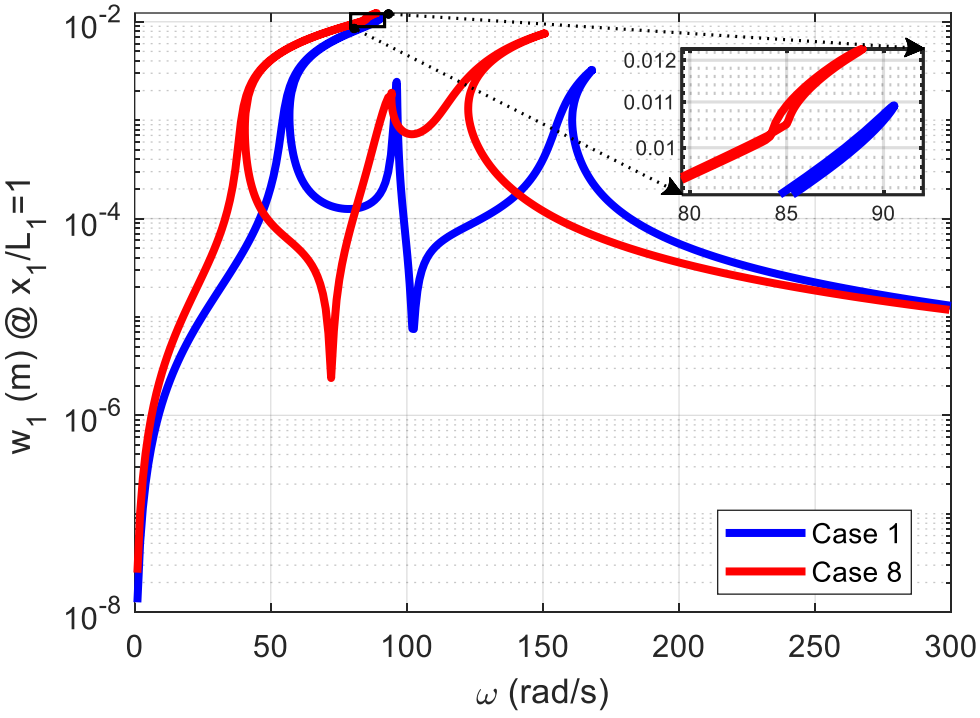

Figure 4.43. Comparison of the FRFs of the Cases 1 and 8 at $x_1 / L_1 = 1$

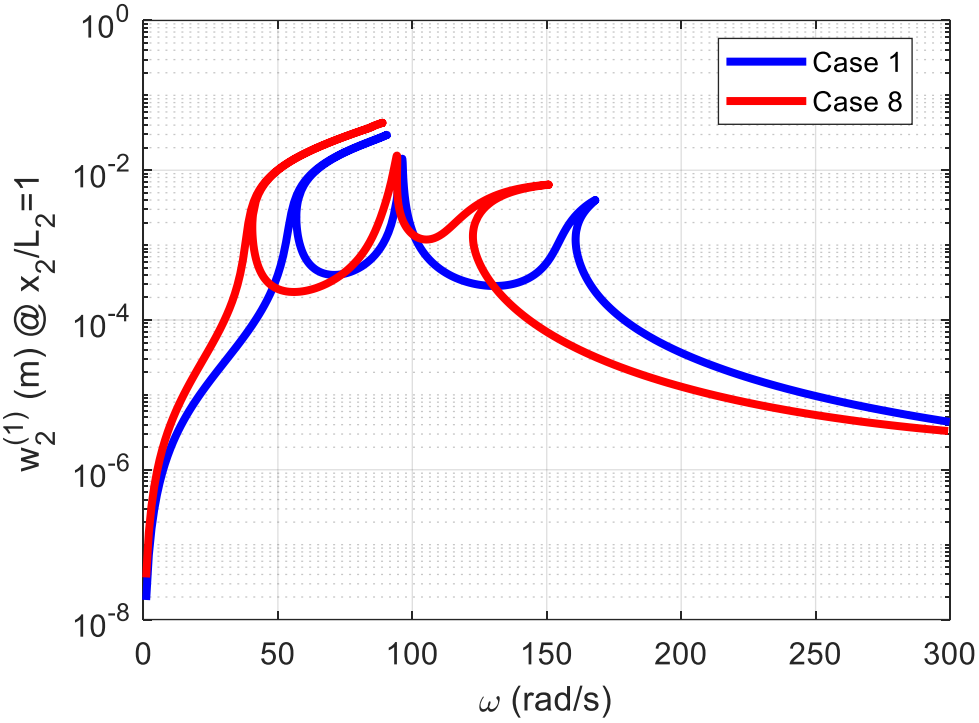

Figure 4.44. Comparison of the FRFs of the Cases 1 and 8 at $x_2 / L_2 = 1$

The effects of nonlinearities are studied in the sixth case study. These are cubic and quadratic nonlinearities. Cubic nonlinearity is proportional to $EA/\left(2L_1^{\,3}\right)$, and quadratic nonlinearity is inversely proportional to L_2 terms. Since the cubic nonlinearity parameter of the second beam is a dependent variable, its effect is not investigated. As seen in Figure 4.45, Figure 4.46, and Figure 4.47, decreasing the cubic nonlinearity parameter decreases its effect on the system, especially on the first and third resonance points, which are related to the deformational modes of the beam. However, a decrease in L_2 has nearly no effect on the system as the plots of Case 1, and Case 10 are nearly the same. It can be concluded that the effect of the cubic nonlinearity is more dominant compared to the squared one.

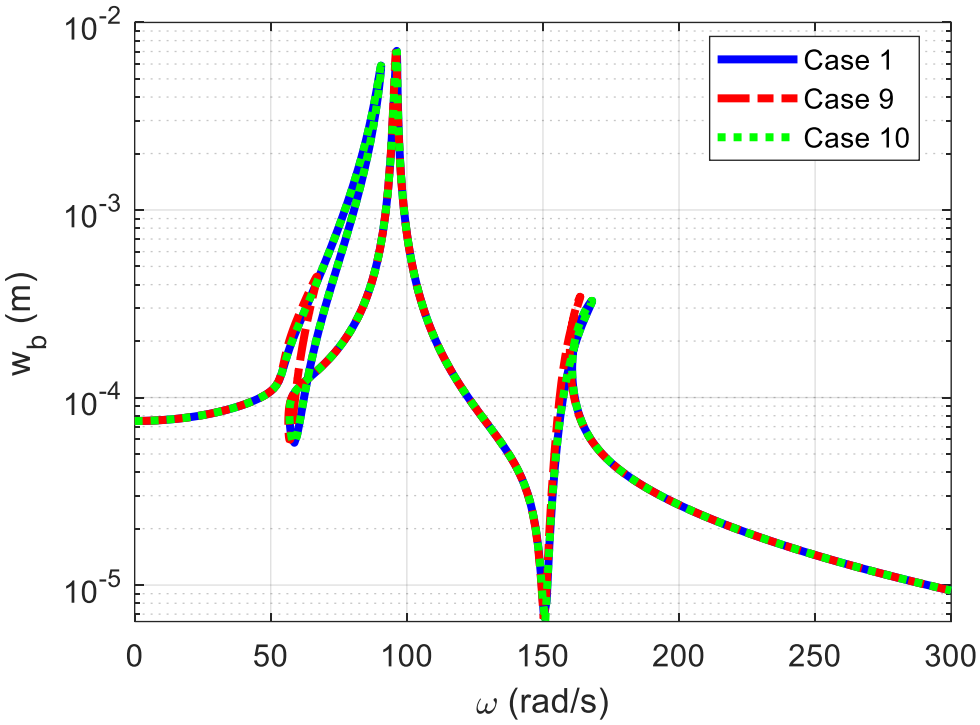

Figure 4.45. Comparison of the FRFs of w_b for the Cases 1, 9 and 10

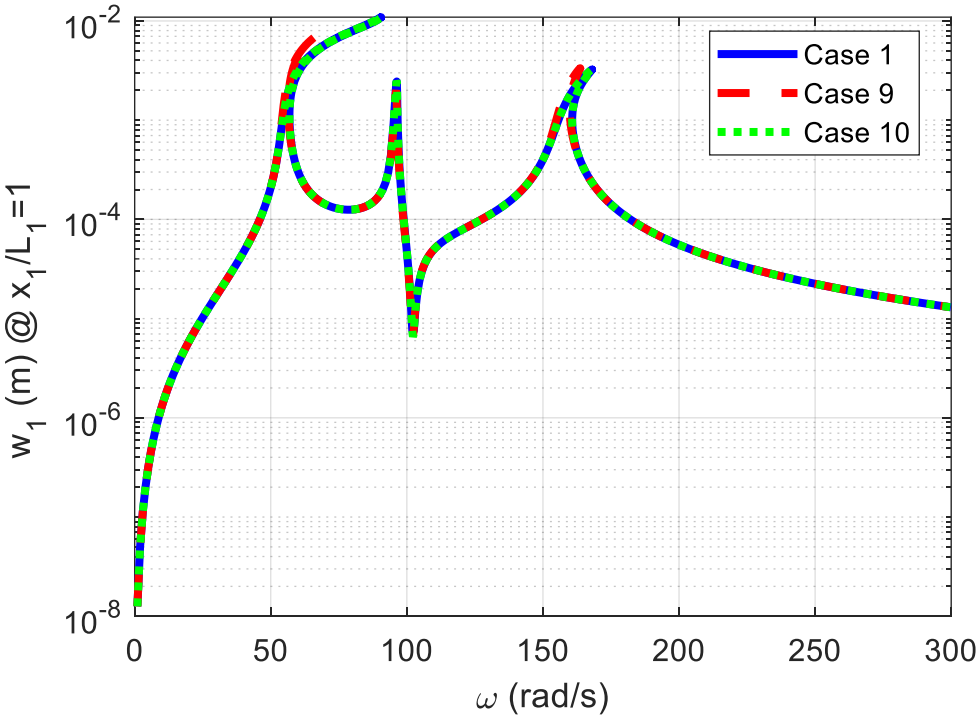

Figure 4.46. Comparison of the FRFs of the Cases 1, 9 and 10 at $x_1 / L_1 = 1$

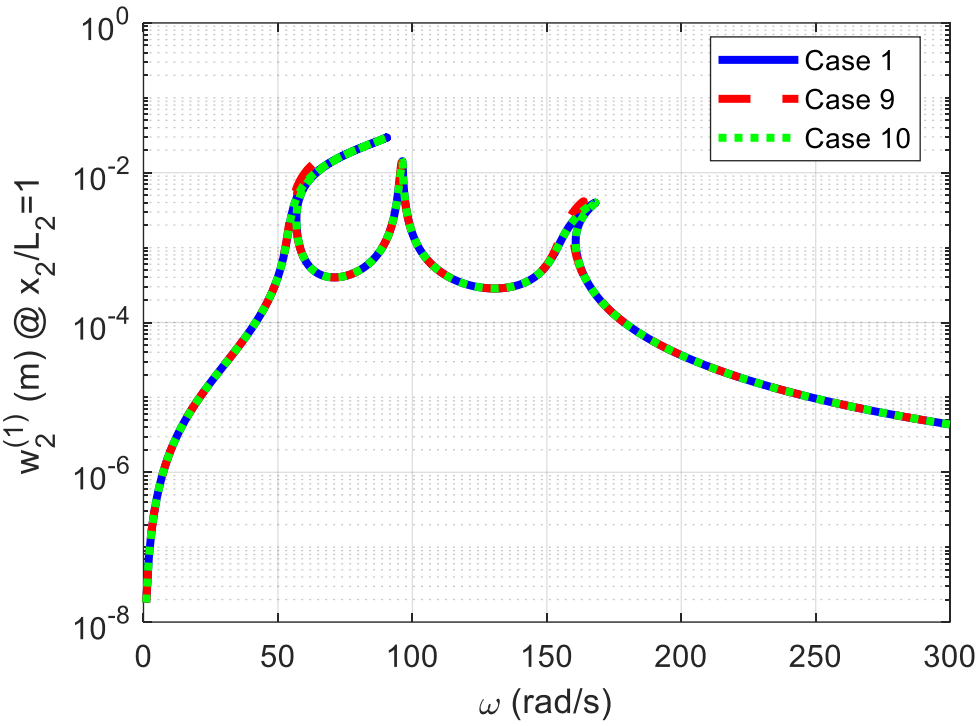

Figure 4.47. Comparison of the FRFs of the Cases 1, 9 and 10 at $x_2 / L_2 = 1$

CHAPTER 5

VIBRATION REDUCTION USING L-SHAPED BEAMS

In this chapter, L-shaped beams are proposed as vibration absorbers as alternatives to tuned mass dampers (TMDs). The system is constructed as a single DOF externally excited base mass to which an L-shaped beam is attached in order to reduce the amplitude of the vibration of the base mass. The schematic of the system can also be seen in Figure 3.1. The system parameters of the nonlinear L-shaped beam are optimized for several combinations of base mass, the spring attached to it, and the forcing applied to it. After that, linear L-shaped beams and cantilever beams are optimized to reduce vibrations on the base mass, and the effects of nonlinearities on the frequency responses of the base are investigated.

5.1 Optimization of the Nonlinear System

The parameters of the nonlinear L-shaped beam are optimized to reduce the maximum amplitude of the vibration of the system. There are 13 independent system parameters of the L-shaped beam needed to be optimized for vibration reduction. Since optimization of these many parameters will take a lot of time and require too much computational power, these parameters are reduced to 10 by assuming the materials, the cross sections, and the structural damping coefficients of the first and the second beams are the same, i.e. $\rho = \rho_1 = \rho_2$, $E = E_1 = E_2$, $A = A_1 = A_2$, $I = I_1 = I_2$, $\gamma = \gamma_1 = \gamma_2$. After reducing the system parameters, the optimization space is bounded by selecting an upper and a lower limit for each parameter. These limits can be seen in Table 5.1.

Table 5.1. Upper and lower limits for system parameters

	$\rho AL_1(kg)$	$\rho AL_2(kg)$	$M_1(kg)$	$M_2(kg)$	$\frac{L_{M_1}}{L_1}$
Lower Limit	0.025	0.025	0.025	0.025	0
Upper Limit	$0.1 \cdot M_b$	$0.1 \cdot M_b$	$0.1 \cdot M_b$	$0.1 \cdot M_b$	1
	$\frac{L_{M_2}}{L_2}$	$\frac{EI}{L_1^3}\left(\frac{N}{m}\right)$	$\frac{EA}{2L_1^3}\left(\frac{N}{m^3}\right)$	$L_2(m)$	γ
Lower Limit	0	150	$85 \cdot 10^4$	0.05	0.001
Upper Limit	1	$15 \cdot 10^3$	$85 \cdot 10^7$	0.5	0.75

Additionally, to limit the total mass of the L-shaped beam, a constraint equation is introduced as,

$$\rho AL_1 + \rho AL_2 + M_1 + M_2 \leq 0.1 \cdot M_b \,. \tag{5.1}$$

The L-shaped beam parameters are optimized for several cases. In each case, different combinations of the base mass (M_b) and the base spring (k_b) are selected, whereas the structural damping ratio of the base spring (γ_b) is selected as 0.01 for all cases. These selected base parameters can be seen in Table 5.2.

Table 5.2. Selected base parameters for each case

CASES	**1**	**2**	**3**	**4**
$M_b(kg)$	5	10	10	15
$k_b\left(\frac{N}{m}\right)$	$10 \cdot 10^4$	$10 \cdot 10^4$	$20 \cdot 10^4$	$15 \cdot 10^4$

The cost function is selected as the maximum amplitude of the frequency response of the base mass (w_b) in a frequency range of 0 and 300 rad/s. Since the cost function is highly nonlinear in the optimization space due to the nature of the nonlinear system, MATLAB's Genetic Algorithm (GA) function is used for optimization. Then, the optimized systems are compared with alternative TMD systems.

5.1.1 Mathematical Formulization of the TMD System

To compare the L-shaped beam system with the TMD counterpart, the governing mathematical equations are obtained. The system is constructed as a two DOF mass-spring system with structural damping, as in the figure below.

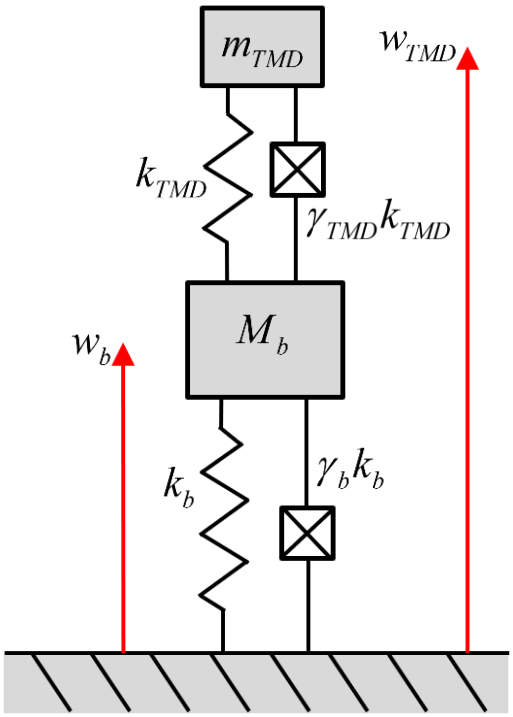

Figure 5.1. Schematic of the TMD System

The governing ODE of the system can be written as,

$$\mathbf{M}_{\mathbf{TMD}}\ddot{\mathbf{q}}_{\mathbf{TMD}} + \left(\mathbf{K}_{\mathbf{TMD}} + \mathbf{i}\mathbf{H}_{\mathbf{TMD}}\right)\mathbf{q}_{\mathbf{TMD}} = \mathbf{f}_{\mathbf{TMD}}, \tag{5.2}$$

where,

$$\mathbf{M_{TMD}} = \begin{bmatrix} M_b & 0 \\ 0 & m_{TMD} \end{bmatrix}, \tag{5.3}$$

$$\mathbf{K_{TMD}} = \begin{bmatrix} k_b + k_{TMD} & -k_{TMD} \\ -k_{TMD} & k_{TMD} \end{bmatrix}, \tag{5.4}$$

$$\mathbf{H_{TMD}} = \begin{bmatrix} \gamma_b k_b + \gamma_{TMD} k_{TMD} & -\gamma_{TMD} k_{TMD} \\ -\gamma_{TMD} k_{TMD} & \gamma_{TMD} k_{TMD} \end{bmatrix}, \tag{5.5}$$

$$\mathbf{q_{TMD}} = \begin{bmatrix} w_b \\ w_{TMD} \end{bmatrix}, \tag{5.6}$$

$$\mathbf{f_{TMD}} = \begin{bmatrix} F_0 \sin(\omega t) \\ 0 \end{bmatrix}. \tag{5.7}$$

In the equations above, m_{TMD}, k_{TMD}, and γ_{TMD} represent the mass of the TMD, the stiffness of the spring connected to base mass, and the structural damping ratio, respectively.

5.1.2 Case Study Results

The frequency responses of the single DOF system, the optimized L-shaped beams for the selected cases under different forcing amplitudes, and their TMD counterparts are compared in the figures below. In order to compare them in the same plot, normalized responses w.r.t the forcing amplitude are obtained. The normalized maximum amplitude results for each case can be seen in Table 5.3, the optimized system parameters are given in Table 5.4-Table 5.7 and the normalized responses of the optimized system can be seen in Figure 5.2-Figure 5.13.

Table 5.3. Maximum Normalized Amplitudes for Each Case Study

	Case 1	Case 2	Case 3	Case 4
Single DOF	$1.000 \cdot 10^{-3}$	$9.992 \cdot 10^{-4}$	$5.000 \cdot 10^{-4}$	$6.661 \cdot 10^{-4}$
TMD	$4.732 \cdot 10^{-5}$	$4.539 \cdot 10^{-5}$	$2.264 \cdot 10^{-5}$	$3.070 \cdot 10^{-5}$
$F_0 = 5N$	$5.109 \cdot 10^{-5}$	$4.972 \cdot 10^{-5}$	$2.625 \cdot 10^{-5}$	$3.221 \cdot 10^{-5}$
$F_0 = 15N$	$5.328 \cdot 10^{-5}$	$5.279 \cdot 10^{-5}$	$2.566 \cdot 10^{-5}$	$3.093 \cdot 10^{-5}$
$F_0 = 30N$	$5.465 \cdot 10^{-5}$	$4.895 \cdot 10^{-5}$	$2.635 \cdot 10^{-5}$	$3.174 \cdot 10^{-5}$

Table 5.4. Optimized System Parameters for Case 1

	$F_0 = 5N$	$F_0 = 15N$	$F_0 = 30N$
$\rho A L_1 (kg)$	0.0803	0.165	0.244
$\rho A L_2 (kg)$	0.206	0.0740	0.0996
$M_1 (kg)$	0.100	0.156	0.0915
$M_2 (kg)$	0.101	0.100	0.0620
$\frac{L_{M_1}}{L_1}$	0.463	0.500	0.448
$\frac{L_{M_2}}{L_2}$	0.612	0.0760	0.202
$\frac{EI}{L_1^3}\left(\frac{N}{m}\right)$	945	1243	1222
$\frac{EA}{2L_1^3}\left(\frac{N}{m^3}\right)$	$9.12 \cdot 10^7$	$4.64 \cdot 10^7$	$1.25 \cdot 10^7$
$L_2 (m)$	0.228	0.144	0.173
γ	0.354	0.347	0.340

Table 5.5. Optimized System Parameters for Case 2

	$F_0 = 5N$	$F_0 = 15N$	$F_0 = 30N$
$\rho A L_1 (kg)$	0.243	0.267	0.200
$\rho A L_2 (kg)$	0.530	0.0675	0.117
$M_1 (kg)$	0.0281	0.273	0.231
$M_2 (kg)$	0.1865	0.390	0.446
$\frac{L_{M_1}}{L_1}$	0.809	0.526	0.849
$\frac{L_{M_2}}{L_2}$	0.774	0.101	0.280
$\frac{EI}{L_1^3}\left(\frac{N}{m}\right)$	1062	1450	2143
$\frac{EA}{2L_1^3}\left(\frac{N}{m^3}\right)$	$1.58 \cdot 10^8$	$5.58 \cdot 10^7$	$2.30 \cdot 10^7$
$L_2 (m)$	0.108	0.193	0.175
γ	0.351	0.383	0.3611

Table 5.6. Optimized System Parameters for Case 3

	$F_0 = 5N$	$F_0 = 15N$	$F_0 = 30N$
$\rho A L_1 (kg)$	0.437	0.177	0.460
$\rho A L_2 (kg)$	0.107	0.395	0.139
$M_1 (kg)$	0.285	0.246	0.172
$M_2 (kg)$	0.130	0.147	0.222
$\frac{L_{M_1}}{L_1}$	0.680	0.599	0.539
$\frac{L_{M_2}}{L_2}$	0.310	0.575	0.215
$\frac{EI}{L_1^3}\left(\frac{N}{m}\right)$	2447	1742	2735
$\frac{EA}{2L_1^3}\left(\frac{N}{m^3}\right)$	$6.36 \cdot 10^7$	$2.96 \cdot 10^7$	$5.13 \cdot 10^7$
$L_2 (m)$	0.128	0.229	0.176
γ	0.330	0.349	0.335

Table 5.7. Optimized System Parameters for Case 4

	$F_0 = 5N$	$F_0 = 15N$	$F_0 = 30N$
$\rho A L_1 (kg)$	0.185	0.0793	0.151
$\rho A L_2 (kg)$	0.126	0.252	0.427
$M_1 (kg)$	0.877	0.448	0.325
$M_2 (kg)$	0.303	0.722	0.595
$\frac{L_{M_1}}{L_1}$	0.770	0.917	0.836
$\frac{L_{M_2}}{L_2}$	0.0807	0.890	0.445
$\frac{EI}{L_1^3}\left(\frac{N}{m}\right)$	2528	2260	1483
$\frac{EA}{2L_1^3}\left(\frac{N}{m^3}\right)$	$4.84 \cdot 10^7$	$3.46 \cdot 10^7$	$4.52 \cdot 10^7$
$L_2 (m)$	0.161	0.150	0.102
γ	0.357	0.379	0.429

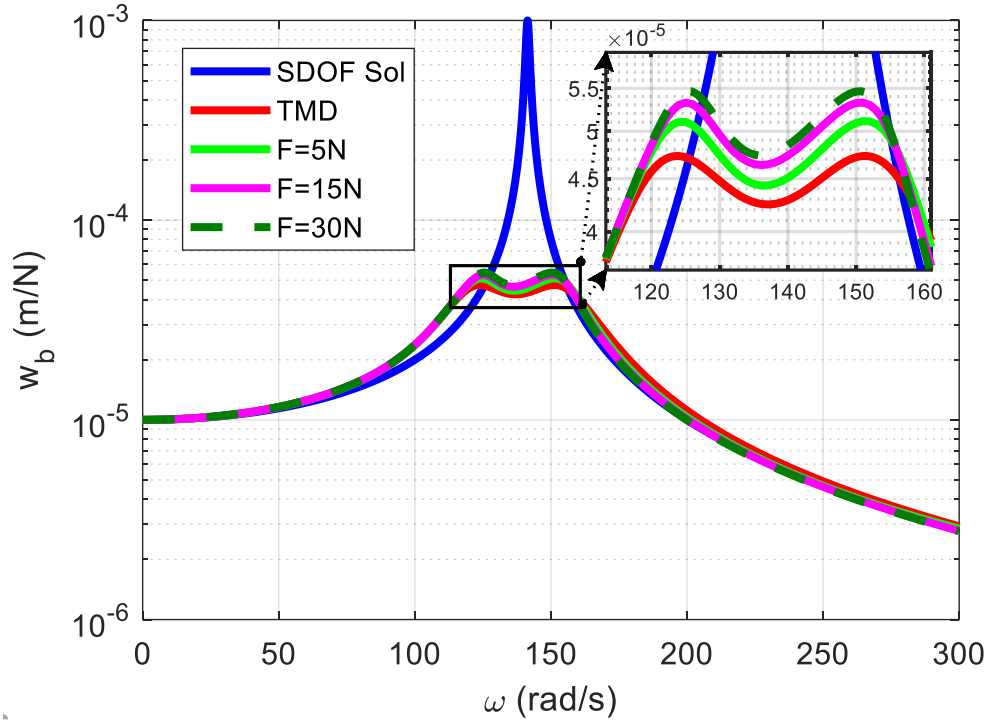

Figure 5.2. Frequency Response of w_b for Case 1

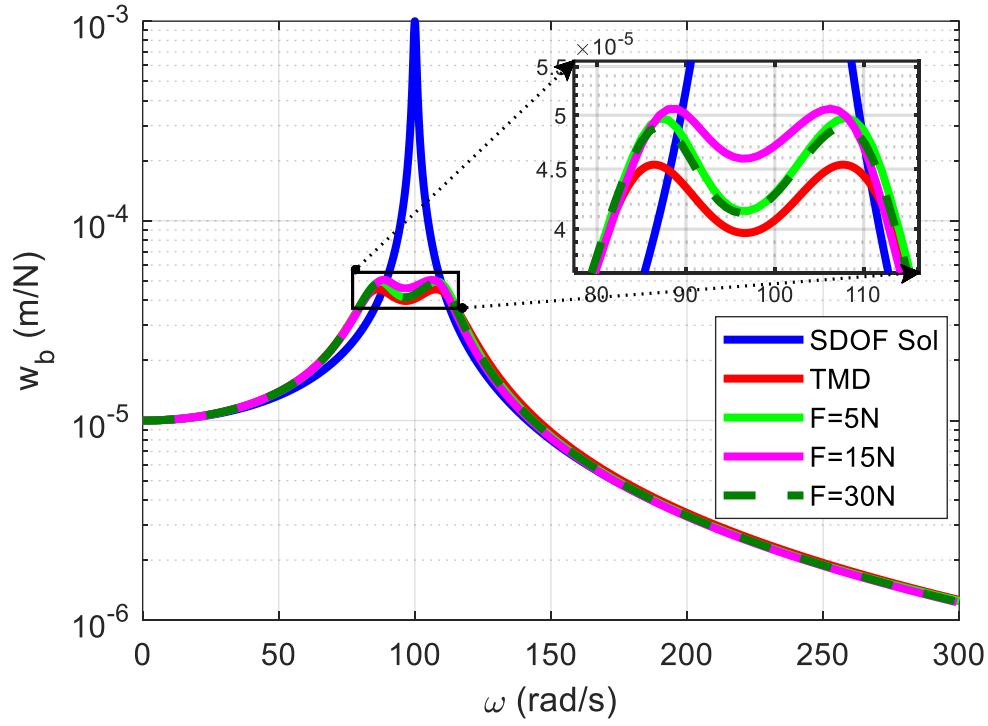

Figure 5.3. Frequency Response of w_b for Case 2

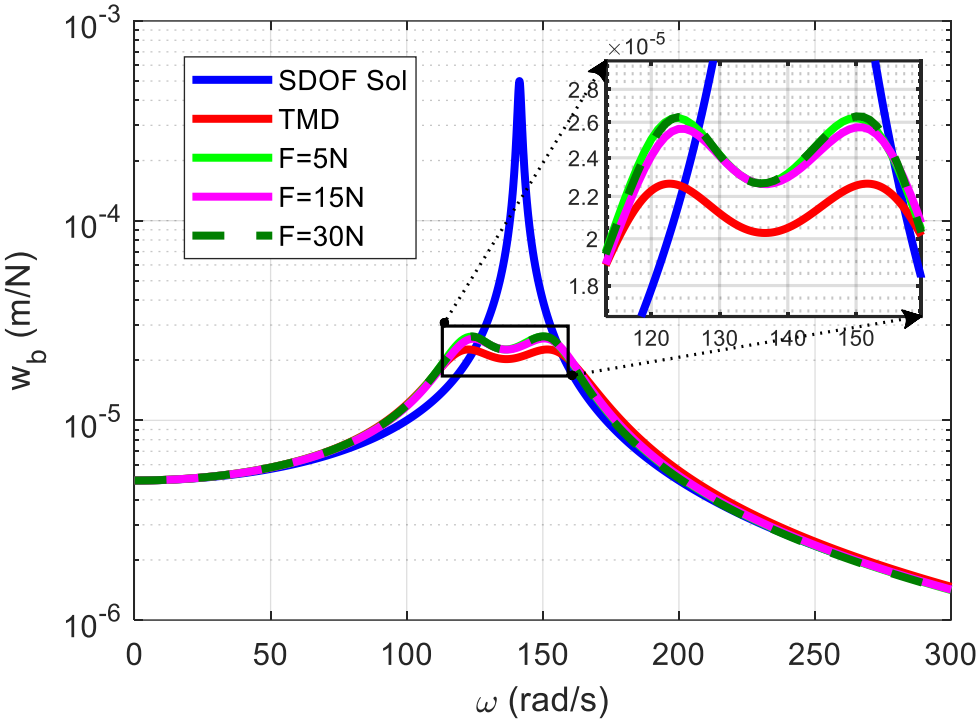

Figure 5.4. Frequency Response of w_b for Case 3

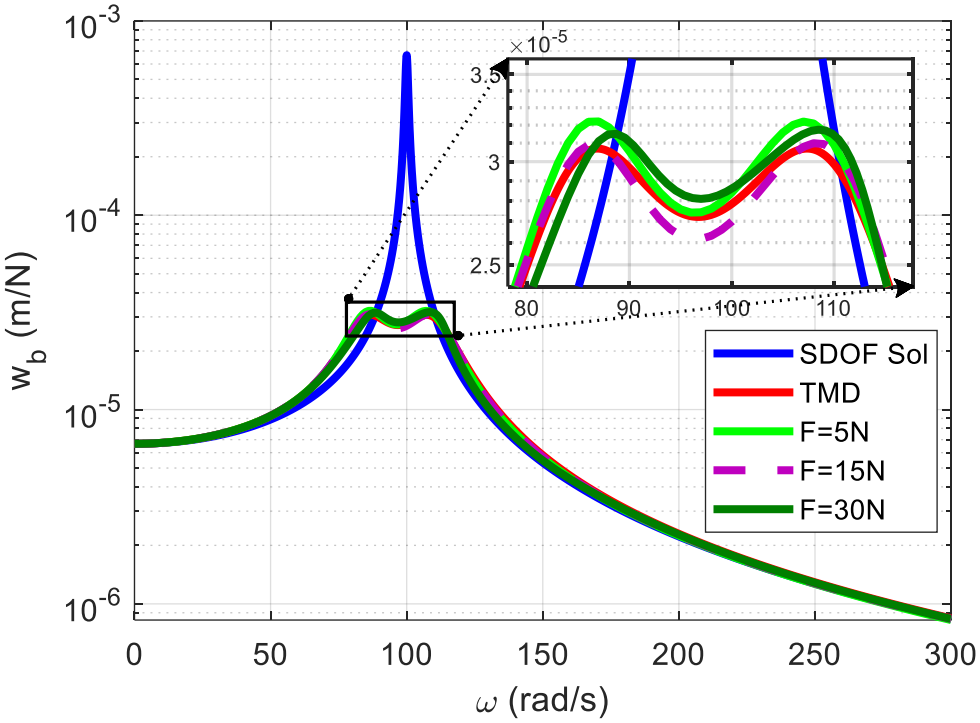

Figure 5.5. Frequency Response of w_b for Case 4

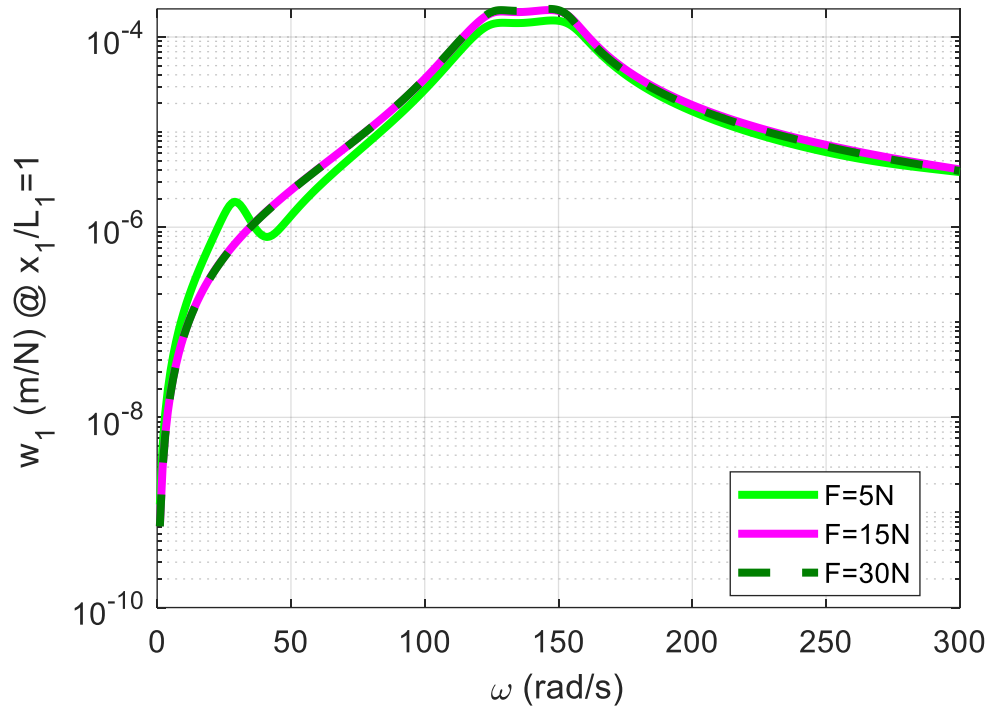

Figure 5.6. Frequency Response for Case 1 at $x_1 / L_1 = 1$

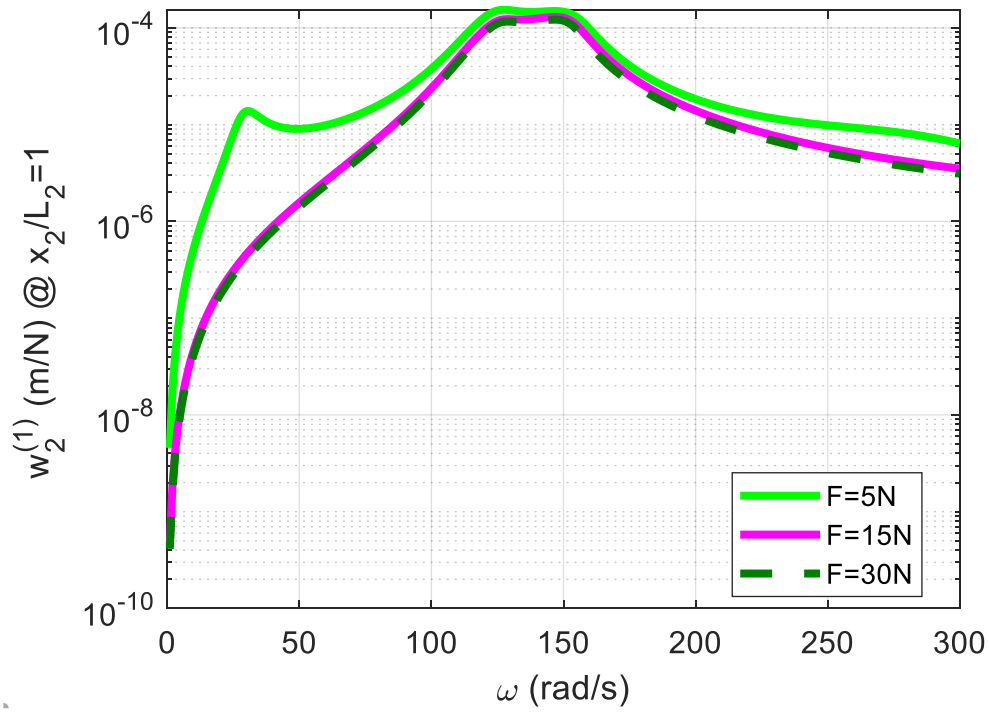

Figure 5.7. Frequency Response for Case 1 at $x_2 / L_2 = 1$

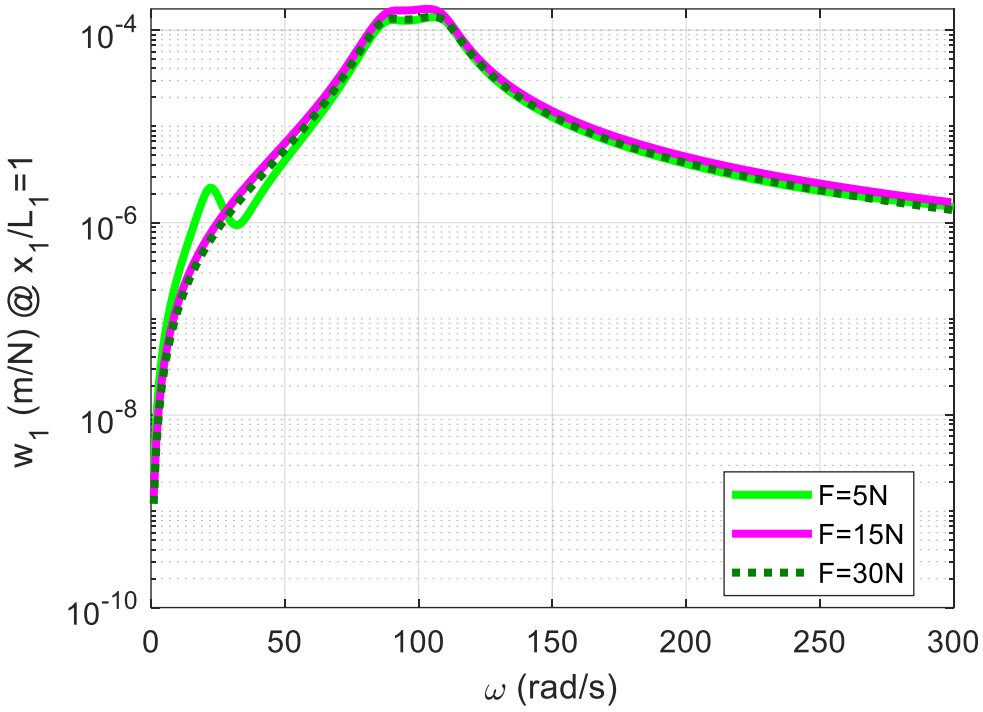

Figure 5.8. Frequency Response for Case 2 at $x_1 / L_1 = 1$

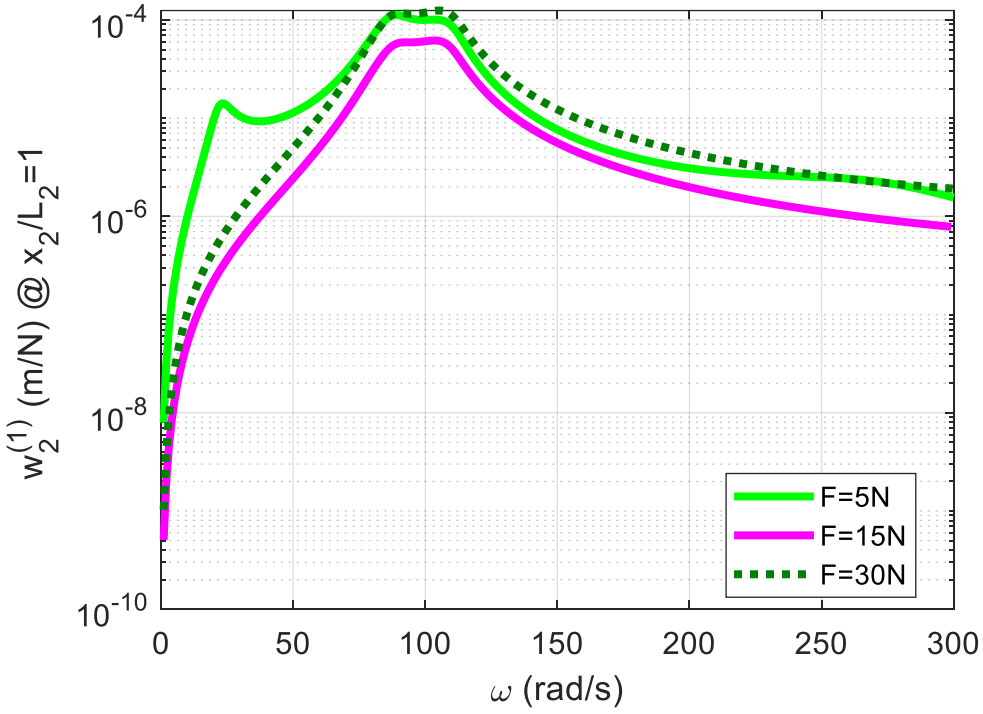

Figure 5.9. Frequency Response for Case 2 at $x_2 / L_2 = 1$

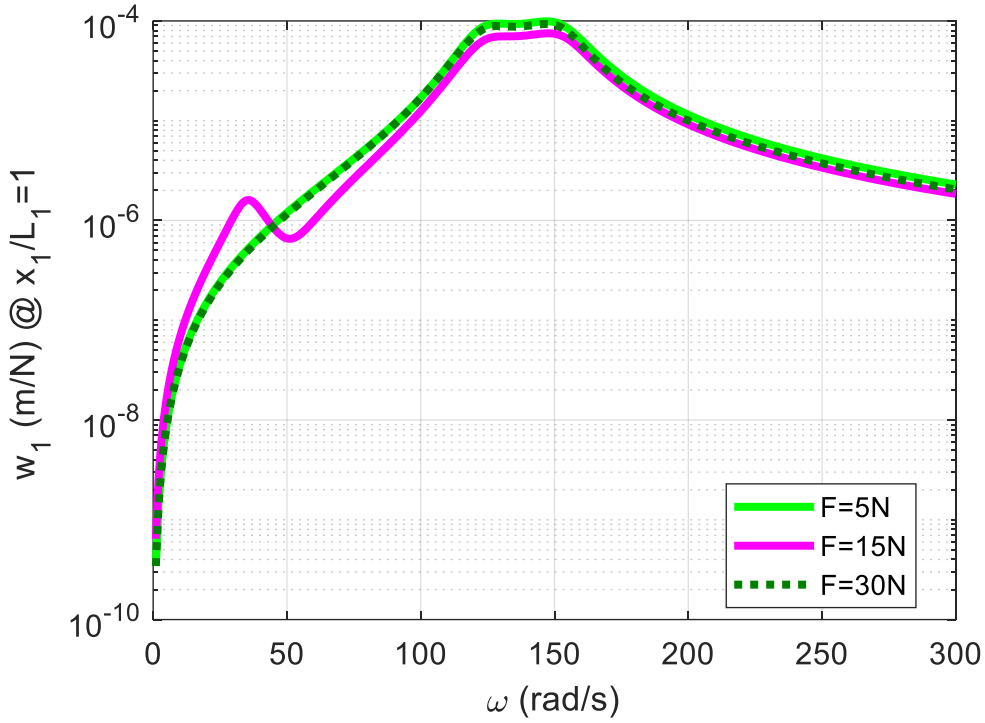

Figure 5.10. Frequency Response for Case 3 at $x_1 / L_1 = 1$

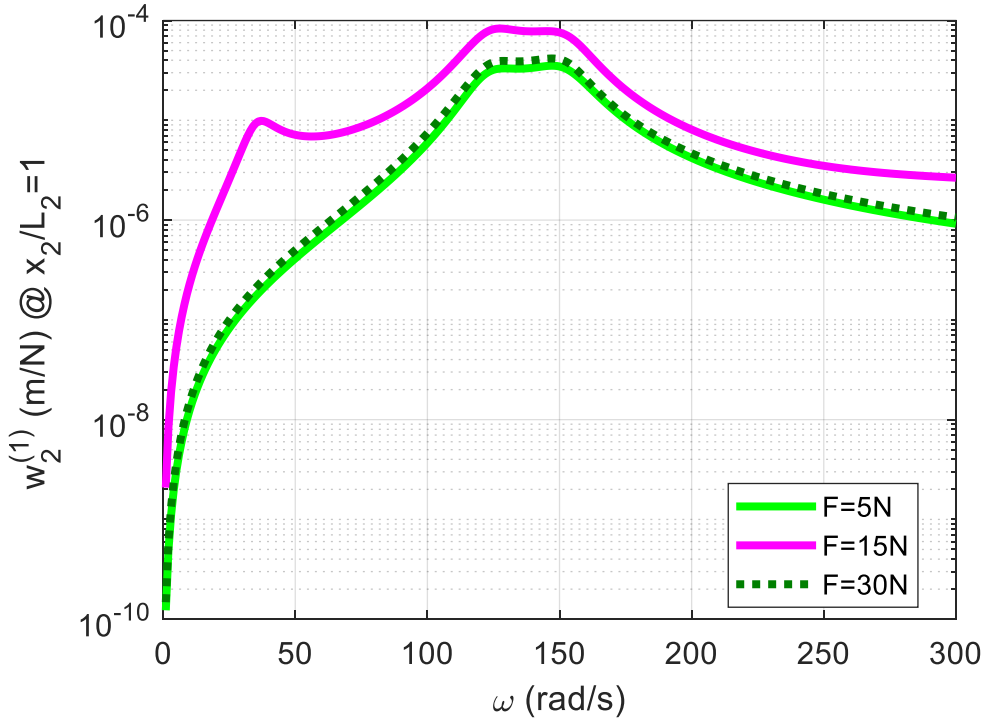

Figure 5.11. Frequency Response for Case 3 at $x_2 / L_2 = 1$

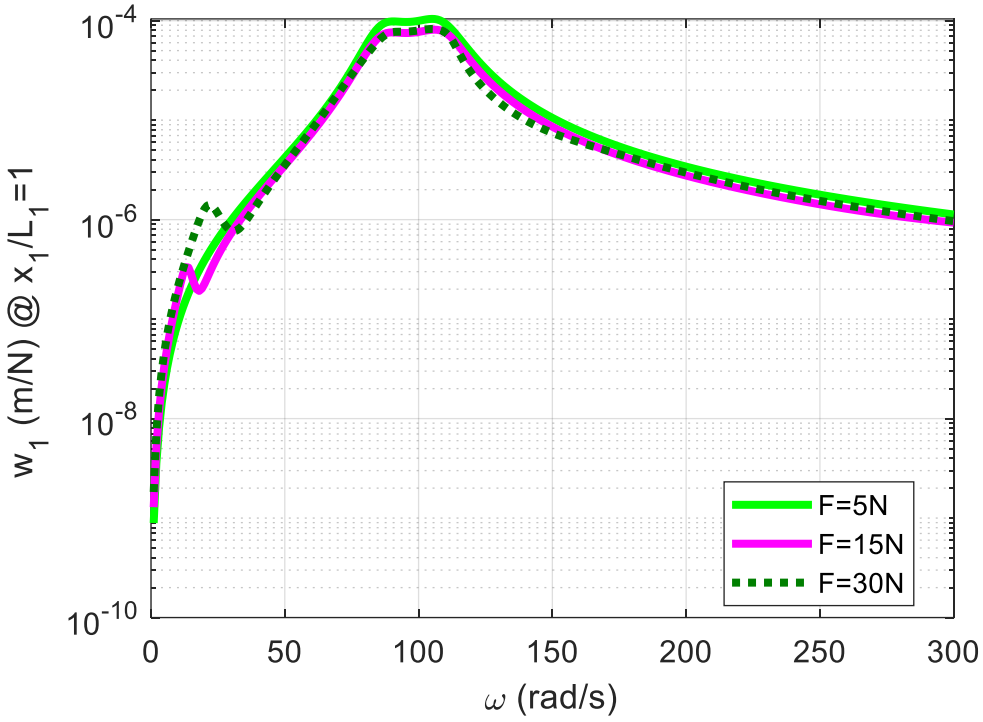

Figure 5.12. Frequency Response for Case 4 at $x_1 / L_1 = 1$

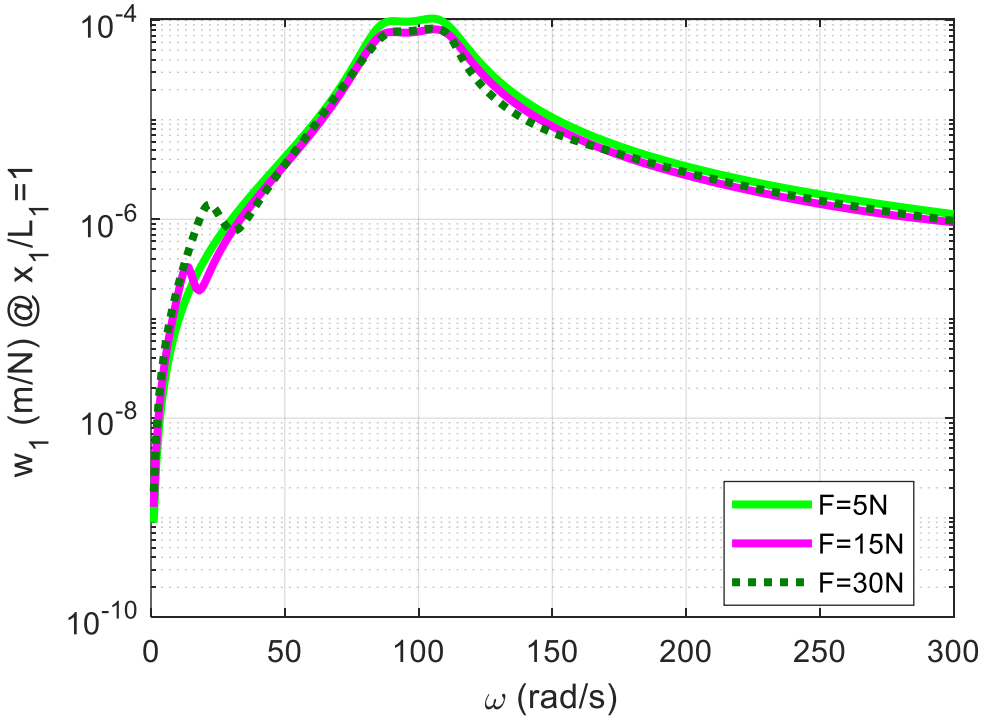

Figure 5.13. Frequency Response for Case 4 at $x_2 / L_2 = 1$

As it can be seen from Figure 5.2-Figure 5.5, vibration is reduced by approximately 20 times both for the TMD case and nonlinear L-shaped beam with different forcing cases. However, TMD gives slightly better results than the L-shaped beam, as seen in Table 5.3. The cause of the differences is probably due to nonlinear optimization not finding the global minimum as the optimization space is high dimensional, and the system is highly nonlinear. If the global minimums of the L-shaped beam cases are found, the responses of them probably converge to the TMD cases. Additionally, investigating the optimized parameters, it is observed that the damping ratio of the beam for all cases ranges between 0.33-0.43. It means that, for optimization, the damping ratio should be between this range.

5.2 Investigation of the Effects of Nonlinearities on the Optimized Linear System

In this section, linear L-shaped beams are used as vibration absorbers, and the frequency responses are obtained for different cases. These results are compared with optimized linear cantilever beam counterparts since cantilever beams are widely used as vibration absorbers in literature such as studies [26]–[30]. Then, the effect of the nonlinearities on frequency responses of both the cantilever beam and the L-shaped beam vibration absorbers are investigated.

For the calculations, a sinusoidal base excitation with an amplitude of 30N is assumed to be applied as in Equation (4.14).

5.2.1 Mathematical Modeling of Nonlinear Cantilever Beams

To investigate the cantilever beam as a vibration absorber, a mathematical model is derived. By disregarding the parts related to the second beam of the mathematical model for the L-shaped beam attached to a SDOF system derived in Chapter 3, the mathematical model for the cantilever beam is obtained as,

$$\mathbf{M}\ddot{\mathbf{q}} + \left(\mathbf{K} + i\mathbf{H}\right)\mathbf{q} + \mathbf{f}_N = \mathbf{f}\,, \tag{5.8}$$

where,

$$\mathbf{M} = \left[\begin{array}{c|ccc} Mbb & M1b_1 & \cdots & M1b_{n_1} \\ \hline Mb1_1 & M11_{1,1} & \cdots & M11_{1,n_1} \\ \vdots & \vdots & \ddots & \vdots \\ Mb1_{n_1} & M11_{n_1,1} & \cdots & M11_{n_1,n_1} \end{array}\right], \tag{5.9}$$

$$\mathbf{K} = \left[\begin{array}{c|ccc} k_b & & & \\ \hline & K_{11_{1,1}} & \cdots & K_{11_{1,n_1}} \\ & \vdots & \ddots & \vdots \\ & K_{11_{n_1,1}} & \cdots & K_{11_{n_1,n_1}} \end{array}\right], \tag{5.10}$$

$$\mathbf{H} = \left[\begin{array}{c|ccc} \gamma_b k_b & & & \\ \hline & \gamma_1 K_{11_{1,1}} & \cdots & \gamma_1 K_{11_{1,n_1}} \\ & \vdots & \ddots & \vdots \\ & \gamma_1 K_{11_{n_1,1}} & \cdots & \gamma_1 K_{11_{n_1,n_1}} \end{array}\right], \tag{5.11}$$

$$\mathbf{q} = \left[\begin{array}{c|ccc} q_b & q_{1,1} & \cdots & q_{1,n_1} \end{array}\right]^T, \tag{5.12}$$

$$\mathbf{f}_N = \left[\begin{array}{c|ccc} 0 & f_{N1_1} & \cdots & f_{N1_{n_1}} \end{array}\right]^T, \tag{5.13}$$

$$\mathbf{f} = \left[\begin{array}{c|ccc} F_b & 0 & \cdots & 0 \end{array}\right]^T. \tag{5.14}$$

5.2.2 Optimization of the Linear Systems

To reduce the dimension of the optimization space, optimization parameters of the linear L-shaped and cantilever beams are reduced by assuming the cross sections and the materials of the first and the second beam are the same as in Section 5.1. By doing that, the number of L-shaped and cantilever beam parameters needed to be

optimized are reduced to eight and five, respectively. The upper and the lower limits for each parameter are selected as the values in Table 5.1.

5.2.3 Nonlinearity Parameters

To investigate the effect of cubic nonlinearity, the cross sections of the beams are assumed rectangular. A schematic of the cross-section can be seen in the figure below.

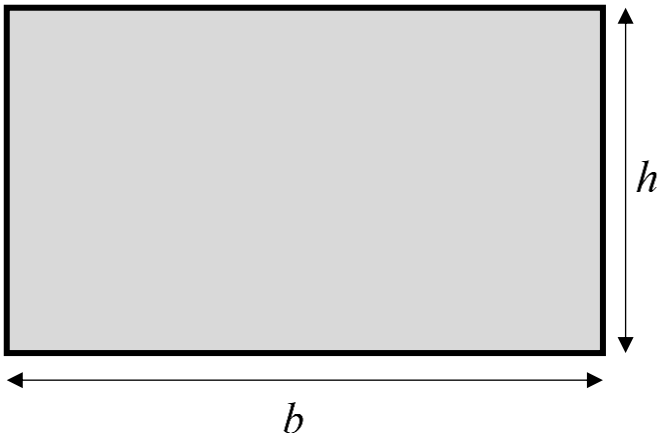

Figure 5.14. Schematic of the cross-section of the beams

Then, the stiffness parameter can be written as,

$$\frac{EI}{L_1^3} = \frac{Ebh^3}{12L_1^3}. \tag{5.15}$$

Using Equation (5.15), the cubic nonlinearity parameter can be written as,

$$\frac{EA}{2L_1^3} = \frac{Ebh}{2L_1^3} = \frac{EI}{L_1^3} \cdot \frac{6}{h^2}. \tag{5.16}$$

As it can be understood from Equation (5.16), the cubic nonlinearity parameter is inversely proportional to the square of the thickness of the beam (h).

Since the effect of the squared nonlinearity is negligible compared to the effect of the cubic nonlinearity, as it is understood from Chapter 4, L_2 is selected as $0.1m$ for

every case, and the effect of its value is not investigated. Additionally, since the cantilever beam consists of a single beam, it has no squared nonlinearity due to this nonlinearity being related to the second beam. The effect of the cubic nonlinearity on the L-shaped and cantilever beam vibration absorbers is investigated by selecting different values for h.

5.2.4 Case Study Results

The frequency responses of the SDOF system, the optimized linear L-shaped and cantilever beams, and the nonlinear counterparts of these systems are compared in the figures below. By doing this, the effect of the nonlinearities on the frequency responses is observed. In order to compare them in the same plot, normalized responses w.r.t the forcing amplitude are obtained. The base parameters for each case are selected as the values in Table 5.2. The optimized parameters for linear L-shaped and cantilever beams are given in Table 5.8 and Table 5.9.

Table 5.8. Optimized Parameters for Linear L-Shaped Beam

	Case 1	**Case 2**	**Case 3**	**Case 4**
$\rho AL_1(kg)$	0.1654	0.240	0.217	0.329
$\rho AL_2(kg)$	0.0468	0.143	0.456	0.0581
$M_1(kg)$	0.0861	0.260	0.111	0.598
$M_2(kg)$	0.202	0.352	0.216	0.516
$\frac{L_{M_1}}{L_1}$	0.379	0.790	0.516	0.659
$\frac{L_{M_2}}{L_2}$	0.223	0.138	0.536	0.279
$\frac{EI}{L_1^3}\left(\frac{N}{m}\right)$	1686	2045	1975	2316
γ	0.323	0.342	0.316	0.354

Table 5.9. Optimized Parameters for Linear Cantilever Beam

	Case 1	**Case 2**	**Case 3**	**Case 4**
$\rho A L_1 (kg)$	0.121	0.345	0.476	0.343
$M_1 (kg)$	0.289	0.621	0.395	1.15
$\frac{L_{M_1}}{L_1}$	0.596	0.568	0.899	0.894
$\frac{EI}{L_1^3}\left(\frac{N}{m}\right)$	512	544	2306	2499
γ	0.338	0.359	0.323	0.393

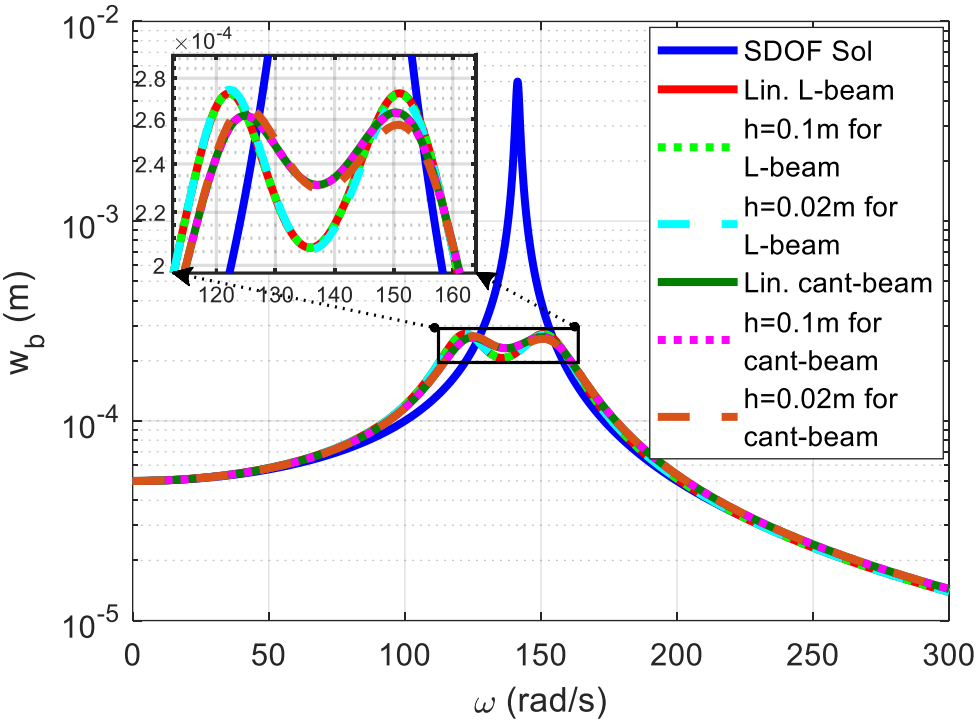

Figure 5.15. Frequency Response of w_b for Case 1, $F_0 = 5N$

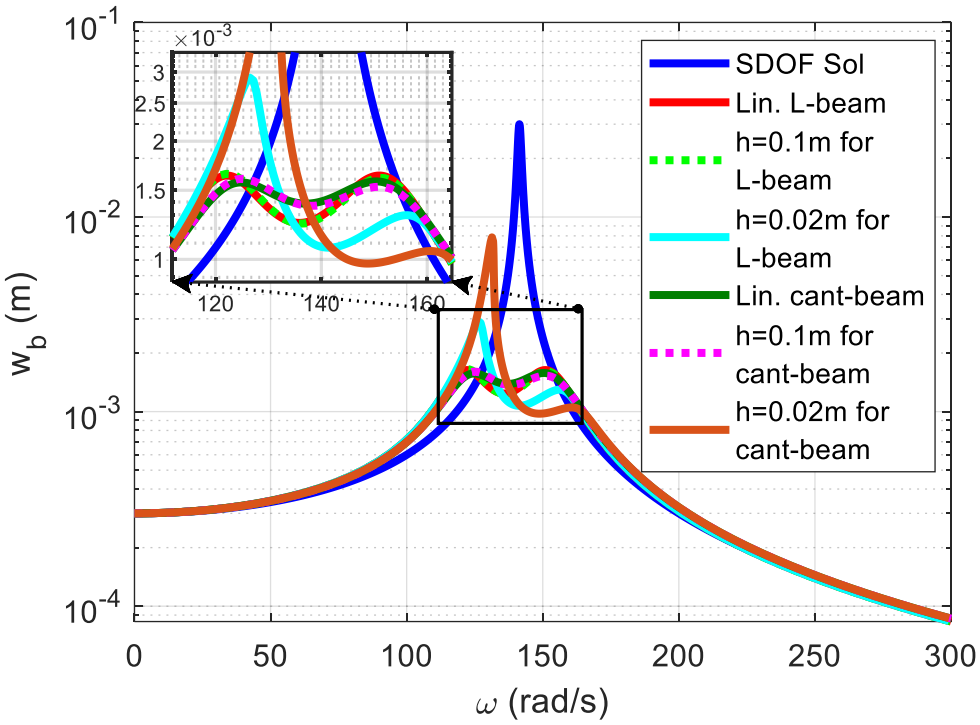

Figure 5.16. Frequency Response of w_b for Case 1, $F_0 = 30N$

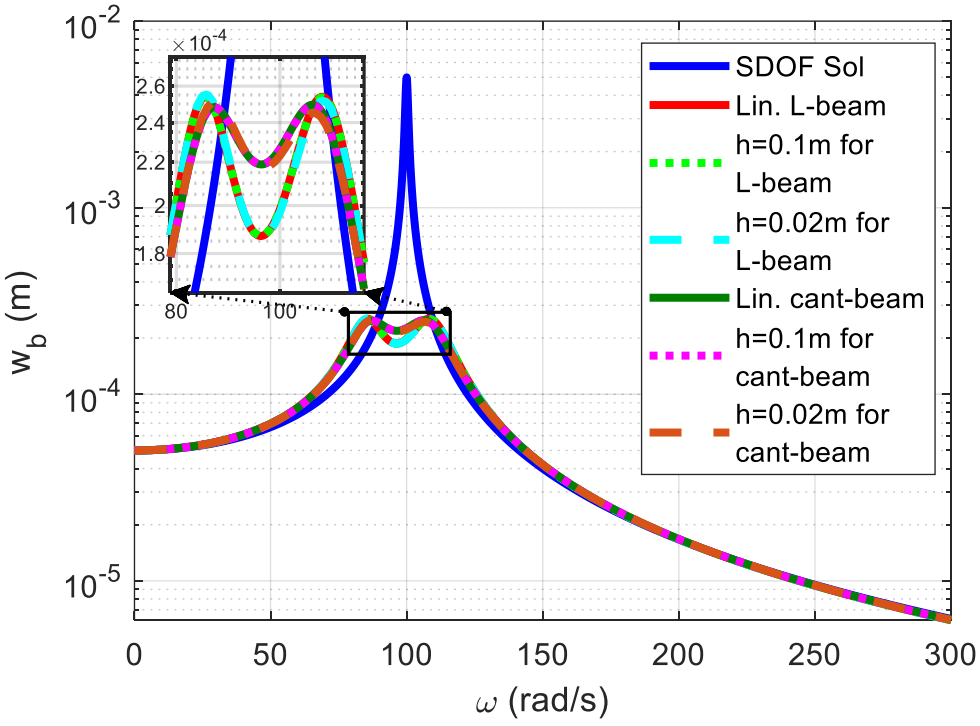

Figure 5.17. Frequency Response of w_b for Case 2, $F_0 = 5N$

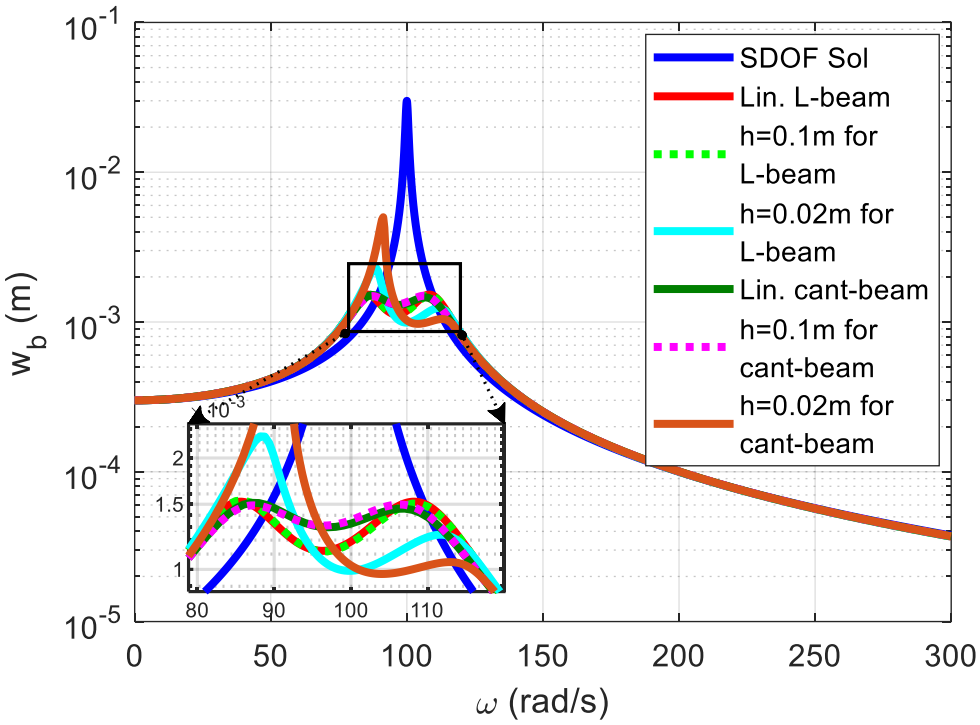

Figure 5.18. Frequency Response of w_b for Case 2, $F_0 = 30N$

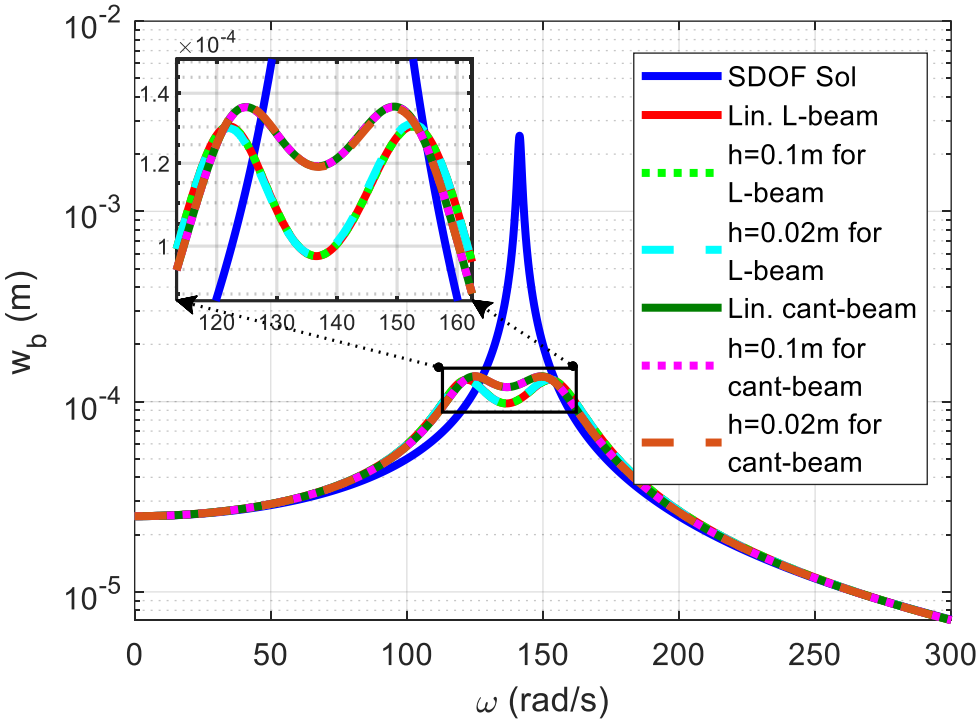

Figure 5.19. Frequency Response of w_b for Case 3, $F_0 = 5N$

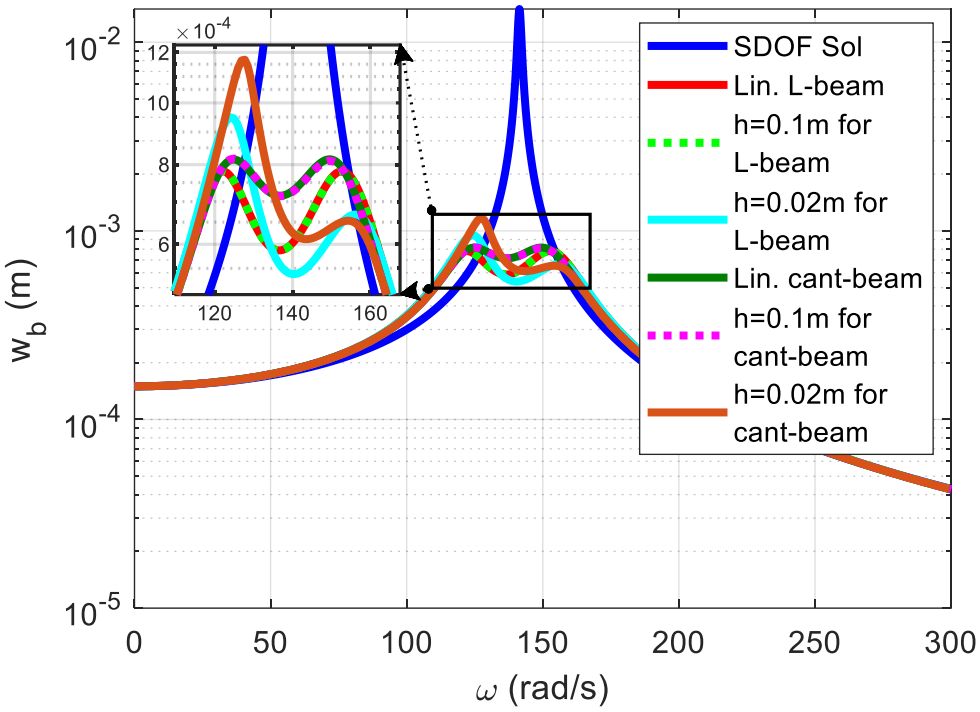

Figure 5.20. Frequency Response of w_b for Case 3, $F_0 = 30N$

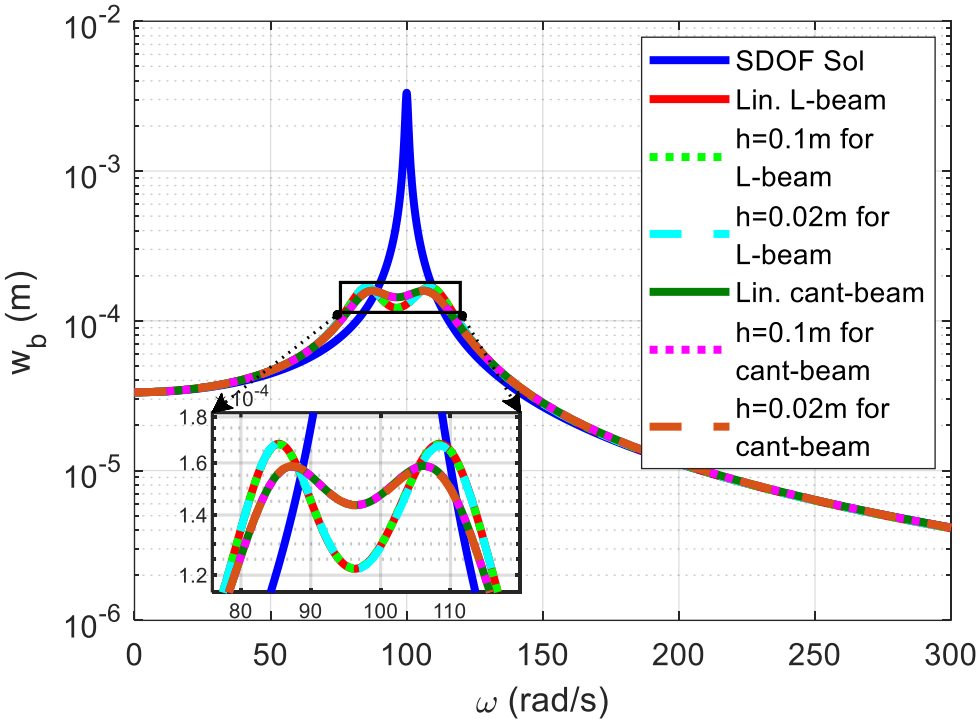

Figure 5.21. Frequency Response of w_b for Case 4, $F_0 = 5N$

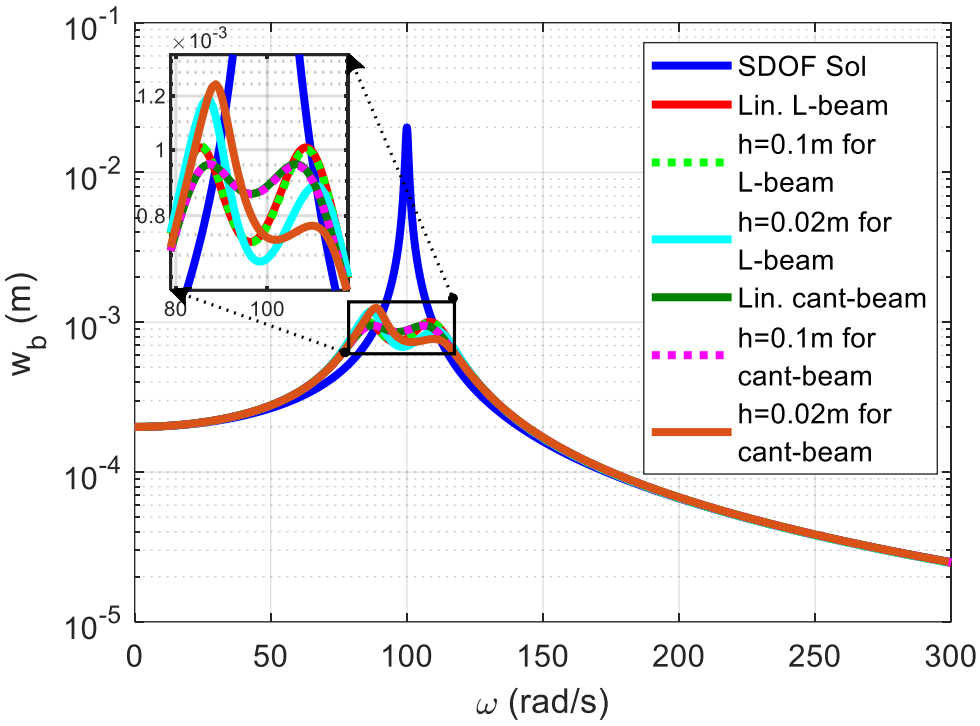

Figure 5.22. Frequency Response of w_b for Case 4, $F_0 = 30N$

As it can be understood from the figures above, increasing the forcing amplifies the effect of nonlinearities. When the forcing with the amplitude $F_0 = 5N$ is applied, the difference between linear and nonlinear solutions is undistinguishable, whereas the effect of nonlinearity becomes apparent. This shows that, under large forces, nonlinearities become significant, and these effects should be taken into account for optimization. Moreover, as the thickness of the beam decreases, the nonlinear effects on the system increase as expected. Additionally, it can be seen by comparing Figure 5.18 and Figure 5.20 that nonlinearity becomes less effective as the stiffness of the base spring increases. One final remark can be made that is the effect of cubic nonlinearity is greater on the cantilever vibration absorbers compared to the L-shaped beam ones.

CHAPTER 6

CONCLUSION

L-shaped beams are commonly used in engineering systems. These beams are used in many applications such as buildings, aerospace structures, naval structures, vehicles, etc. Because of these, many studies investigated these beams both mathematically and experimentally.

In this thesis, a nonlinear mathematical model is derived for an L-shaped beam attached to a SDOF system. The model is derived by applying Hamilton's method to the Euler Bernoulli Beam Theory. Nonlinear Von Karman displacement field and strain relationship is used for the calculation of potential energy. Galerkin's method is applied to discretize the obtained nonlinear PDEs into nonlinear ODEs. Mathematical models for fixed L-shaped beam and cantilever beam attached to a SDOF system are derived using the governing ODEs of the L-shaped beam attached to a SDOF system. Then, Harmonic Balance method is applied in order to transform the nonlinear ODEs into nonlinear algebraic equations. These equations are solved in a frequency range using Newton's method with Arc-Length Continuation and Homotopy Continuation in order to obtain the steady-state frequency response of the system.

The linearized models for both fixed L-shaped beam and L-shaped beam attached to a SDOF system are validated using the commercial FE analysis program ANSYS. Then, case studies are carried out in order to observe the effects of the system parameters on the frequency responses. In these case studies, the effects of the amplitude of the forcing applied, the masses of the beams and the concentrated masses, the locations of the concentrated masses, the stiffness of the beams, the cubic and the quadratic nonlinearities are investigated and discussed.

Finally, these beams are proposed as vibration absorbers, and the structural parameters of the nonlinear beams are optimized to reduce the vibration of the base mass. To investigate the effectiveness of L-shaped beams, they are compared with TMDs, and it is concluded that their effect on vibration reduction is very similar to the TMD devices. Moreover, the nonlinear effects on the optimized linear L-shaped beam and cantilever beam vibration absorbers are studied, and these are compared with each other to see how much nonlinearities change the frequency responses of each beam. It is deduced from this study that, under large forces, nonlinearities play a significant role in the responses of the beams.

For future works, these analyses can be experimentally validated. Moreover, a more complex mathematical model can be derived using the Timoshenko beam theory, which can be compared with the mathematical model obtained in this thesis. Lastly, these beams can be proposed as vibration amplifiers to harvest energy like the piezoelectric energy harvesters.

REFERENCES

[1] H. Samandari and E. Cigeroglu, “Nonlinear vibrations of a flexible L-shaped beam using differential quadrature method,” in *Conference Proceedings of the Society for Experimental Mechanics Series*, 2016, vol. 1, pp. 145–154. doi: 10.1007/978-3-319-15221-9_12.

[2] S. S. Rao, *Vibration of continuous systems*. wiley, 2019. doi: 10.1002/9781119424284.

[3] D. Wagg and S. Neild, “Nonlinear vibration with control,” *Solid Mechanics and its Applications*, vol. 170, pp. 215–254, 2010, doi: 10.1007/978-90-481-2837-2_1.

[4] F. Tornabene, N. Fantuzzi, F. Ubertini, and E. Viola, “Strong formulation finite element method based on differential quadrature: A survey,” *Applied Mechanics Reviews*, vol. 67, no. 2, Mar. 2015, doi: 10.1115/1.4028859.

[5] E. Cigeroglu and H. Samandari, “Nonlinear free vibrations of curved double walled carbon nanotubes using differential quadrature method,” *Physica E: Low-Dimensional Systems and Nanostructures*, vol. 64, pp. 95–105, 2014, doi: 10.1016/j.physe.2014.07.010.

[6] C. A. Morales, “Dynamic analysis of an L-shaped structure by Rayleigh-Ritz substructure synthesis method,” *Meccanica*, vol. 44, no. 3, pp. 339–343, Jun. 2009, doi: 10.1007/s11012-009-9200-8.

[7] L. Meirovitch and M. K. Kwak, “Rayleigh-ritz based substructure synthesis for flexible multibody systems,” *AIAA Journal*, vol. 29, no. 10, 1991, doi: 10.2514/3.10794.

[8] C. A. Morales, “L-shaped structure mass and stiffness matrices by substructure synthesis,” *Meccanica*, vol. 45, no. 2, pp. 279–282, Apr. 2010, doi: 10.1007/s11012-009-9245-8.

[9] H. Bang, “Analytical solution for dynamic analysis of a flexible L-shaped structure,” *Journal of Guidance, Control, and Dynamics*, vol. 19, no. 1, pp. 248–250, 1996, doi: 10.2514/3.21608.

[10] M. Gürgöze, “Comment on ‘analytical solution for dynamic analysis of a flexible l-shaped structure,’” *Journal of Guidance, Control, and Dynamics*, vol. 21, no. 2, pp. 359–359, 1998, doi: 10.2514/2.4244.

[11] M. Gürgöze, “On the dynamic analysis of a flexible L-shaped structure,” *Journal of Sound and Vibration*, vol. 211, no. 4. Academic Press, pp. 683–688, Apr. 09, 1998. doi: 10.1006/jsvi.1997.1375.

[12] , D Oguamanam, J. Hansen, and G. Heppler, “Vibration of Arbitrarily Oriented Two-Member Open Frames with Tip Mass,” 1998.

[13] F. Georgiades, J. Warminski, and M. P. Cartmell, “Linear modal analysis of L-shaped beam structures,” *Mechanical Systems and Signal Processing*, vol. 38, no. 2, pp. 312–332, Jul. 2013, doi: 10.1016/j.ymssp.2012.12.006.

[14] J. Wei, D. Cao, Y. Yang, and W. Huang, “Nonlinear dynamical modeling and vibration responses of an L-shaped beam-mass structure,” *Journal of Applied Nonlinear Dynamics*, vol. 6, no. 1, pp. 91–104, 2017, doi: 10.5890/JAND.2017.03.007.

[15] F. Georgiades, “Nonlinear equations of motion of L-shaped beam structures,” *European Journal of Mechanics, A/Solids*, vol. 65, pp. 91–122, Sep. 2017, doi: 10.1016/j.euromechsol.2017.03.007.

[16] A. G. Haddow, A. D. S. Barr, and D. T. Mook, “Theoretical and Experimental Study of Modal Interaction in a Two-Degree-of-Freedom Structure,” 1984.

[17] A. H. Nayfeh and L. D. Zavodney, “Experimental Observation of Amplitude-and Phase-Modulated Responses of Two Internally Coupled

Oscillators to a Harmonic Excitation," 1988. [Online]. Available: http://www.asme.org/about-asme/terms-of-use

[18] A. H. Nayfeh, B. Balachandran, M. A. Colbert, and M. A. Nayfeh, "An Experimental Investigation of Complicated Responses of a Two-Degree-of-Freedom Structure," 1998. [Online]. Available: http://www.asme.org/about-asme/terms-of-use

[19] A. H. Nayfeh and B. Balachandran, "Experimental Investigation of Resonantly Forced Oscillations of a Two-Degree-of-Freedom Structure."

[20] B. Balachandran and A. H. Nayfeh, "Nonlinear Motions of Beam-Mass Structure."

[21] B. Balachandran and A. H. Nayfeh, "Observations of Modal Interactions in Resonantly Forced Beam-Mass Structures," 1991.

[22] A. Erturk, J. M. Renno, and D. J. Inman, "Piezoelectric energy harvesting from an L-shaped beam-mass structure," in *Active and Passive Smart Structures and Integrated Systems 2008*, Mar. 2008, vol. 6928, p. 69280I. doi: 10.1117/12.776211.

[23] M. Yao, P. Liu, L. Ma, H. Wang, and W. Zhang, "Experimental study on broadband bistable energy harvester with L-shaped piezoelectric cantilever beam," *Acta Mechanica Sinica/Lixue Xuebao*, vol. 36, no. 3, pp. 557–577, Jun. 2020, doi: 10.1007/s10409-020-00956-1.

[24] M. Krack and J. Gross, *Harmonic Balance for Nonlinear Vibration Problems*. Cham: Springer International Publishing, 2019. doi: 10.1007/978-3-030-14023-6.

[25] J. N. Reddy, *An Introduction to Nonlinear Finite Element Analysis, 2nd Edn*. 2015. doi: 10.1093/acprof:oso/9780199641758.001.0001.

[26] S. Gebai, G. Cumunel, M. Hammoud, G. Foret, E. Roze, and E. Hainque, "Upper Limb Involuntary Tremor Reduction Using Cantilever Beam

TMDs," *JVC/Journal of Vibration and Control*, 2022, doi: 10.1177/10775463211051869.

[27] J. Enriquez-Zarate, H. F. Abundis-Fong, and G. Silva-Navarro, "Passive Vibration Control in a Building-Like Structure Using a Tuned-Mass-Damper and an Autoparametric Cantilever Beam Absorber," in *Active and Passive Smart Structures and Integrated Systems 2015*, Apr. 2015, vol. 9431, p. 94312Z. doi: 10.1117/12.2083779.

[28] R. G. Jacquot, A. Professor, and J. E. Foster, "Optimal Cantilever Dynamic Vibration Absorbers," 1977. [Online]. Available: http://www.asme.org/about-asme/terms-of-use

[29] G. Silva-Navarro and H. F. Abundis-Fong, "Passive/Active Autoparametric Cantilever Beam Absorber with Piezoelectric Actuator for a Two-Story Building-Like Structure," *Journal of Vibration and Acoustics, Transactions of the ASME*, vol. 137, no. 1, 2015, doi: 10.1115/1.4028711.

[30] M. Cavacece and L. Vita, "Optimal Cantilever Dynamic Vibration Absorbers by Timoshenko Beam Theory," IOS Press, 2002.